

https://dspace.org/

Hydraulic characterization of the kinsere geology, Democratic Republic of the Congo

Moswathupa, Hamilton Thabang Segana

2019

https://hdl.handle.net/10539/28084

Downloaded from a DSpace repository. https://dspace.org/

HYDRAULIC CHARACTERISATION OF THE KINSEVERE GEOLOGY, DEMOCRATIC REPUBLIC OF THE CONGO

Hamilton Thabang Segana Moswathupa

A Research Report submitted to the Faculty of Science, University of the Witwatersrand, in partial fulfilment of the requirements for the degree of Master of Science in Hydrogeology

June 2019



Supervisor: Prof. Tamiru Abiye

School of Geosciences

University of the Witwatersrand, Johannesburg





Declaration

I, Hamilton Thabang Segana Moswathupa, declare that this research report is my own, unaided work, undertaken in tandem with SRK Consulting (SA) Pty Ltd (SRK), a consulting firm appointed by Kinsevere and my employer. SRK and I collected the data presented, analysis of which was undertaken by myself, independent from that undertaken by SRK and without bias. This report is being submitted for the Degree of Master of Science in Hydrogeology at the University of the Witwatersrand, Johannesburg. It has not been submitted before for any degree or examination at any other University.



(Signature of candidate)

10th day of June 2019 at Johannesburg

Abstract

The Kinsevere mine operation extracts copper oxide ore that occurs within the Tshifufiamashi, Tshifufia and Kinsevere Hill fragments at the Mashi, Central and Kinsevere Hill pits, respectively. Copper oxide ore mining is expected to continue until 2021, following which, copper sulphide ore mining could be initiated and undertaken until 2027, entailing extension and deepening of the pits. Hydraulic tests were undertaken to determine and characterise hydraulic attributes of various siliceous and dolomitic rock units underlying the pits so as to understand the influence of mine progression on groundwater dynamics, inflows and pore pressures. From this, effective planning, safe mining and sound groundwater management may be undertaken.

Hydraulic test data were acquired through pumping, airlift and slug testing of 39 boreholes intersecting the various rock units. The data were analysed using specified methods and characterised based on common hydraulic and lithologic attributes of the various rock units tested. Saprolite and saprock derivatives of the Kundelungu shale and siltstone units had a low hydraulic conductivity (K) of $8.0x10^{-3}$ – $2.6x10^{-2}$ m/d, while the derivative of the Mines Series shales dolomitiques (SD) unit had a K of $1.6x10^{-1}$ – $7.0x10^{-1}$ m/d. The RAT siltstone (RSL) and RAT breccia (RBX) units had a moderate K of $3.3x10^{-3}$ – $1.5x10^{-2}$ m/d and $1.7x10^{-2}$ – $5.4x10^{1}$ m/d, respectively. The Mines Series SD and calcaire à minerais noir (CMN) units had a high K of $4.2x10^{-3}$ – $1.5x10^{0}$ m/d and $1.3x10^{0}$ – $1.6x10^{2}$ m/d, respectively. Hydraulic and lithologic attributes influence the capacity of the various rock units to receive, store and transmit groundwater, thereby defining three aquifer units (siliceous, polymictic and dolomitic) at Kinsevere.

Mine progression is expected to remove storage, increasing the groundwater sink towards the pits, leading to increased groundwater inflows via moderate to high permeability zones (RSL, RBX, SD and CMN) on the highwalls and pit floors under hydrostatic drive stemming from higher groundwater levels and upward pressures. Inflows into the Mashi Pit could increase from 125 L/s to 171 L/s, while the Central Pit could experience an increase from 545 L/s to 1 103 L/s when terminal depths are reached. Negligible inflows were observed in the Kinsevere Hill Pit. Projected inflows into the Kinsevere Hill North and South pits could be 27 L/s and 135 L/s, respectively. The inflows exceed dewatering discharge of 280 L/s. Most inflows stem from the highwalls, resulting in increased pore pressures that could compromise stability within rock units of low permeability and weakened self-retainability.

Acknowledgements

I wish to thank the following individuals and institutions for their assistance and cooperation:

- Minerals and Metals Group (Pty) Ltd for having authorised this study;
- Kinsevere's exploration, mining and environmental departments for assisting with field investigations;
- Mr. B. Mabenge (Principal Hydrogeologist) and Mr. I. Mahomed (Principal Hydrogeologist and Partner) of SRK Consulting (SA) Pty Ltd for their continued technical mentorship and motivation;
- Prof. R. Gibson, Head of School at the University of the Witwatersrand, for his assistance during the authorisation process; and
- Prof. T. Abiye of the University of the Witwatersrand for his patience, technical contribution and guidance. Time spent in his lectures was inspiring, thought provoking and instilled independent thinking.

The following, presented in my mother's tongue (Sepedi), gives acknowledgement and appreciation to my family for their love and support:

- Ke rata go leboga Dineo, Mokgadi le Mankgarube Moswathupa. Ngwanammaka, ke ka baka la lerato le hlohleletšo ya gago ke sa eme. Khego le papa, ke leboga kgodišo, thekgo le lerato. Ba go ba le moratho le batswadi ba go swana le lena ba a balega;
- Ke leboga thekgo ya Kelebogile Mokoena, Morongwa Kekana, Sello le Rahab Motswi. Dithapelo tša lena di kwagetše; le
- Bogologolo ke rata go leboga Badimo ba Ga- Moswathupa, Motswi, Masekwameng le ba Ga-Phalamohlaka. Ke leboga bophelo, tšhireletšo, lerato le dimpho tšeo le nkadimilego tšona, le tšeo di sa tlago.

Table of Contents

1 Introduction 1

1.1 Background and Rationale for the Research 1

1.2 Problem Statement 2

1.3 Objectives 4

2 Literature Review 4

2.1 Groundwater Flow Dynamics and Mechanism 4

2.2 Hydraulic Characterisation 4

2.2.1 Ruashi Cu-Co Mine (DRC) 4

2.2.2 Dikulwe, Mashamba West and Mashamba East Cu-Co Mines (DRC) 5

2.2.3 Konkola Cu-Co Mine (Zambia) 6

3 Methodology 8

3.1 Data Review 8

3.2 Hydrocensus 8

3.3 Drilling and Construction 8

3.3.1 Drilling Techniques 8

3.3.2 Construction 10

3.4 Hydraulic Testing 12

3.4.1 Pumping Test 12

3.4.2 Airlift Tests 13

3.4.3 Slug Tests 14

3.5 Hydraulic Test Data Analysis 14

3.5.1 Pumping Test Data Analysis 14

3.5.2 Airlift Test Data Analysis 15

3.5.3 Slug Test Data Analysis 15

3.6 Pore Pressure Assessment 16

3.7 Groundwater Recharge Determination 16

3.8 Inflow Determination- Steady State Analytical Solution 16

3.9 Conceptual Hydrogeological Model 17

4 Study Site 18

4.1 Climate 18

4.2 Topography and Surface Water 19

4.3 Geology 19

4.3.1 Depositional Setting and Regional Stratigraphy 19

4.3.2 Lithostratigraphy 23

4.3.3 Structural Evolution and Architecture 27

4.4 Hydrogeology 28

4.4.1 Groundwater Recharge 28

4.4.2 Groundwater Flow and Levels and Strikes 28

4.4.3 Hydrostratigraphy 29

5 Observations and Findings 30

5.1 Hydrocensus 30

5.1.1 Groundwater Level Measurements and Abstraction 30
5.1.2 Observed Groundwater Inflows 33
5.2 Pore Pressure Assessment 35
5.3 Drilling 38
5.3.1 Rock Units Intersected 41
5.4 Hydraulic Testing 45
5.4.1 Pumping Test 45
5.4.2 Airlift Tests 48
5.4.3 Slug Tests 49
5.5 Groundwater Recharge 55
5.6 Groundwater Inflow Calculations 55
6 Discussion 56
6.1 Hydraulic Characterisation 56
6.1.1 Saprolite and Saprock Units 56
6.1.2 RSL Unit 56
6.1.3 RBX Unit 56
6.1.4 SD Unit 57
6.1.5 CMN Unit 57
6.1.6 Bulk Units 57
6.2 Pore Pressures 57
6.3 Groundwater Inflows 57
7 Hydrogeological Conceptual Model 59
8 Conclusions and Recommendations 61
References 62

List of Figures

Figure 1-1: Locality map (Source: SRK, 2015). 1

Figure 1-2: Site layout map (Source: SRK, 2016). 2

Figure 1-3: Photographs of Kinsevere pits as taken in 2018 – A. Mashi Pit (facing NE); B. Central Pit (facing SE); and C. Kinsevere Hill Pit (facing NE). 3

Figure 3-1: Photograph of CSRC rig setup for drilling of a dewatering borehole on the saddle between the Mashi and Central pits saddle. 9

Figure 3-2: Schematic of CCRC (A), CSRC (B) and DC (C) drilling techniques (Source: Marjoribanks, 2010). 9

Figure 3-3: Photographs of borehole development (A), airlift yield measurement during drilling (B), borehole headworks (C&D) and generic DEW borehole construction (E- Source: SRK, 2016). 11

Figure 3-4: Schematic of pumping well dynamics (A, modified from Summa, 2010) and photograph of a positive displacement pumping test rig (B). 12

Figure 3-5: Generic setup of airlift test (Source: SRK, 2016). 13

Figure 3-6: Slug test, pre-test (A), water injection type (B) and slug piece type (C, with photograph). 14

Figure 3-7: Groundwater inflow generic analytical model (Source: Marinelli and Niccoli, 2000). 17

Figure 4-1: Hyetograph showing rainfall distribution from January 2011 to February 2018 (Source: Kinsevere weather station). 18

Figure 4-2 Location of the Lufilian Arc in relation to the Kalahari and Congo cratons and other belts (Source: Kampunzu and Cailteux, 1999). 19

Figure 4-3 Katanga Supergroup stratigraphy in the DRC (Source: Francois, 2006). 22

Figure 4-4: The Kinsevere geological map (Source: SRK, 2018). 23

Figure 4-5: Field appearance of the RSL unit. 24

Figure 4-6: Field appearance of the SD unit. 25

Figure 4-7: Field appearance of the CMN unit. 26

Figure 4-8 Stratigraphy of Kinsevere geology as classified by McMaster *et al.* (2016). 26

Figure 4-9: The Kinsevere structural architecture (Source: Kazadi, 2012). 28

Figure 4-10 Map of Kinsevere topography, hydrology and piezometric heads in 2010 (base map source: SRK, 2018). Borehole water level and piezometric contour data collated by author. 29

Figure 5-1 Boreholes identified during the hydrocensus (Base map source: SRK, 2018). Borehole data collated by author. 30

Figure 5-2: Piezometric map (Base map source: SRK, 2018). Borehole water level and piezometric contour data collated by author. 31

Figure 5-3: Daily abstraction volume for 2016 to 2018 (Source: Kinsevere Pumping Sheets, 2018). 32

Figure 5-4: Temporal groundwater level monitoring plot between 2010 and 2016 (Data source: SRK, 2016). 32

Figure 5-5: Photographs of groundwater conditions at Kinsevere. 35

Figure 5-6: HTH01 Plot– evidence of rainfall influence on groundwater levels (Data source: SRK, 2016). 36

Figure 5-7: HTH05 Plot– evidence of rainfall influence on groundwater levels (Data source: SRK, 2016). 37

Figure 5-8: HTH02 Plot– evidence of hydraulic connectivity and upward hydrostatic pressures (Data source: SRK, 2016). 37

Figure 5-9: HTH03 Plot– evidence of hydraulic connectivity and upward hydrostatic pressures (Data source: SRK, 2016). 37

Figure 5-10: HTH04 Plot– evidence of hydraulic connectivity and upward hydrostatic pressures (Data source: SRK, 2016). 38

Figure 5-11: HTH06 Plot– evidence of disconnection between upper CMN and underlying RSL and CMN units (Data source: SRK, 2016). 38

Figure 5-12: Map showing boreholes drilled during research (Base map source: SRK, 2018). Borehole data collated by author. 39

Figure 5-13: Photographs of rock units intersected during drilling. 45

Figure 5-14: Step drawdown data vs. time graph of DEW08 overlain by the Non-Linear FC Method line of best fit (pink). 46

Figure 5-15: Diagnostic plots showing trends observed during pumping test (Source: Renard, 2005b). 47

Figure 5-16: Log-log Diagnostic Plot of DEW08 constant drawdown data. 47

Figure 5-17: Derivative Plot of DEW08 constant drawdown data. 47

Figure 5-18: Residual drawdown data plot of DEW08. 48

Figure 5-19: Analysis of DEW33 Airlift testing data using Theis (1935) Recovery Method (Source: SRK, 2017). Analysis spreadsheet updated by author. 49

Figure 5-20: Slug test analysis for SRC069 using Bouwer-Rice (1976) in Aquifer Test Pro (2015.1). 50

Figure 5-21: Location of boreholes subjected to hydraulic tests (Base map source: SRK, 2018). Borehole data collated by author. 51

Figure 6-1: Hydraulic conductivity values determined from hydraulic tests plotted over generic results presented in USGS (2003). 58

Figure 7-1: Hydrogeological conceptual model (Source: SRK, 2016). Updated and modified by author. 60

List of Tables

Table 2-1: Summary of hydraulic attributes determined at Ruashi Mine. 5

Table 2-2: Summary of hydraulic attributes determined in the DIMA area. 6

Table 2-3: Summary of hydraulic attributes determined at Konkola Mine. 7

Table 5-1: Details of HTH boreholes installed. 36

Table 5-2: Details of pilot boreholes drilled. 39

Table 5-3: Details of dewatering boreholes. 40

Table 5-4: Details of resource exploration boreholes. 40

Table 5-5: Details of rock units intersected by dewatering pilot boreholes and their respective lithological attributes. 42

Table 5-6: Summary of rock units intersected by resource exploration boreholes in the TSF3 area. 43

Table 5-7: K and T ranges determined from newly drilled pilot boreholes and an additional 22 boreholes. 49

Table 5-8: K and T ranges determined from eight resource exploration boreholes. 50

Table 5-9: Summary of hydraulic conductivity (K) and transmissivity (T) data determined from airlift tests. 52

Table 5-10: Summary of hydraulic conductivity (K) and transmissivity (T) data determined from slug tests. 54

Table 5-11: Input parameters used for recharge calculation. 55

Table 5-12: Summary of pit inflows determined. 55

List of Abbreviations

Abbreviation	Description
CACB	Central African Copper Belt
CDRT	Constant Discharge Rate Test
cm	Centimeter
CMN	Calcaire à Minerais Noir
D Strat	Dolomites Stratifiées
GBS	Grey Banded Shale
ICSL	Interbedded Calcareous Siltstone and Shale
K	Hydraulic Conductivity
km	Kilometer
KP	Knight Piésold Consulting (Pty) Ltd
Ku	Kundelungu Group
L/s	Liter per Second
LSH	Lower Shale
LMU	Laminated Magnesitic
m	Meter
Ma	Million Annum
MAE	Mean Annual Evaporation
magl	Meter Above Ground Level
MAP	Mean Annual Precipitation
MAR	Mean Annual Recharge
mamsl	Meter Above Mean Sea Level
mbgl	Meter Below Ground Level
MNZ	Middle Nodular Zone
mm	Millimeter
Ng	Nguba Group
Q	Discharge
OS	Ore Stockpile
R	Roan Group
RAT	Roches Argilo-Talqueuses
RBX	RAT Breccia
RSC	Roches Siliceuses Cellulaires
RSF	Roches Siliceuses Feuilletées
RSL	RAT Siltstone
SD	Shales Dolomitiques
SDRT	Stepped Discharge Rate Test
SRK	SRK Consulting (South Africa) (Pty) Ltd
T	Transmissivity
TDA	Telescope Down Approach
TSF	Tailings Storage Facility
WRD	Waster Rock Dump

1 Introduction

1.1 Background and Rationale for the Research

Kinsevere is an opencast copper mine and a heavy media separation plant operation with an electric arc furnace, located *c*.35 km north-northeast (NNE) of Lubumbashi, Kipushi Territory, Katanga Province, Democratic Republic of the Congo (DRC) (Figure 1-1). The mine and plant are owned and operated through a joint venture between the Mining Company Katanga SPRL (MCK) and the Minerals and Metals Group (Pty) Ltd (MMG). MMG is a mid-tier global resource company, having the China Minmetals Corporation (CMC) as its main shareholder (74%). MMG owns 95% of Kinsevere, while MCK owns 5%. MMG and MCK have a lease agreement with La Génerale des Carrieres et des Mines (Gécamines), a state-owned mining company. MMG acquired majority ownership of the operation in 2012 from Anvil Mining Ltd (Anvil).

The operation extracts copper oxide and sulphide ore occurring within four mineralised siliceous and dolomitic fragments belonging to the Roches Argilo-Talqueuses (RAT) and Mines Series subgroups of the Roan Group, Katanga Supergroup, through the Mashi, Central and Kinsevere Hill pits. The fragments occur in the northern portion of the Lufilian Arc. Mining is ongoing in the Mashi Pit, with the pit floor located at 60 meters below ground level (mbgl), 1 150 meters above mean sea level (mamsl). The Central Pit is undergoing a cutback and has a pit floor depth of 140 mbgl (1 070 mamsl). Mining in the Kinsevere Hill Pit ceased at a depth of 30 mbgl (1 170 mamsl).

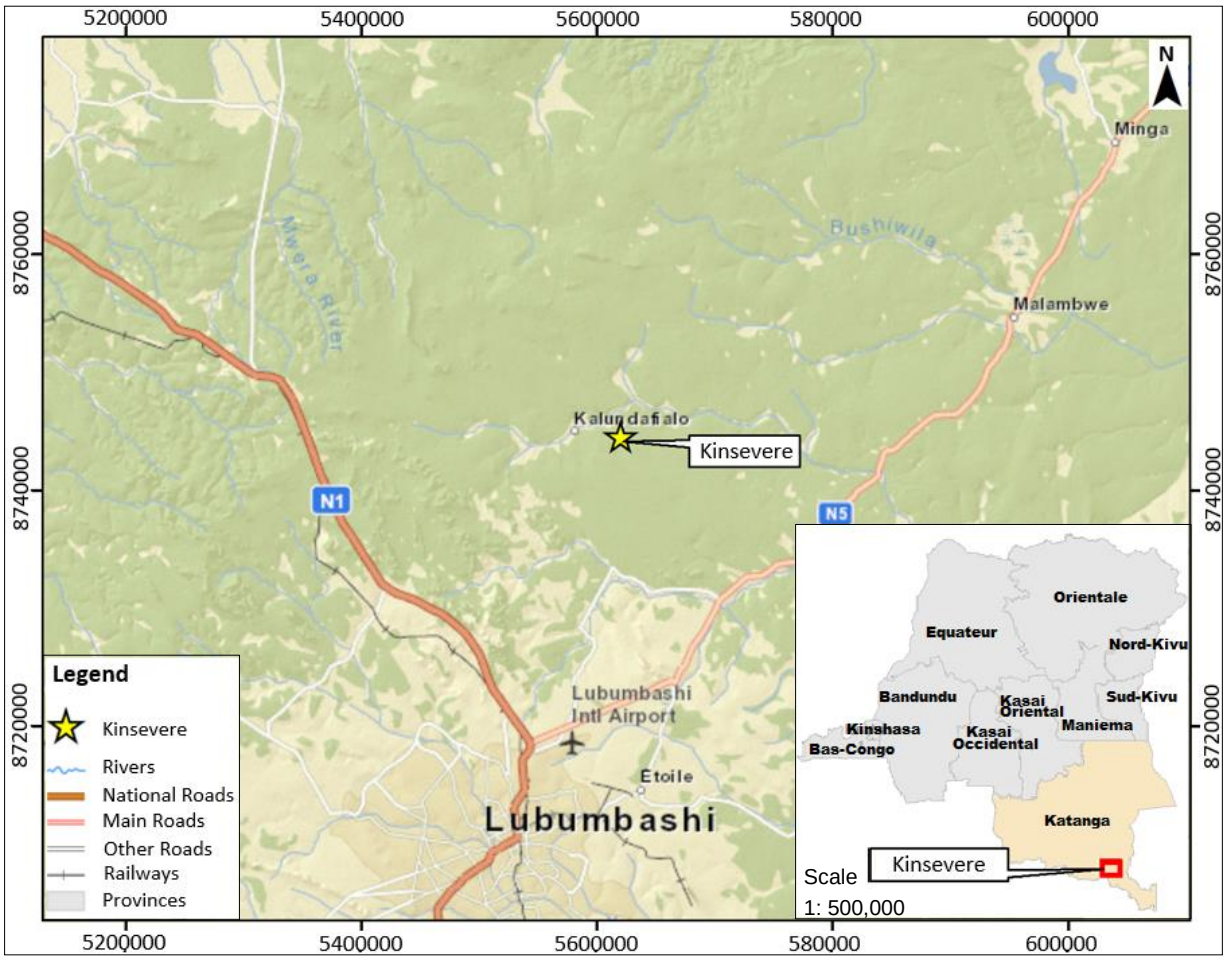


Figure 1-1: Locality map (Source: SRK, 2015).

Mining of copper oxide ore is set to run until 2021, by which, depths of 80 mbgl (1 130 mamsl) and 170 mbgl (1 040 mamsl) could be reached in the Mashi and Central pits, respectively. Mining of copper sulphide ore could continue from 2021 to 2027, entailing deepening and merging of the two pits into one large split pit. Planned terminal depths for the Mashi and Central pits are 135 mbgl (1 075 mamsl) and 305 mbgl (905 mamsl), respectively. The Kinsevere Hill Pit and a demarcated area to its immediate south could be mined for copper sulphide ore, making the current pit Kinsevere Hill North and the new pit Kinsevere Hill South, with planned terminal depths of 40 mbgl (1 160 mamsl) and 85 mbgl (1 115 mamsl), respectively. See Figure 1-2 for the final planned layout of the four pits and Figure1-3 for photographs of the pits.

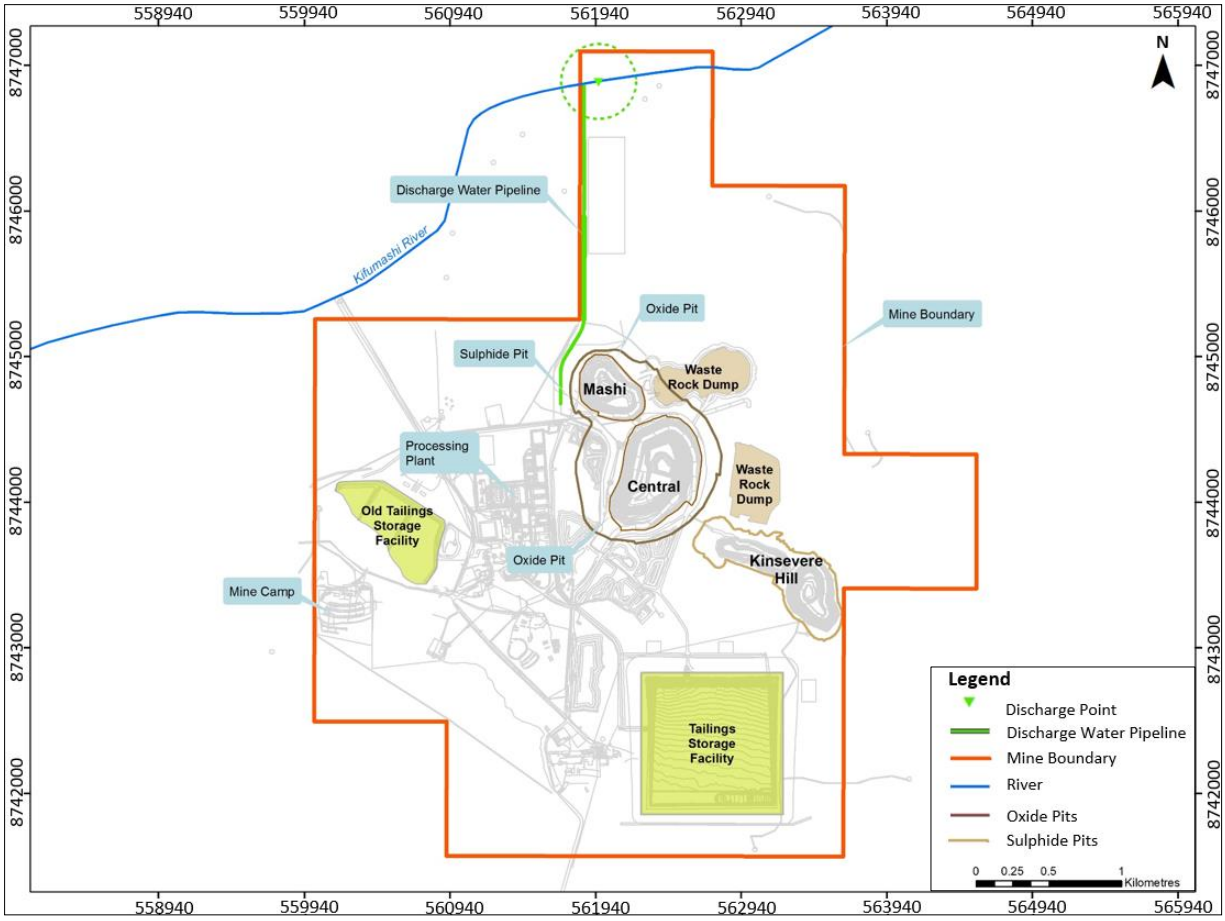


Figure 1-2: Site layout map (Source: SRK, 2016).

1.2 Problem Statement

The mine progression is expected to further expose the underlying siliceous and dolomitic rock units together with geological structures of the Tshifufiamashi, Tshifufia, Kilongo and Kinsevere Hill fragments. The Tshifufiamashi and Tshifufia fragments mined at the Mashi and Central pits, respectively, occur along a major north (N) to south (S) oriented fracture and are disjointed by a northeast (NE) to southwest (SW) oriented sinistral strike-slip fault. The Kilongo and Kinsevere Hill fragments could be mined at the Kinsevere Hill North and South pits, respectively. The two fragments occur along a major northwest (NW) to southeast (SE) oriented fracture and are dislodged from the Tshifufiamashi and Tshifufia fragments by an east (E) to west (W) oriented strike-slip sinistral fault (Kazadi, 2012). The mine progression could be accompanied by increased groundwater inflows into the pits together with slope failure within oversaturated rock units of low permeability and weakened self-retainability. The increase in groundwater inflows and slope failure need to be better understood and articulated through hydraulic testing and characterisation so as to mitigate flooding and slope failure, thereby ensuring safe mining conditions. Therefore, this work aims to provide relevant answers to the problem.



Figure 1-3: Photographs of Kinsevere pits as taken in 2018 – A. Mashi Pit (facing NE); B. Central Pit (facing SE); and C. Kinsevere Hill Pit (facing NE).

1.3 Objectives

The objective of this research was to determine and characterise hydraulic attributes of saprolites, saprock, shale, siltstone, RAT Siltstone (RSL), RAT Breccia (RBX), Shales Dolomitiques (SD) and Calcaire à Minerais Noir (CMN) together with geological structures underlying the Kinsevere concession using various specified methods and their respective analyses.

2 Literature Review

2.1 Groundwater Flow Dynamics and Mechanism

Groundwater flow and storage is dependent on lithologic and hydraulic attributes of the rock units and structures it occurs within and interacts with, driven by variations in pressures (lithostatic and hydrostatic) and gradients (topography, density, thermal, and hydraulic head) (Evans *et al.* 1991). The flow and storage capacity of rock units and structures are primarily quantified by hydraulic conductivity (K), transmissivity (T) and storativity (S), determined through their respective governing equations as per hydrogeological conditions encountered, variations therein, and specific test methods applied.

2.2 Hydraulic Characterisation

For relation purposes, this research reviewed various operations found across the Lufilian Arc, with common geology as Kinsevere to deduce the hydraulic characterisation of the rock units and the response of groundwater dynamics as affected by common operational activities. Hydraulic attributes of rock units intersected were reviewed to determine their influence on the extent of the response.

2.2.1 Ruashi Cu-Co Mine (DRC)

The mine is located *c*.50 km south of Kinsevere, within the Luano River Catchment, having drainage occurring via this river and the Kebumba River flowing to the NW and NE direction, respectively, with groundwater following the same trend. The orebody occurs within NE dipping layers of siliceous dolomitic schist (SDS, herein referred to as SD and as per Katangan nomenclature) in a locally overturned syncline having a thick lateritic cap, mined through three pits (Pit 1, Pit 2 and Pit 3). The mine concession sits on siliceous and dolomitic rock units of the Katangan Supergroup, comprising rock units of the Roan (RAT and Mines Series – DStrat, RSF, RSC, SD, and CMN) and Kundelungu (shale, sandstone, dolomitic shale and minor limestone) groups.

Chironga (2013) undertook studies to characterise the various rock units using drilling and hydraulic testing data to develop a dewatering plan for the mine following concerns of significant volumes of groundwater being introduced into the pits and increased pore water pressures that led to slope failure. The following aquifers and hydraulic attributes of their respective rock units (common to Kinsevere) were deduced (Table 2-1):

- **Shallow Aquifer** – low yielding and comprised laterites, siliceous RAT Subgroup and Kundelungu Group rock units acting as confining beds in places. The laterites and RAT units had a K of $1.0x10^{-2}$ m/d, with the RAT unit having airlift yields of 0.3 L/s, increasing to 11 L/s when brecciated. The Kundelungu sandstone unit was interbedded with siltstone, mudstone and shale (occasionally dolomitic) units, having a K of $1.0x10^{-1}$ m/d, average airlift yields of 3 L/s and S of 0.03 due to porosities of 5 – 15%. Water strikes within this aquifer were intersected at depths of 5 – 40 mbgl.

The shallow water strikes were attributed to recharge from the water mounds underlying the tailings storage facility (TSF) and waste rock dump (WRD). The low permeability in this aquifer promotes perched conditions. Increases in water levels and resultant increase in saturation in this aquifer led to increased pore pressures and slope failure; and

- **Deep Aquifer** – high yielding relative to the Shallow Aquifer and comprised the Mines Series dolomitic units. Groundwater occurrence and yields are largely controlled by geological structures and dissolution features. The SD unit had a porosity range of 20 – 25%, K of $3.0x10^{0}$ m/d, T of $2.5x10^{2}$ m^2/d and airlift yields of up to 111 L/s attributed to moderate weathering, vugs and sub-horizontal fractures as connection conduits. The RSC and DStrat units were not tested and could not be assigned K values. The RSF unit had a porosity of 15 – 25%, K of $2.0x10^{0}$ m/d and T of $2.0x10^{2}$ – $4.0x10^{2}$ m^2/d. The CMN unit had a K of $1.0x10^{-1}$ – $5.0x10^{-1}$ m/d, T of $1.0x10^{0}$ – $5.0x10^{0}$ m^2/d, storativity of 0.02 and airlift yields of 1 – 6 L/s. Water strikes within this aquifer occurred at depths of 35 – 220 mbgl. The dolomitic rock units (predominantly SD) intersected by the pits contributed significant volumes of water into the pits due to their respective high hydraulic attributes.

Table 2-1: Summary of hydraulic attributes determined at Ruashi Mine.

Aquifer	Rock Type	K (m/d)	T (m^2/d)	S	Yield (L/s)
Shallow	Laterite and RAT	$1.0x10^{-2}$	-	0.001	0.3
	Kundelungu sandstone interbedded with mudstone and shale	$1.0x10^{-1}$	-	0.03	-
Deep	SD	$3.0x10^{0}$	$2.5\ x10^{2}$	-	111
	RSC and D Strat	-	-	-	-
	RSF	$2.0x10^{0}$	$2x10^{2}$ – $4x10^{2}$	-	-
	CMN	$1.0x10^{-1}$ – $5.0x10^{-1}$	$1x10^{0}$ – $5x10^{0}$	0.02	1 – 6

- Not provided

Chironga (2013) further constructed a three-dimensional numerical model using the aforementioned attributes to simulate and predict groundwater inflows into the pits from 2012 to 2022. The total inflows into Pit 1 were determined to be 130 L/s, while Pit 2 and Pit 3 were projected to have total inflows of 98 L/s and 250 L/s, respectively. Groundwater inflows were projected to increase with depth. The increase in groundwater inflows was predicted to influence pore pressures, leading to more slope failures if not managed. Abstraction for dewatering purposes drew groundwater towards the pits, thereby promoting hydrostatic loading of the highwalls of the pit which could lead to failure.

2.2.2 Dikulwe, Mashamba West and Mashamba East Cu-Co Mines (DRC)

Straskraba *et al*. (1985) undertook hydrogeological investigations for mine dewatering and water management purposes in the Dikulwe, Mashamba West and Mashamba East (DIMA) open pit mines and the Kamoto Underground Mine (KUM), located in the southwestern portion of the Kolwezi Mining District. Drainage encompassed the S – N flowing Potopoto and Luilu rivers forming a confluence north of the mining area. The north central portion of the DIMA area comprised the Lac D'Exhaure Sinkhole, previously used as a discharge point for the KUM and its concentrator. Dolomitic and siliceous Mines Series and Kundelungu rock units underlie the DIMA area. The structural architecture of the area comprised several interconnected anticline and syncline blocks trending SE – NW, with the main anticlinal structures moderately and steeply dipping east and northeast, respectively.

Straskraba *et al*. (1985) delineated the dolomitic and siliceous rock units (common to Kinsevere) and their respective hydraulic attributes into the following aquifers (Table 2-2):

- **Shallow Aquifer** – comprised the RAT unit of relatively low permeability and primary porosity, limiting groundwater storage and transport to the rock unit matrix, unless enhanced by structures and weathering (evolving to secondary porosity). The unit generally had limited hydraulic connections, thereby promoting semi-confined to confined conditions; and
- **Deep Aquifer** – of unconfined character where it outcropped, comprising the CMN and SD units, having secondary porosity, with groundwater storage and transport influenced by the extent of cavity and fracture connectivity. Hydraulic pumping tests undertaken within these units determined a bulk K of $7.0x10^{-1}$ – $2.0x10^{1}$ m/d, T of $4.0x10^{3}$ – $4x10^{4}$ m^2/d and S of 0.006 – 0.2.

Straskraba *et al*. (1985) did not report total groundwater inflows, however, ex-pit pumping of 722 L/s and 500 L/s in the KUM and the DIMA pits were respectively reported. These could be assumed as minimum inflows due to the high hydraulics associated with the dolomitic units. The Lac D'Exhaure Sinkhole was determined to be a major recharge point for the area.

Table 2-2: Summary of hydraulic attributes determined in the DIMA area.

Aquifer	Rock Type	K (m/d)	T (m^2/d)	S	Yield (L/s)
Shallow	RAT	-	-	-	-
Deep	CMN	$7.0x10^{-1}$ – $2.0x10^{1}$	$4.0x10^{3}$ – $4.0x10^{4}$	0.006 – 0.2	-
	SD				

- Not provided

2.2.3 Konkola Cu-Co Mine (Zambia)

Mulenga (1991) and Straskraba *et al*. (2012) undertook hydrogeological studies to develop inflow predictions for the progression of the Konkola Underground Mine located on the northern portion of the Zambian Copperbelt. Mining in the area primarily focuses on three orebodies: the Kirilambombwe, Konkola and Fitolwa (Mulenga, 1991). The orebody in the area is hosted within the shale formation, sandwiched between the Footwall and Hangingwall formations, structured as a system of W – NW plunging folds forming part of the Kafue Anticline. The mine area is juxtaposed between the Lubengele and Luansobe faults in the north and south, respectively. The two faults form a conjugate shear set with lateral displacement. The fault houses the Kirilambombwe Anticline Axis and the Cross-Anticline Axis faults.

The Footwall Formation comprised siliceous rocks, predominantly quartzites, feldspathic sandstones and conglomerates, while the Hangingwall Formation comprised dolomites, limestones, dolomitic siltstones and shales (Mulenga, 1991). The rock units, structural architecture and inherent hydraulic attributes determined through discharge and pressure build-up tests define four aquifers in the mine area as follows (Table 2-3):

- **Footwall Quartzite Aquifer** – the lower most aquifer unit comprising Lower Porous Conglomerate and the lower part of the footwall quartzite. The Lower Porous Conglomerate limited water to its siliceous matrix and vugs, making permeability to be predominantly primary, with a K of $8.4x10^{0}$ m/d. The overlying footwall quartzite was extensively jointed and fissure controlled, making permeability to be secondary and the K to be relatively higher at $7.0x10^{0}$ – $1.8x10^{2}$ m/d;

- **Footwall Aquifer** – underlies the orebody, comprising the Porous Conglomerate, Footwall Sandstone and Footwall Conglomerate formations underlying the orebody. The formations had a bulk K of $9.0x10^0 – 1.6x10^2$ m/d. The conglomerates within this aquifer had similar hydraulic attributes as the one in the Footwall Quartzite Aquifer. The Footwall Aquifer unit had a highly porous and permeable matrix, promoting significant groundwater flow, with yields of 60 L/s. Fissured zones had yields up to 120 L/s;
- **Hangingwall Aquifer** – comprised Hangingwall Formation, gritty shale and Upper Roan Dolomites. The shale units had primary permeability, limiting groundwater storage and transport to within the matrix, unless intersected by structures, thereby promoting secondary permeability. The dolomitic units had predominantly secondary permeability and had a relatively high hydraulic connection due to dissolution features and faults, making them the highest yielding units within this aquifer. The bulk K of this unit ranged from $1.8x10^0$ to $2.6x10^2$ m/d. This unit promotes the greatest amount of inflows into the mine workings as it overlies the orebody; and
- **Kakontwe Limestone Aquifer** – overlies the Hangingwall aquifer and outcrops near the mine. Groundwater recharge occurs through this unit. This carbonate unit and its karst features had a relatively high K, expediting groundwater recharge from precipitation and the leaking Kakosa Stream and Lubengele River, together with its tributary, the Mingombe River.

Straskraba *et al*. (2012) constructed a finite-difference numerical model to simulate and predict inflows. From this study, maximum groundwater inflows of 4 630 L/s in 1987 were determined. The Inflows were projected to decrease with mine progression down to 1 620 L/s by 2017 due to decreased permeability with depth.

Table 2-3: Summary of hydraulic attributes determined at Konkola Mine.

Aquifer	Rock Type	K (m/d)	S	Yield (L/s)
Footwall Quartzite	Conglomerate	$8.0x10^0$	-	-
	Quartzite	$7.0x10^0 – 1.8x10^2$	-	-
Footwall	Conglomerate	$9.0x10^0 – 1.6x10^2$	-	60
	Sandstone			
	Footwall Conglomerate			
Hanging	Shale	$1.8x10^0 – 2.6x10^2$	-	-
	Dolomite		-	-
Kakontwe Limestone	Limestone	-	-	-
	Dolomite			

- Not provided

3 Methodology

3.1 Data Review

A review of surface water and groundwater related information from literature and as provided by SRK and MMG was undertaken throughout the course of this research to establish prevailing hydrogeological conditions at Kinsevere and its immediate surrounds. The review encompassed a thorough analysis of the following:

- Hydrological, geological and hydrogeological reports, published papers and maps;
- Case studies of operations in similar settings;
- Surface water and groundwater monitoring and management programmes;
- Lithological logs of boreholes drilled;
- Groundwater level monitoring data; and
- Hydraulic testing data.

3.2 Hydrocensus

A hydrocensus was conducted to verify water related information. Surface water bodies together with structures having water standing atop, within, and at the toe (as seepage) were considered in the assessment. These included the discharge channel, Kifumashi River, sediment ponds, WRDs, TSFs and ore stockpiles (OSs). A network of groundwater monitoring and dewatering boreholes was visited and reviewed, noting information pertaining to identifiers, use, location (area and coordinates), collar height (and elevation), depth drilled and water level. Boreholes earmarked for exploration, dewatering and monitoring drilling during the course of this research were included. A visit to the pits was undertaken, noting the extent of groundwater ingress and ex-pit management.

3.3 Drilling and Construction

3.3.1 Drilling Techniques

Kinsevere had ongoing resource exploration, monitoring and dewatering drilling programmes, on which this research piggybacked. The Diamond Core (DC) drilling technique was applied for drilling vertical dewatering pilot boreholes (3) for feasibility purposes to deduce whether the various rock units and geological structures intersected had sufficient hydraulic capacity to induce significant drawdown to the groundwater level should they be completed as dewatering boreholes. The boreholes were advanced down to depth using a Telescope-Down Approach (TDA), where drilling started at a large diameter and decreased with depth until end of the borehole. The DC drill bit was advanced by rotary action, cutting rock units intersected into core, which collected in the lifter tube and moved up the core barrel, then hoisted onto surface by wireline where it was washed, placed in core trays, lithologically logged and stored for future reference. This technique was ideal in that the core retrieved adequately represented conditions of the various rocks at specified depth. The three boreholes were drilled on the northern side of the Mashi Pit, between the Mashi and Central pit saddle and to the immediate south of the Kinsevere Hill Pit.

The Conventional-Crossover (CCRC) and Centre-Sample Return Circulation (CSRC) percussion drilling techniques were applied for drilling vertical exploration (8), monitoring (3), pilot (1) and dewatering (3) boreholes, following the TDA. Drilling advanced using a pneumatic reciprocating piston-driven hammer with a bit at the end, crushing and grinding the various rock units and structures intersected with depth into small chips.

Exploration drilling used the CCRC technique, whereby compressed air injected through the rods brought a mix of aerated water and drill chips to surface through the space between the borehole annulus and rods. Ejection pressures destabilized the borehole sidewalls, leading to collapse in unstable rocks. The eight exploration boreholes were drilled, using CCRC, on the eastern portion of the Kinsevere concession, in an area earmarked for the construction of a tailings storage facility (TSF3). Boreholes drilled for monitoring, pilot and dewatering purposes used the CSRC drilling technique, where the water/drill chip-mix was brought to surface through the rod inner tube, thereby limiting pressures to within the rods and keeping the boreholes open longer for casing installation.

The three monitoring boreholes were drilled around TSF3 and the one pilot dewatering borehole was drilled on the saddle between the Mashi and Central pits. Two dewatering boreholes were drilled on the saddle between the pits, while the third was drilled on the northern portion of the Mashi Pit. Groundwater strikes intersected during drilling using both CCRC and CSRC techniques were recorded, and the final airlift yield measured using a V-notch Weir. Drill chips ejected on surface were washed, logged, placed in chip trays and stored for future reference. See Figure 3-1 for photograph of CSRC drill rig setup and Figure 3-2 for schematic of drilling sample retrieval per technique applied.



Figure 3-1: Photograph of CSRC rig setup for drilling of a dewatering borehole on the saddle between the Mashi and Central pits saddle.

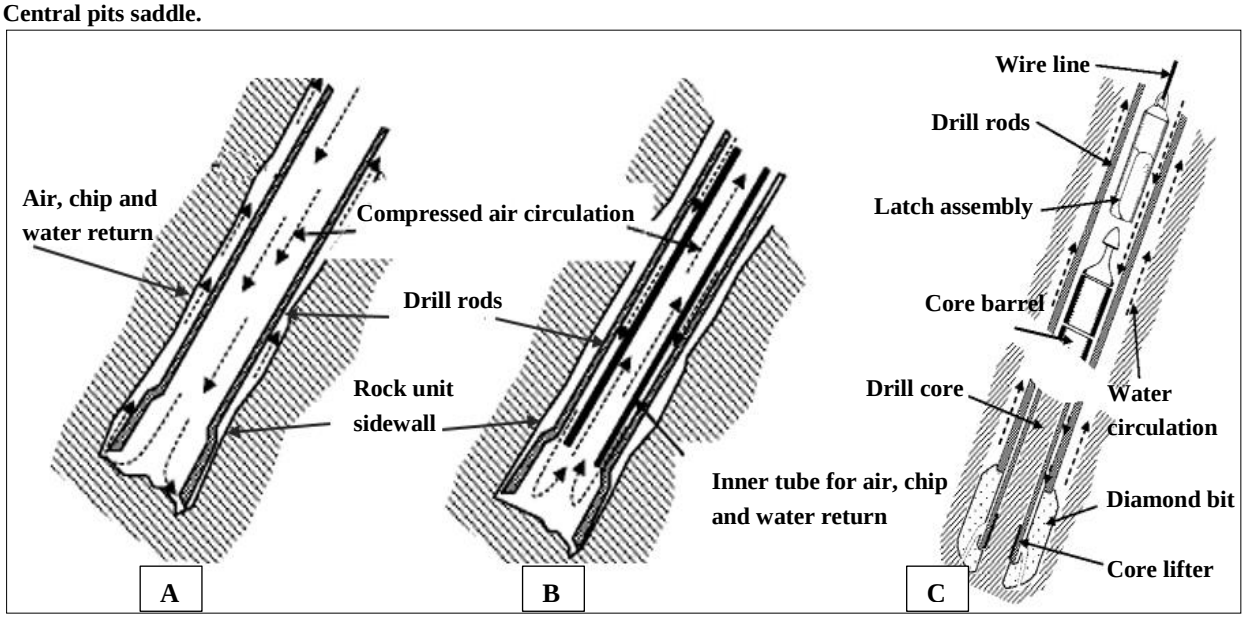


Figure 3-2: Schematic of CCRC (A), CSRC (B) and DC (C) drilling techniques (Source: Marjoribanks, 2010).

3.3.2 Construction

Dewatering Boreholes

Construction of dewatering boreholes followed the TDA approach similar to drilling, whereby the casing diameter decreased with depth from 60.96 cm to 40.64 cm. Solid steel casing was installed above the groundwater level while the perforated casing was installed below groundwater level to the bottom of the borehole. Casing was installed as drilling progressed. Silica gravel was poured down the borehole, between the casing and borehole annulus, filling the boreholes from the bottom to 2 m above the groundwater level. The gravel acts as filtration membrane, restricting fine ingress into the borehole.

The boreholes were developed until the water was clean and the gravel settled. A final airlift yield was determined by channelling the water ejected along a trench to a V-notch Weir where the flow was measured. A bentonite plug was installed above the silica gravel to restrict potential ingress of contaminants washed down through the unsaturated zone during rainy seasons. Drill cuttings were then used to backfill the section overlying the bentonite plug. A sanitary seal comprising a cement-bentonite mix was installed around the protruding casing and down to 1 m depth (constituting headworks) to restrict on-surface contaminant ingress. The protruding casing was fitted with a lockable cap for protection.

Monitoring Boreholes

Construction of monitoring boreholes entailed the installation of two types of casing, a slightly larger solid steel starter casing of 17.78 cm diameter and a smaller unplasticized polyvinyl chloride (uPVC) casing of 10.16 cm diameter. The solid steel starter casing was installed to restrict the borehole side walls at the top weathered sections from collapsing and for protection. Solid uPVC casing was installed above the groundwater level, while the perforated uPVC casing was installed from then down to end of borehole. Installation of uPVC casing only occurred after drilling down to the end of the borehole. Silica gravel was poured down the borehole between the borehole annulus and the uPVC casing. The boreholes headworks were then completed, and the airlift yield measured as outlined previously.

See Figure 3-3 for photographs of borehole drilling, development, airlift measurements, borehole headworks and generic borehole construction schematic.

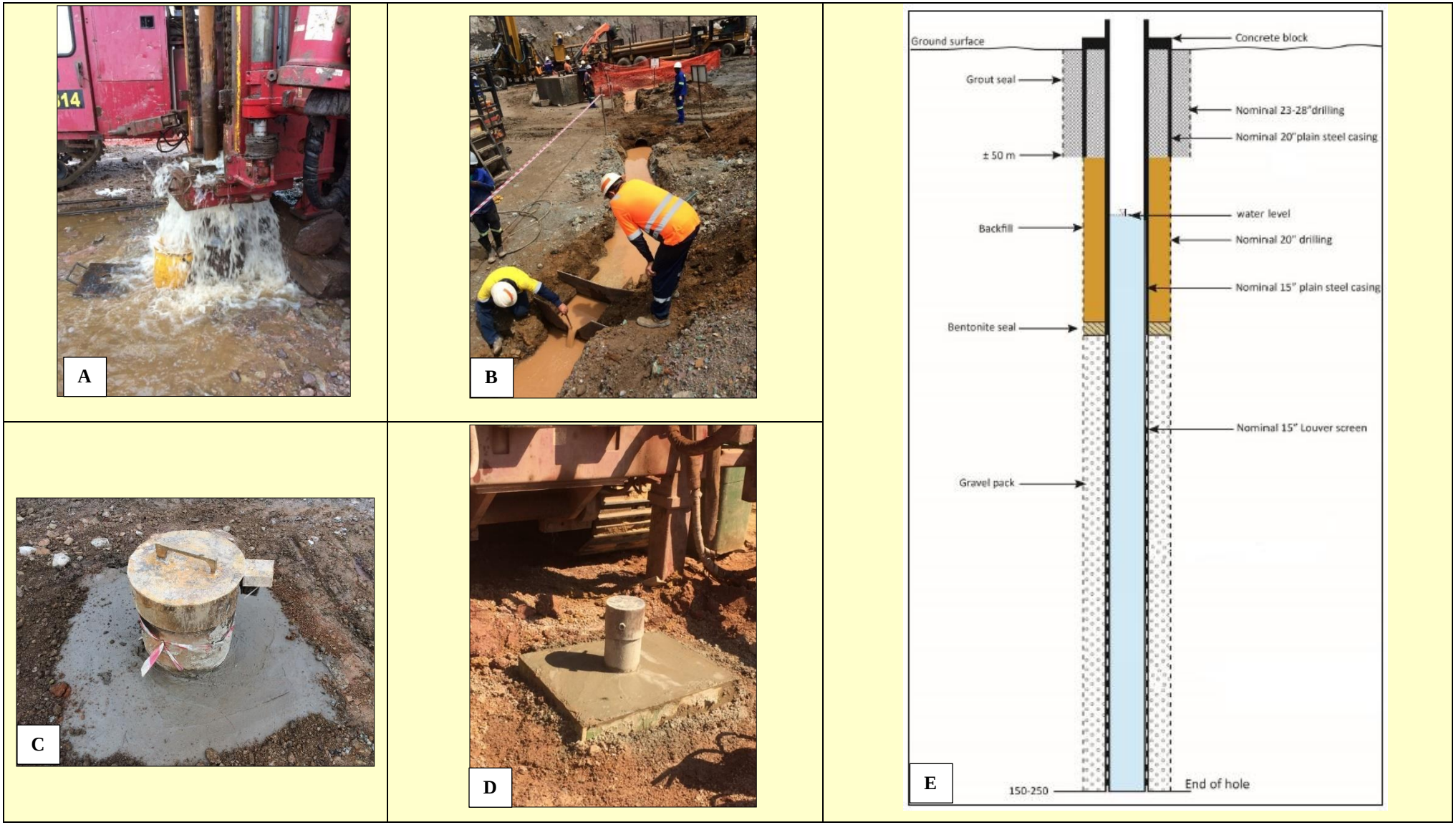


Figure 3-3: Photographs of borehole development (A), airlift yield measurement during drilling (B), borehole headworks (C&D) and generic DEW borehole construction (E- Source: SRK, 2016).

3.4 Hydraulic Testing

3.4.1 Pumping Test

A pumping test was undertaken in a decommissioned dewatering borehole drilled in 2010 by Anvil, located on the northeastern portion of the Mashi Pit to determine bulk hydraulic attributes and to deduce the feasibility of recommissioning it. Details pertaining to the log, borehole depth, water level, identification of two observation boreholes, water strikes intersected during drilling and the airlift yield were recorded and assessed prior to initiating the test. The test encompassed the use of a positive displacement pump connected to a pump head (driven by a diesel motor fitted with a gearbox, accelerator and clutch) by shafts, leading down the borehole, ensuring a constant water discharge throughout the test. The pump head was connected to a discharge line (lay-flat). The discharge rate was measured using a flow gauge fitted before the discharge line. An electronic water level depth sounder of 0.01 m accuracy was used to measure changes in the water level before, during and after pumping. See Figure 3-4 for pumping test schematic and rig photograph. The pumping test entailed the following:

- **Step Drawdown Test (SDT)** – carried out as an initial phase of the test, entailing pumping in steps of 60-minute interval, each with a higher constant discharge than the previous. The pumping rate and drawdown were measured at 1, 2, 3, 5, 7, 10, 15, 20, 25, 30, 40, 50 and 60-minute intervals. The residual drawdown measurements were undertaken immediately after termination of the final step, over the pumping duration;
- **Constant Drawdown Test (CDT)** – carried out over 48 hours, at a constant rate, with drawdown in the pumping and observation boreholes being measured during the test at 1, 2, 3, 5, 7, 10, 15, 20, 25, 30, 40, 50 and 60-minute intervals during the first hour, then at 30-minute intervals and ultimately at hourly intervals until termination of the test; and
- **Recovery Test (RT)** – carried out immediately after termination of the CDT test, where the residual drawdown in the pumped and observation boreholes were measured over the pumping duration or until a minimum 95% recovery was achieved.

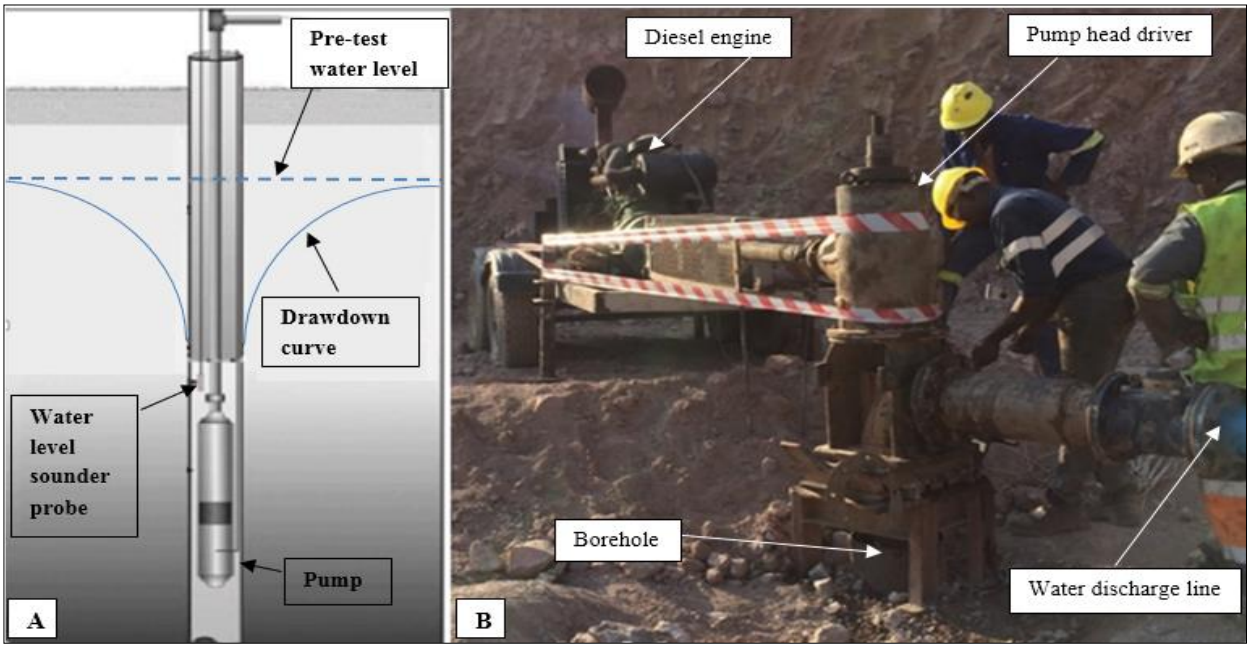


Figure 3-4: Schematic of pumping well dynamics (A, modified from Summa, 2010) and photograph of a positive displacement pumping test rig (B).

3.4.2 Airlift Tests

Three dewatering pilot boreholes were subjected to multiple airlift tests, where rock units and geological structures were tested in isolation at depth, to determine their respective hydraulic attributes. Isolation was achieved by pulling the DC rods to a specified depth, following a lithological assessment of the core retrieved. The tests were ideal in that small diameter boreholes intersecting highly conductive rock units and structures could be pumped at higher rates, inducing significant drawdown for measuring. The initial (pre-test) groundwater level was measured to determine submergence (equation 1), a proportion of an airline (HDPE pipe) under water, to deduce whether drawdown can be induced.

$$Submergence = \frac{\text{length of airline under water}}{\text{Total length of airline}} \times 100 \quad (1)$$

Once sufficient submergence (minimum 40%) was determined, the airline (fitted with a weighted foot piece) was lowered down the borehole through the core rods, with the top of the airline connected to a wellhead fastened to the core rods on surface. The bottom of the airline and foot piece were perforated to increase air distribution, thereby increasing surface area and reducing water density, creating enough lift force when compressed air was injected down the borehole via the airline. A water discharge line leading from the wellhead to a Baski Cutthroat Flume was connected, followed by connecting a pneumatic hose to a compressor leading to the wellhead and airline for air supply. See Figure 3-5 for airlift test setup. Testing encompassed a discharge of aerated water over an hour using compressed air injected down the borehole via the airline. Discharge measurements were undertaken at 3, 5, 7, 10, 15, 20, 25, 30, 35, 40, 50 and 60-minute intervals to ensure constant discharge using the flume. The compressor was shutoff and the air pressure bled off following the last discharge measurement. The residual drawdown was measured over the discharge duration.

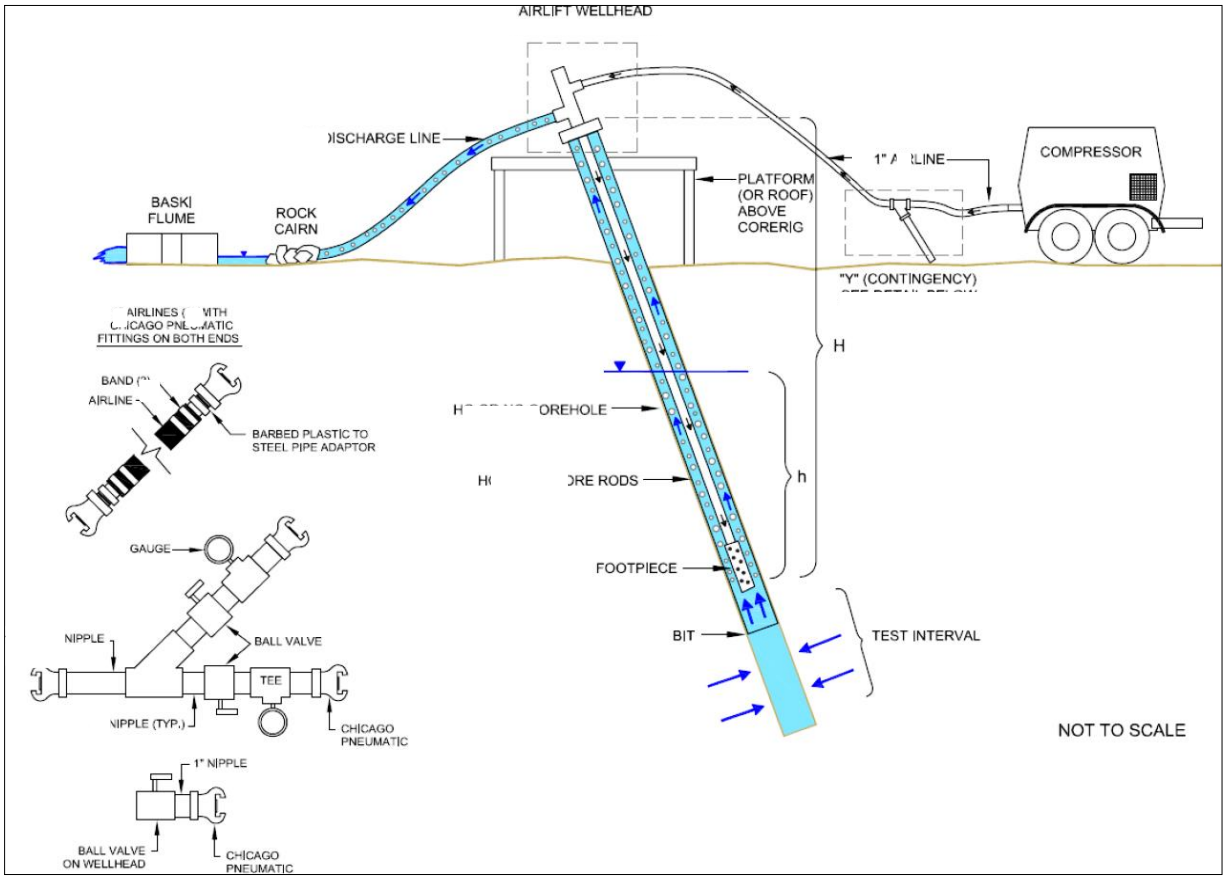


Figure 3-5: Generic setup of airlift test (Source: SRK, 2016).

3.4.3 Slug Tests

Slug tests were undertaken in eleven open exploration boreholes in the TSF3 area, encompassing an instantaneous displacement of the groundwater level within each borehole through adding a known volume of water via a discharge pipe from a water tanker, filling each borehole to the brim and measuring that time, from which the discharge rate was determined. The initial groundwater level, borehole radius, borehole depth, minimum volume of water to be injected down the borehole and saturated thickness were determined. The residual drawdown was measured at 1, 3, 5, 7, 10, 15, 20, 25, 30, 35, 40, 50 and 60-minute intervals or until the groundwater level reverted to its initial depth. Water was used to induce displacement in eight boreholes, while a 16 L slug was used to test the three boreholes. The slug piece was lowered down using a rope (slug line). Resultant water level displacement and residual drawdown were measured over the aforementioned intervals. See Figure 3-6 for schematic of slug tests.

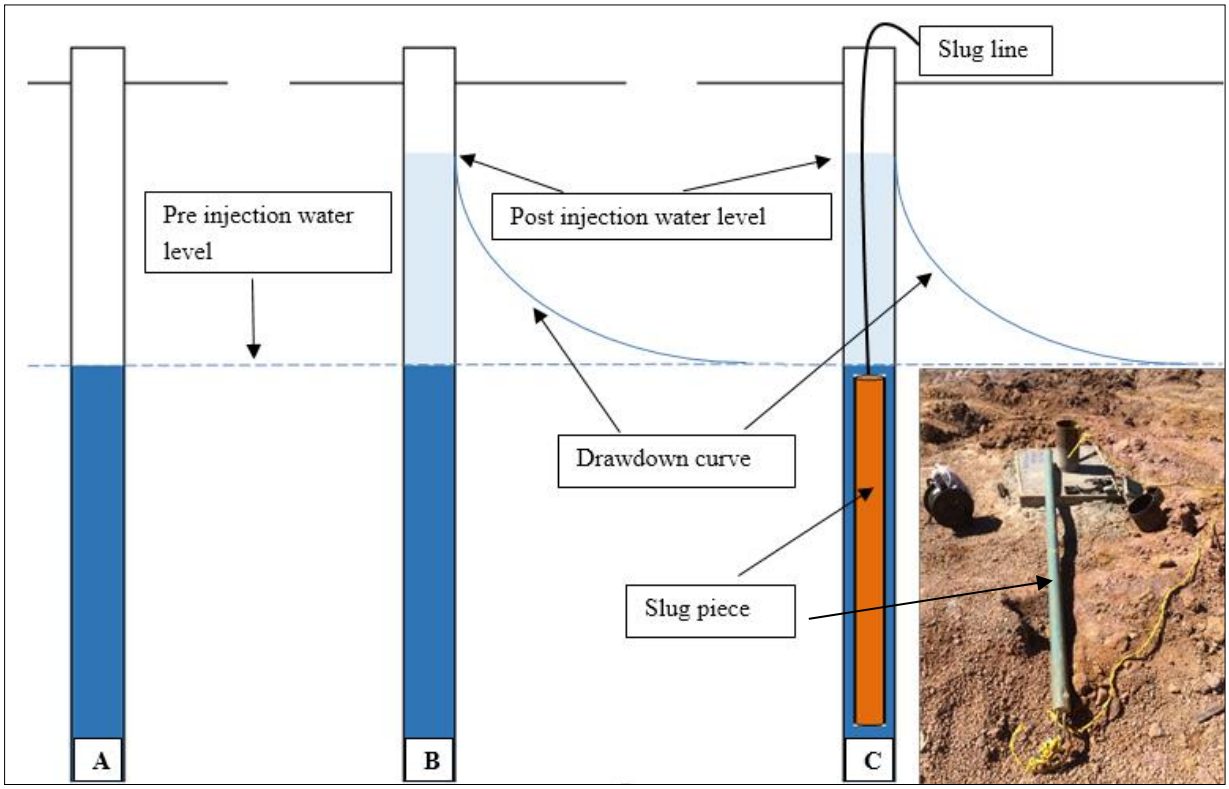


Figure 3-6: Slug test, pre-test (A), water injection type (B) and slug piece type (C, with photograph).

3.5 Hydraulic Test Data Analysis

3.5.1 Pumping Test Data Analysis

As an initial step, pumping test data analysis encompassed a review of the dewatering and observation borehole lithological logs, groundwater strikes, groundwater levels and drawdown data to verify confining and unsteady-state conditions induced by the siliceous and dolomitic rock units at depth as reported by SRK (2016). Specific analytical methods to be applied were deduced from this review. The groundwater levels (13 mbgl) in the boreholes sat above groundwater strikes intersected at depth (between 59 mbgl and 63 mbgl), suggesting confining conditions. Groundwater strikes were intersected within the siliceous and dolomitic rock unit matrix, fractures and dissolution features, suggesting double porosity. The drawdown of the groundwater levels in the three boreholes was not constant during pumping, suggesting unsteady state flow conditions.

Pumping test data were analysed using the latest version (2014) of the multi-optional Flow Characteristics (FC) Method excel-based program to determine bulk hydraulic attributes (van Tonder *et al.,* 2014). Determination of bulk T, K and S encompassed the following:

- **SDT Drawdown Data Analysis** – a scatter plot of Drawdown vs. Time was graphically analysed using an interactive line of best fit from the Non-linear FC Method. S and T were determined from the best fit, and then translated to K based on their $T = Kb$ relationship, where *b* is the saturated thickness;
- **CDT Drawdown Data Analysis** – diagnostic and derivative plots of Drawdown derivative vs. Time derivative were analysed to determine hydraulic boundaries, flow models, water bearing units and their respective depths. This method was ideal in that subtle drawdown variations are exaggerated (Bourdet *et al*., 1983, Bourdet *et al*., 1989; Renard *et al*., 2005, Renard *et al*., 2008); and
- **RT Data Analysis** – residual drawdown data provided a more accurate representation of the hydraulic capacity of rock units and geological structures tested as it did not succumb to the influence of fluctuation associated with pumping (Kruseman and de Ridder, 1994). Groundwater ingress into the borehole occurred without external influence. The Theis (1935) Recovery Method was identified as the appropriate method to use for confined and unsteady state conditions reported by SRK (2016) and confirmed through review of lithological logs, groundwater strikes, groundwater levels and drawdown data of the boreholes. The method (equation 2) was applied to determine T from the Residual drawdown vs. Time Scatter Plot produced. T was translated to K.

$$T = \frac{0.183Q}{\Delta s} \quad (2)$$

Where: T = transmissivity(m^2/d), Q = discharge (m^3/d) and Δs = drawdown change (m) per log cycle.

3.5.2 Airlift Test Data Analysis

Airlift test data collected from the three boreholes were analysed using the Theis (1935) Recovery Method to determine T from analysing the Residual drawdown data vs. Time Scatter Plot. T was translated to K based on the saturated thickness. The method was preferred as airlift tests induce significant stress beyond the borehole, resulting in a more representative response (Howell, n.d.). Unsteady-state and confined conditions induced by the siliceous and dolomitic rock units warranted the use of the Theis (1935) Recovery Method. Data from 22 additional boreholes tested previously by SRK was analysed and included in the airlift test dataset.

3.5.3 Slug Test Data Analysis

K and T were determined from slug test data analysed using the Bouwer-Rice (1976) Method (equation 3), an option found in Aquifer Test Pro (2015.1) software. The method was best suited as it accounted for the geometry of the borehole and may be applied in partially to fully penetrating and perforated or open boreholes, intersecting confined or unconfined conditions (Summers, 1983; Bouwer, 1989; Campbell *et al.*, 1990).

$$K = \frac{r_c^2 Ln(\frac{R_c}{r_w})}{2L_e} \frac{1}{t} Ln \frac{y_0}{y_t} \quad (3)$$

Where: r_c= casing radius (m), R_e= a dimensionless ration describing system geometry, r_w= screen radius (m), L_e=screen length (saturated) (m), y_0= difference between initial water level and water level after slug (m) and y_t= water level at time t (m)

3.6 Pore Pressure Assessment

Groundwater levels within six hydrogeological test boreholes (HTH- multilevel piezometers) installed in 2015, each fitted with three vibrating wire transducers (VWTs) targeting specific rock units were assessed to determine the influence of rainfall, groundwater inflows, hydraulic connectivity, dewatering and upward pressure contribution on pore pressures. Hydrostatic pressures were determined through converting the height of the groundwater levels above each VWT into pressure by dividing it by *10.197442889221* and reporting it in Megapascal (MPa).

3.7 Groundwater Recharge Determination

Calculation of the groundwater recharge in the Kinsevere pit area and surrounds was undetaken using th CMB method to validate historical estimates presented by KP (2007, 2010) and SRK (2016). The method was used due to its low cost and reasonable precision. It assumes steady state conditions between the chloride flux on surface and the chloride flux beneath the evapotranspiration and mixing zones (Eriksson and Khunakasem, 1969; Bredenkamp *et al.,* 1995; Beekman *et al.,* 1997; Beekman, 2000). Recharge is defined by equation 4 below:

$$R = P\frac{Cl_p^-}{Cl_{GW}^-} \quad (4)$$

Where: R= mean groundwater recharge in mm/yr, P = mean annual precipitation depth (mm/yr), Cl_p^- *= average chloride concentration in precipitation (mg/L) and* Cl_{GW}^- *= average chloride concentration in groundwater (mg/L)*

3.8 Inflow Determination- Steady State Analytical Solution

Groundwater ingress into the pits was estimated using the Dupuit-Forchheimer Analytical Method (McWhorter and Sunada, 1977) to verify inflows modelled by SRK (2018). The method was ideal in that it considers the influence of decreased saturated thickness near the pits, upward flow contribution and pit-lake conditions (Marinelli and Niccoli, 2000). The method divides the pits into two flow zones (Figure 3-7) to account for the aforementioned considerations, with each zone having an independent analytical solution.

The solution for Zone 1 assumed the following:

- The pit walls were cylindrical and intersected the rock units at a right angle;
- Lateral groundwater flow towards the pit was dominant and axially asymmetric;
- The static water level (pre-mining) was horizontal; and
- All recharge within the pit radius of influence was captured by the pit.

The following equation (5) applied to the aforementioned assumptions and conditions:

$$h_0 = \sqrt{h_p^2 + \frac{W}{K_{h1}}\left[r_0^2 \ln(\frac{r_0}{r_p}) - \frac{(r_0^2 - r_p^2)}{2}\right]} \quad (5)$$

Where: h_0*= pre-mining saturated thickness (m),* h_p*= mining saturated thickness (m), W= distributed recharge flux (m/d),* K_{h1}*= horizontal hydraulic conductivity of rock units intersected (m/d),* r_0*= radius of influence (m) and* r_c*= pit radius (m)*

The pit radius of influence (r_0) was determined through reiteration, as other parameters were known. From this, inflows (Q_1) into Zone 1 were determined by equation 6:

$$Q_1 = W\,\pi\,(r_0^2 - r_p^2) \quad (6)$$

The solution for Zone 2 assumed the following:

- Hydraulic head was initially uniform and equal to the pre-mining water level in Zone 1;
- The pit lake had a constant head, if completely dewatered, the head was equal to the pit floor elevation;
- Groundwater ingress was three-dimensional and axially symmetric; and
- Rock units and inherent hydraulic conductivities were anisotropic.

The following equation (7) applied to the aforementioned assumptions and conditions:

$$Q_2 = 4\, r_p \left(\frac{K_{h2}}{m_2}\right)(h_0 - d) \quad (7)$$

Where Q_2= inflows (m^3/d), r_p= pit radius (m), K_{h2}= horizontal hydraulic conductivity of rock units intersected, m_2= anisotropy parameter, h_0= pre-mining saturated thickness, d=depth of the pit lake.

The anisotropy parameter was determined by the following equation (8):

$$m_2 = \sqrt{\frac{K_{h2}}{K_{v2}}} \quad (8)$$

Where m_2= anisotropy parameter K_{h2}= horizontal hydraulic conductivity of rock units intersected, K_{v2}= Vertical hydraulic conductivity of rock units intersected

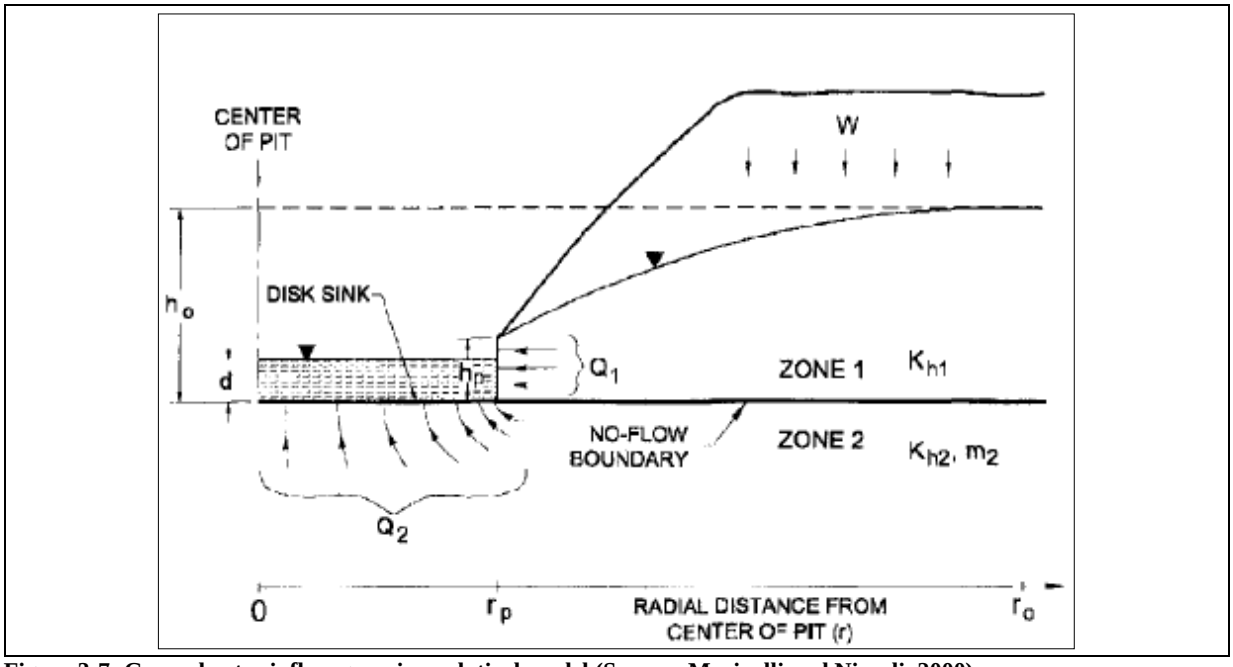


Figure 3-7: Groundwater inflow generic analytical model (Source: Marinelli and Niccoli, 2000).

3.9 Conceptual Hydrogeological Model

A conceptual model presenting a concise, coherent and quantitative description of hydrogeological and hydrological elements found at Kinsevere was collated. The model provided a fundamental understanding of how these elements interacted and how they were affected by changes in hydraulic stresses induced by precipitation, mining and dewatering. Hydrogeological elements included rock units, faults, fractures, dissolution features, hydrostratigraphy, groundwater levels, boreholes acting as conduits to flow and hydraulic attributes of rock units. Water flowing in and out of the system as rainfall, runoff, recharge, evaporation and groundwater discharge was accounted for and presented. Conceptualization of the Kinsevere concession area further presented details of the confining conditions, aquifer types, groundwater strikes and levels as per findings outlined in Sections 4 to 6.

4 Study Site

4.1 Climate

Regionally, the DRC climate is defined by atmospheric conditions associated with the seasonally mobile Inter Tropical Convergence Zone (ITCZ) across the equator. Trade winds of varying temperatures and pressures from the Northern and Southern hemispheres collide, giving rise to high clouds, frequent thunderstorms and heavy convective rainfall. The radiation balance values of the DRC surface were relatively high throughout the year due to the equator transecting across the country, resulting in seasonal differences on either side (Bohlweki, 2007)

The Kinsevere mine area is located 11° south of the equator, experiencing a mean annual precipitation (MAP) of 1 084 mm/yr (Kinsevere weather station data, 2011 – 2018). Precipitation data plotted on a hyetograph revealed unimodal distribution, with most rainfall occurring between months of November and March, indicative of a humid subtropical climate (Figure 4-1). The rainy season was dominated by monsoon effect, induced by temperature variations between the ocean and continent. High pressures from the South Atlantic, resulting in higher showers and thunderstorms, supplemented humid air flowing to the west. Dry months occurred during the migration of the anticyclone towards the equator, conveying dry and warm air from the southeast, leading to the end of the rainy season (Bohlweki, 2007).

The mean annual evaporation (MAE) at Kinsevere was 1 017 mm/yr, exceeding precipitation during dry months with the converse being true for rainy season. Kinsevere experienced SSE trending winds throughout the year, with an average speed of 2.5 m/s, and wind gusts recorded as high as 78.9 m/s during the rainy seasons (KP, 2007; KP, 2012). Average minimum temperatures across Kinsevere ranged between 11°C and 18°C in July and October months, respectively. Average maximum temperatures ranged between 26°C and 32°C during the aforementioned months (Kinsevere weather station).

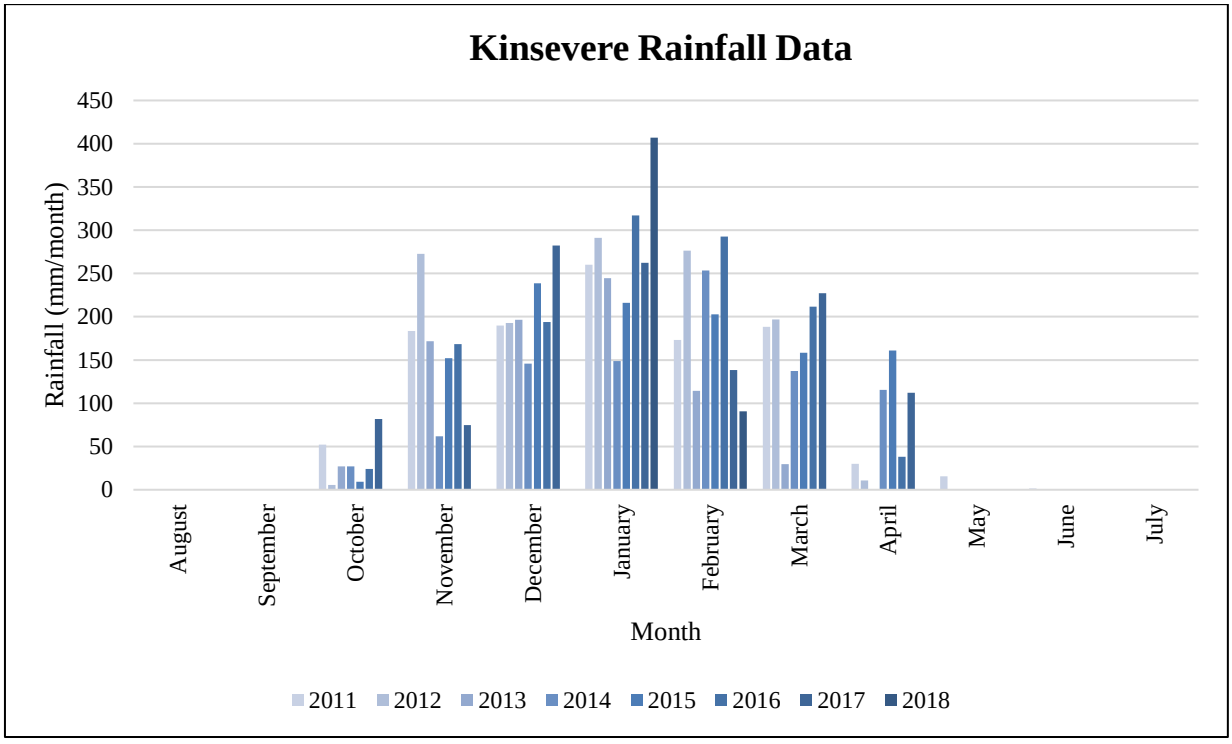


Figure 4-1: Hyetograph showing rainfall distribution from January 2011 to February 2018 (Source: Kinsevere weather station).

4.2 Topography and Surface Water

Regionally, Kinsevere sits on the Luiswhishi River Basin, within a watershed of a gently sloping plateau, incised by the Luapula River (and its tributaries), flowing north to form a confluence with the Congo River via Lake Moero, together with the Luvua and Lualaba rivers. The plateau has elevations ranging between 1 150 and 1 300 mamsl (KP, 2007). Kinsevere mine infrastructure define the concession topography, which was otherwise characterised by gently rolling and slightly undulating features, sloping north towards the WSW – ENE flowing Kifumashi River, a first order perennial tributary of the Luapula River, characterised by a low gradient (2%) and an extensive sedge dominated by a 300 m wide Dambo marshland (Nepid, 2006; KP, 2009). Elevations across Kinsevere range between 1 180 and 1 291 mamsl, with topographic highs in the south and the lows in the north.

4.3 Geology

4.3.1 Depositional Setting and Regional Stratigraphy

Kinsevere mines the basal Neoproterozoic sedimentary rocks of the Katangan Supergroup occurring as fragments within the northern portion of the cupriferous Lufilian Arc (referred to as the Central African Copperbelt, CACB), a *c*.800 km long SE – NW trending orogenic belt (Figure 4-2). The arc is generally characterised by north-verging convex structures, shear zones, folded and thrusted terranes juxtaposed between the Congo and Kalahari cratons. It straddles along the border between the DRC (south) and the Republic of Zambia (north) (Unrug, 1983; Cahens *et al*., 1984; Kampunzu and Cailteux, 1999; Porada and Berhorst, 2000; Cailteux *et al*., 2005; Batumike *et al*., 2006).

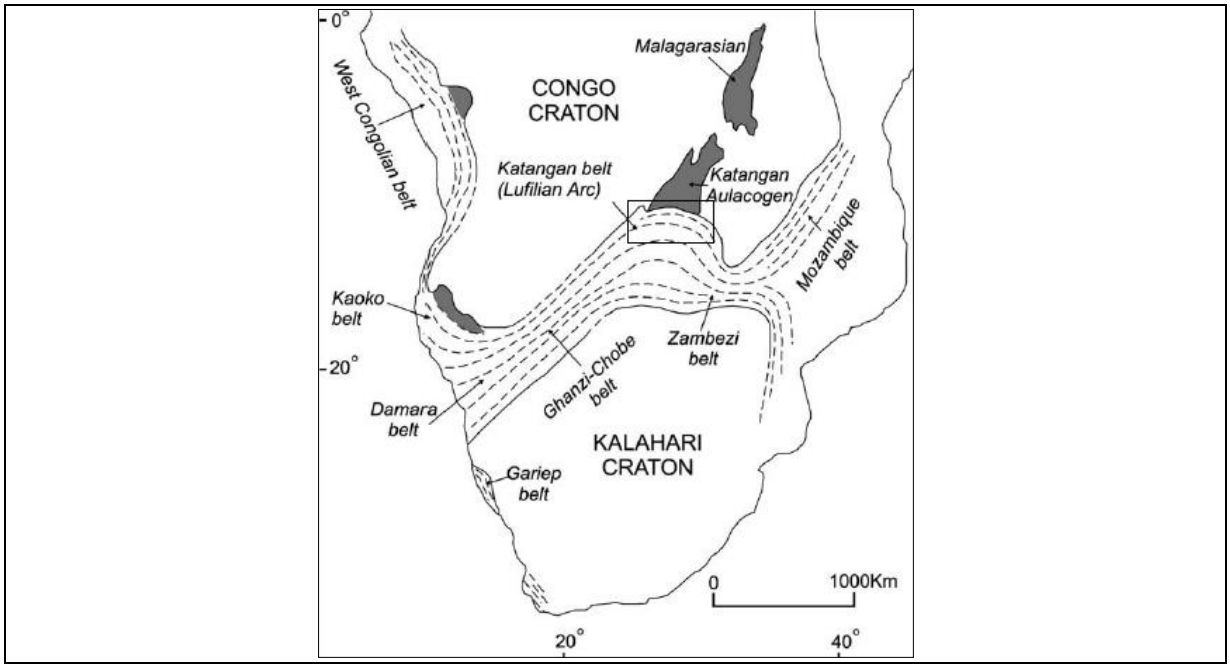


Figure 4-2 Location of the Lufilian Arc in relation to the Kalahari and Congo cratons and other belts (Source: Kampunzu and Cailteux, 1999).

The Katangan Supergroup comprises a succession of 5 – 10 km thick mixed carbonate and siliceous rocks, deposited 880 – 460 Ma onto the Kibaran Supergroup basement rocks through a Wilson Cycle, whereby the Congo Craton rifted from the Rodinian Supercontinent towards the end of the Kibaran Orogeny 1 300 – 1 000 Ma. The craton was later integrated into the Gondwana Supercontinent during the Lufilian Orogeny (Buffard, 1988; Unrug, 1988; Okitaudji, 1989; Cailteux *et al*., 1994; Porada and Berhost, 2000; Kampunzu *et al.*, 2000; Bumby and Giraud, 2005; Master *et al*., 2005; Armstrong *et al*., 2005).

The Katanga Supergroup is divided into the Roan (R), Nguba (Ng) and Kundelungu (Ku) groups (in ascending order), separated by two marker diamictite units, the Grand Conglome´rat (above R) and the Petit Conglome´rat (above Ng), related to two Cyrogenian glacial events, the Sturtian (750 – 700 Ma) and Marinoan-Varangian (650 – 635 Ma) glacial events, respectively (Zeintek *et al*., 2010). The Roan sediments were deposited in an intra-continental rift basin that evolved to a proto-oceanic rift basin, whereas the Nguba Group sediments were deposited in a relatively wider basin and those of the Kundelungu Group represent the compressional foreland basin settings (Buffard, 1988; Kampunzu *et al*., 1991; Cailteux *et al*., 1994; Batumike *et al*., 2002; Bull *et al*., 2010). See Figure 4-3 for Katangan stratigraphy. The following paragraphs only emphasize units found within the Kinsevere concession.

Roan Group (R)

The group predominantly comprises carbonaceous sediments, divided into the four subgroups, ascending from the Roches Argilo-Talqueuses (RAT, R.1), Mines Series (R.2), Dipeta (R.3) to Mwashya (R.4), and occurring as variable sedimentary facies due to structural discontinuities and influence (Wendorff, 2005).

- **RAT Subgroup (R.1)** – forms the base of the group with a thickness of 230 m, comprising a sequence of red and grey, massive to irregularly bedded siliceous terrigenous rocks truncated against breccia. The red coloured RAT occupies the lower part of this subgroup, with the colour stemming from the presence of hematite in the form of authigenic plates, staining authigenic dolomites, tourmaline and quartz. The grey colour stems from a chloritic-dolomite cement increasing towards the top of the subgroup. Differences in colour stem from variable redox, petrographic and geochemical conditions associated with the evolution of the depositional environment (Moine *et al*., 1986; Cailteux, 1994; Zientek *et al*., 2010).
- **Mine Series Subgroup (R.2)** – unconformably overlies the Grey RAT unit, has a thickness of 370 m, occurring as the most ore bearing subgroup, and is divided into the Musonoi, Long, Kilamusembu, Kalumbwe and Menda facies based on a variable combination of the following carbonate formations in places, in ascending order (Francois, 1974; Cailteux, 1994; Zientek *et al*., 2010):
    - **Kamoto Dolomites (R.2.1)** – ore bearing and comprises stratified (D Strat, Dolomites Stratifiées), siliceous and laminated (RSF, Roches Siliceuses Feuilletées), and massive and stromatolitic (RSC, Roches Siliceuses Cellulaires) units, in ascending order. The D Strat unit marks a major marine transgression and inherent lithological change, containing finely bedded impure and silicified dolomites with characteristic clasts and nodules. The RSF unit is lithologically similar to the D Strat unit, with the exception of having thinner beds of algal origin, minimal nodules and progressive increase in silicification intensity up the unit. The RSC unit comprises clasts, minor interbeds and non-silicified siltstone;
    - **Dolomitic Shale (SD, "Shales Dolomitiques", R.2.2)** – ore bearing, characterised by fine-grained siltstone and laminated dolomite with carbonaceous shale; and
    - **Kambove Dolomite (CMN, "Calcaire à Minerais Noir", R2.3**) – characterised by finely laminated dark dolomite enriched by organic matter and "clean" interbedded chloritic-dolomitic siltstone.

- **Dipeta Subgroup (R.3)** – overlies the Mines Series Subgroup, has a thickness of 600 m and comprises the following four units, each with variable proportions of siltstone and dolomite in ascending order (Cailteux, 1994; Zeintek *et al*., 2010):
    - **RGS ("Roches Greso-Schisteuses", R.3.1)** – characterised by argillaceous dolomitic siltstone;
    - **Argillaceous dolomitic siltstone** interbedded with sandstone or white dolomite and intrusive Gabbro **(R.3.2)**;
    - **Mofya Formation (R3.3)** – comprises dolomites, arenitic dolomite and dolomitic siltstone; and
    - **Kansuki Formation (R3.4)** – comprised dolomite with volcanolastic beds.
- **Mwashya Subgroup (R.4**) – unconformably overlies the Dipeta Subgroup of 520 m thickness, and is divided into the following three formations, in ascending order (Cailteux, 1994; Cailteux *et al*., 2007):
    - **Kamoya Formation (R4.1**) – characterised by dolomitic, silty shale, siltstone and sandstone;
    - **Kafubu Formation (R4.2)** – characterised by finely bedded and slightly dolomitic shale; and
    - **Kanzadi Formation (R4.3)** – characterised by interchanging feldspathic sandstone and black shale or siltite.
- **Roan Breccia** – characterised by angular and slightly rounded clast zones of 1 – 10 km sizes (termed as megaclasts), hosting fragments of the RAT and Mines Series sediments, within a chloritic dolomitic talcose siltstone matrix of grey or lilac colour. It occurs along detachment zones of anticlines, synclines, overthrusted klippen, discordant diapiric intrusions and oblique strike slip zones (Binda and Porada, 1995; Jackson *et al*., 2003; Kazadi, 2012).

Nguba Group (Ng)

The Nguba Group has a thickness range of 1 to 3 km, comprising mixed dolomitic shale and siliceous rocks with minimal carbonates. It is divided into the **Muombe (Ng.1, Formerly known as Likasi) and Bunkeya (Ng.2)** subgroups. The Muombe is marked by the Grand Conglome´rat at the base, overlain by silty shale to calcareous dolomite formations of the Kaponda, Kakontwe and Kipushi formations (from bottom to top), displaying regional facies change from clastic to carbonate rocks. The Bunkeya Subgroup comprises clastic and dolomitic rocks, characterised by an abundance of mafic igneous rock grains (Francois, 1974; Cailteux, 1994; Batumike *et al*., 2007; Zientek *et al*., 2010).

Kundelungu Group (Ku)

The Kundelungu Group is 300 m thick, comprising argillaceous to sandy clastics and diamictites, divided into the **Gombela (Ku.1), Ngule (Ku.2) and Biano (Ku.3)** subgroups, in ascending order. The Gombela Subgroup is marked by the Petit Conglome´rat diamictite (at the base), which overlies the Nguba Group with an erosional unconformity, and is overlaid and capped by the Lusele Formation Dolomites, having a shale and sandstone component. Deposition of the conglomerate occurred through glaciation, during which, the underlying Nguba and Roan clastics were dragged and striated. The occurrence of the clastics give record of exhumation of the aforementioned groups during the Lufilian Orogeny.

The Ngule Subgroup (Ku.2) comprises, from bottom to top, the Mongwe (Ku.2.1), Kiubo (Ku.2.2) and Sampwe (Ku.2.3) formations. The Mongwe and Kiubo Formations were folded and deposited in a shallow foreland basin that developed to the north of the Lufilian Arc. The Sampwe Formation was deposited in the northernmost portion of the foreland basin. It was undeformed, unmetamorphosed and sub horizontal. (Kampunzu and Cailteux, 1999; Wendorff, 2003; Batumike *et al*., 2007).

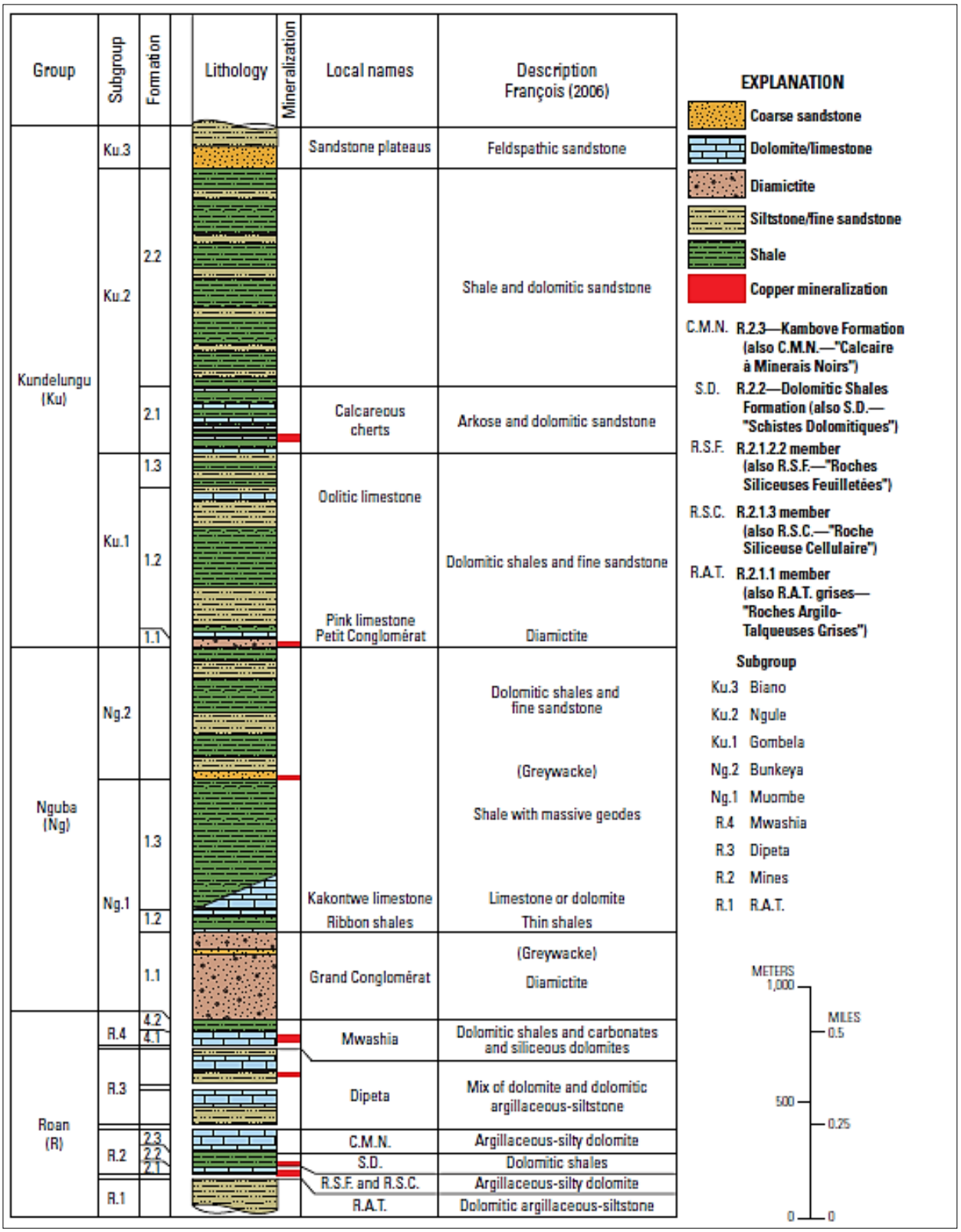


Figure 4-3 Katanga Supergroup stratigraphy in the DRC (Source: Francois, 2006).

4.3.2 Lithostratigraphy

Kinsevere mines the Menda Facies of the Mines Series Subgroup, characterised by the absence of the RSC unit and the presence of three graphitic beds within the SD unit (Francois, 1973; Kazadi, 2012). McMaster *et al.* (2016) refined the Kinsevere stratigraphy based on lithological attributes observed in each rock unit to remove geological bias in logging and to improve identification of marker horizons. Kinsevere geology holistically comprises the RAT (RSL and RBX), SD (inclusive of RSF and DStrat) and CMN units of the Roan Group, together with unclassified shale and siltstone units of the Kundelungu Group (Figure 4-4).

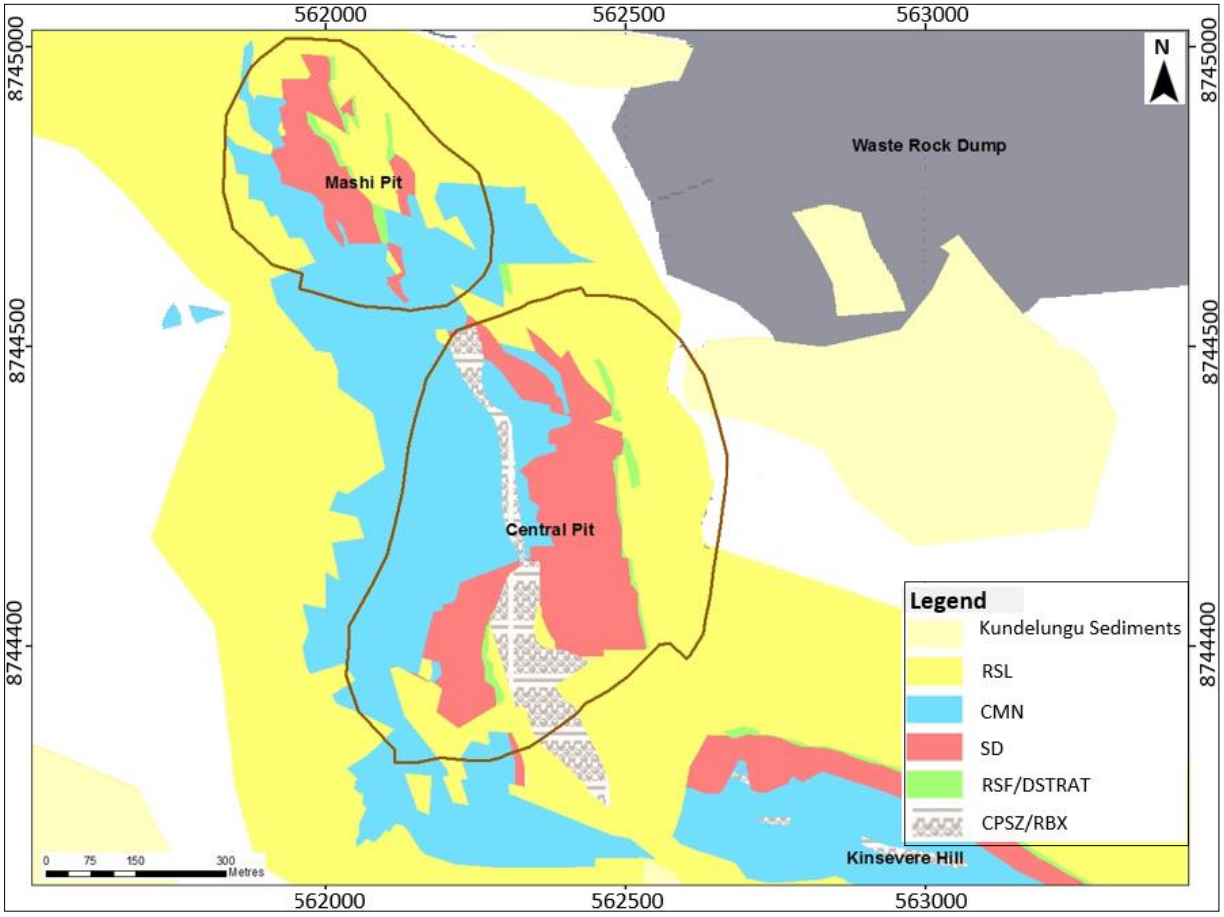


Figure 4-4: The Kinsevere geological map (Source: SRK, 2018).

Roches Argilo-Talqueuses (RAT)

McMaster *et al*. (2016) divided the RAT into RAT Siltstone (RSL – correlates with Red RAT on Katangan nomenclature) and the RAT Breccia (RBX- correlates with the Grey RAT and brecciated polymictic Roan Breccia) units. The RSL occurs as oxidized, bleached and massive siltstone comprising variable amounts of hematite, minor chlorite and talc, predominantly occupying the eastern portions of the pits (Figure 4-5). The RBX unit occurs as polymictic breccia comprising a siltstone and carbonate mix of variable clast sizes, occupying the fault and contact zones of the CMN, RSL and SD units, acting as preferential fluid pathways and weathering zones, found in the centre of the Central and Kinsevere Hill pits and bordering parts of the eastern and western portions of the Mashi Pit.

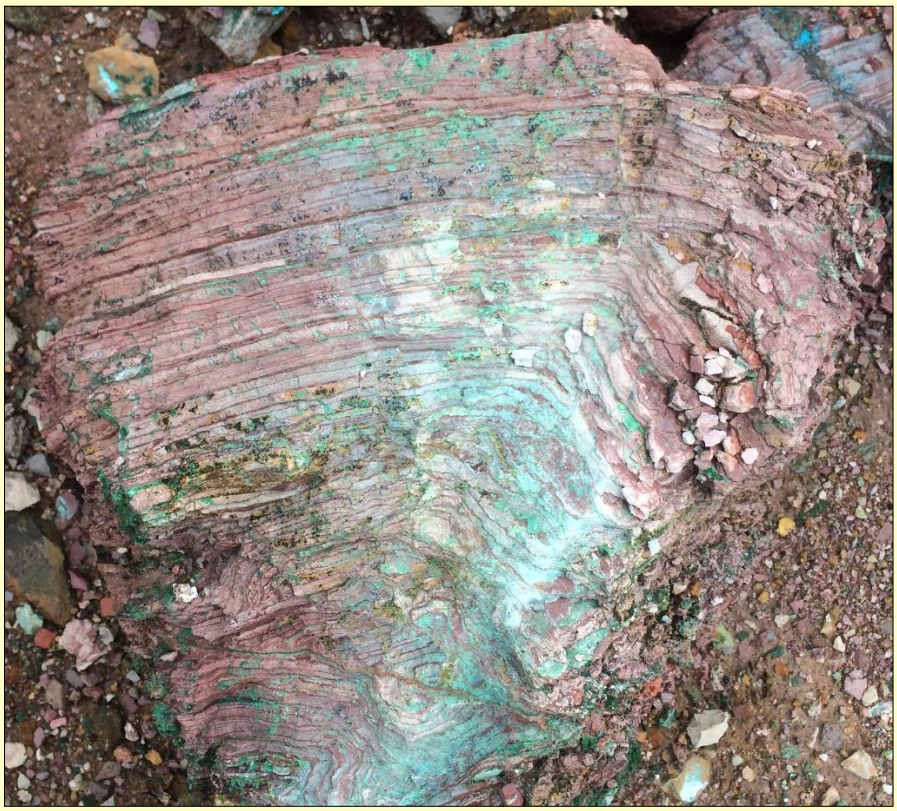


Figure 4-5: Field appearance of the RSL unit.

Shales Dolomitiques (SD)

The unit is 40 – 70m thick, characterised by fine laminations of pyrite parallel to bedding, limiting oxidation to within the beds, reduced and organic rich shales marking zones of localised deformation, containing muscovite-bearing clays (Figure 4-6). Alteration of magnesite occurred throughout the unit but was more pronounced at its base and at the contacts with the overlying CMN unit, having shales occurring as thin beds of less than 5 m thickness. It occupies the central and eastern portions of the pits. It is divided into two lithostratigraphic packages and their respective sub-units (McMaster *et al.,* 2016):

- **Lower Shale (LSH) Unit** – characterised by laminated, fine carbonaceous shale hosting coarse aggregates of chalcopyrite and carrolite within thick (10 – 20 cm) equigranular carbonate-quartz veins. It is divided into the following sub-units:
    - **Lower Nodular Unit (LNU)** – correlates to the D Strat unit on Katangan nomenclature. It constitutes the base of the LSH unit, characterised by discrete 1 – 2 cm ellipsoidal concretions;
    - **Grey Banded Shale Unit (GBS)** – overlies the LNU and is characterised by rhythmically bedded siltstone and shale units, correlates with the RSF unit on Katangan nomenclature; and
    - **Middle Nodular Zone Unit (MNZ)** – occupies the top of the LNU and is characterised by elongate, sigmoidal poly-crystalline carbonate nodules that were replaced by pyrite and chalcopyrite.
- **Interbedded Calcareous Siltstone and Shale (ICSL) Unit** – marks the gradational transition into the overlying CMN unit and is characterised by grey dolomitic siltstone interbedded with carbonaceous shale. High-grade copper mineralisation in the form of fine-grained stratiform disseminations is dominant in the carbonaceous shale interbeds than the dolomitic siltstone.



Figure 4-6: Field appearance of the SD unit.

Calcaire à Minerais Noir (CMN)

The unit predominantly occurs on the western portion of the pits, characterised by grey, dolomitised and magnesitic carbonate and siltstone of variable organic matter (Figure 4-7). It is divided into the following lithostratigraphic packages and their respective sub-units (McMaster *et al.*, 2016):

- **Lower CMN Unit** – hosts primary sulphide mineralisation in the form of veins, grains and pore fill material, characterised by extensive vein density, decreasing up the unit. Oxidation weathering and alteration caused increased pore spaces (micron scale), vugs (mm to cm scale) and cavities (cm to m scale). It is divided into the following sub-units:
    - **Lower Intercalated Dolomite and Shale Unit (IDSH)** – characterised by nodules of irregular shape filled with sulphides, comprising intercalated recrystallized carbonates of wavy lamination with carbonaceous shales. The contact between this unit and the underlying ICSL (SD) had underlying localised deformation from faulting and shearing; and
    - **Laminated Magnesitic Unit (LMU)** – characterised by crystalline dolomitic-magnesite altered carbonates with wavy carbonaceous laminations, with copper mineralisation occurring as vein and void fill.
- **Upper CMN Unit** – characterised by thick pale pink dolomites and grey-green siltstone (GSL) with silicified nodules (SDOL) in places. This unit has less organic matter, relative to the Lower CMN Unit. It comprises weak hypogene mineralisation. It is more predominant in the western portion of the Central Pit Shear Zone (CPSZ).

The undifferentiated sedimentary rocks of the Kundelungu Group predominantly occur on the eastern portions of the concession surrounds, respectively, comprising siltstone and shale. Saprolite and saprock units represent the variably weathered derivatives of the parent rocks. They retain the lithological fabric of all aforementioned units and are predominant across Kinsevere, having a thickness of up to 130 m in places. See Figure 4-8 for Kinsevere stratigraphy as divided by McMaster *et al*. (2016).



Figure 4-7: Field appearance of the CMN unit.

Schematic Kinsevere Strat Column	Domain code and name	Marker name + Code		Description	Katangan Correlates
	SDOL Interbedded silcified dolomite and green siltstone	Green Siltstone Silicified Dolomite	GSL SLD	Cream white to grey dolomites with dark silified bands/nodules, interbedded with green massive siltstones. Lower contact often structurally controlled. Strain partitioning between SDOL and LMU Often contains entrained HBX (heterogeneous breccia zones).	Kambove Dolomite (R2.3) Upper CMN
Structurally influenced	LMU Laminated Dolomite and Magnesite			Crinkly laminated, often coarsely re-crystalised and magnesite altered carbonate (likely after dolomite). Crystalline texture defined by cm scale magnesite/dolomite crystals with no apparent defined orientation. Carbonaceous laminae throughout.	Kambove Dolomite (R2.3) Lower CMN
	IDSH Interbedded dolomite and shale	Upper Nodular	UNZ	Interbedded laminated dolomite and shale. Dolomites can be intensely magnesite altered. Especially in Central pit. Gradational unit into upper laminated dolomite unit. UNZ - Upper Nodular Zone defines the lower contact of this unit. Comprised of elongate and irregular carbonate concretions/psedomorphs within a carbonaceous siltstone/shale.	
	ICSL Calcareous Siltstone with Shale			Interbedded calcareous siltstone and shale. Siltstone often dolomitic with weak primary minerlisation Shale interbeds often display strong veining with primary copper minerlisation - mostly as chalcopyrite This unit can be quite thick throughout the Mashi region	Shales Dolomit-iques R2.2 (SD)
Structurally influenced	LSH Lower Shale Package	Middle Nodular Grey Banded Shale Lower Nodular	MNZ GBS LNU	Shale dominated package; carbonaceous and variably magnesite altered. MNZ - S0 parallel, sheared carbonate pseudomorphs after evaporites. Frequently selectively replaced by Cu sulphides. GBS - Rythmic, evenly space bands of alternating shale and calcareous siltstone. LNU - Black shale with round circular, to ellipsoid shaped concretions (correlate; D-Strat) Lower contact with RSL often tectonic with abundant veining and mineralisation	D.Strat
	RSL Footwall Siltstone			Purple/red, ferruginous massive siltstone and/or green, sericitic massive silstone Both units can either be interbedded or gradational and contain; Ferroan dolomite veins, specular hematite, chalcocite near the upper contact with the LSH, mg-chlorite and talc	R.A.T R1
	RBX Footwall Breccia			Polymict heterogeneous breccia. Disseminated specular hematite	

Figure 4-8 Stratigraphy of Kinsevere geology as classified by McMaster *et al.* (2016).

4.3.3 Structural Evolution and Architecture

The structural architecture and evolution of the Lufilian Arc occurred through three major deformational phases (Francois,n1973; Unrug, 1983; Cahen *et al.,* 1984; Cailteux, 1994; Kampunzu and Cailteux, 1999; Batumike *et al*., 2007; Bull *et al*., 2010; Johnson, 2014):

- **Kolwezian Phase (D1)** – compressional event representing the initial integration phase of the Congo Craton into the Gondwana Supercontinent, occurring 800 – 710 Ma, peaking at 790 – 750 Ma, resulted in folds, faults and thrust sheets with a general northward transport direction forming duplexes comprising preserved Katangan stratigraphy within. The thrust sheets were associated with breccias transecting the Roan Group at sub-vertical angels. Folds related to the D1 phase are characterised by SE – NW strike with NE dip, SW – NE strike with NW dip, and E – W strike with S and N dip;
- **Monwezian Phase (D2)** – compressional event occurring 690 – 540 Ma, characterized by several E – W sinistral strikes-slip faults, which were sequentially activated, leading to the re-orientation of D1 structures clockwise and the development of the convex nature of the Lufilian Arc. Southward dipping fault plans obliquely cut across the D1 fold axes; and
- The **Chilatembo Phase (D3)** – spanning 530 – 507 Ma and characterised by upright fold structures which transverse the Lufilian Arc trend in the SW – NE direction, together with faults of S – N and E – W trend.

Kazadi (2012) developed a kinetic model to explain the structural complexities observed in the Kinsevere concession, from which it was deduced that the area comprised a thrusted and refolded syncline with steeply dipping dismembered limbs, with the Tshifufiamashi, Kinsevere Hill and Kilongo fragments constituting the western limb while the Tshifufia Fragment represents the east-dipping limb of the synformal anticline. Small scale folds within the western limb dip SW suggestive of the D1 event, whereas the NW dip in the eastern limb occurring between two sinistral strike-slip faults was indicative of the D1 event and its clockwise rotation induced by the D2 event.

The D2 event was accompanied by a fracture system of SW – NE and SE – NW orientation and occasionally, E – W and S – N, associated with the SE – NW and SE – NE oriented conjugate strike-slip faults, possibly related to early D3 deformation. The D3 event was characterised by SW – NE and SE – NW oriented normal faults. The D1 and D2 fractures had characteristic mineralisation while those of the D3 had none. The fragments were bisected by N – S shear zone. See Figure 4-9 for the structural architecture of Kinsevere as modelled by Kazadi (2012).

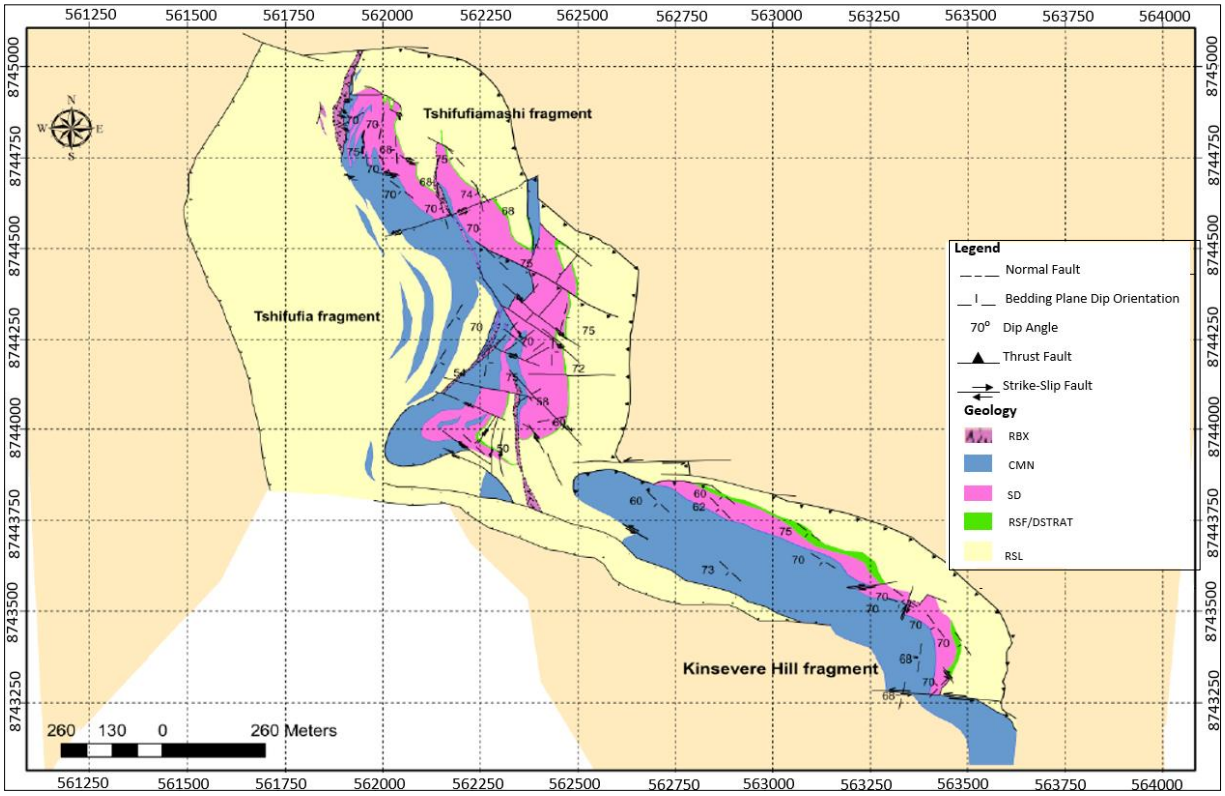


Figure 4-9: The Kinsevere structural architecture (Source: Kazadi, 2012).

4.4 Hydrogeology

4.4.1 Groundwater Recharge

Groundwater recharge calculated using the Chloride Mass Balance Method (CMB) was determined to be 27% of MAP (293 mm/yr) in the pit area, while the concession surrounds received 8% of MAP (90 mm/yr) (KP, 2007; KP, 2010; SRK, 2016). The high groundwater recharge in the pit area was predominately attributed to exposed fractures and dissolution features of high hydraulic capacity, while that of the concession surrounds was attributed to the relatively low permeability of the weathered zones.

4.4.2 Groundwater Flow and Levels and Strikes

The earliest (2010) available groundwater level data suggested groundwater flow was to the NNE towards the Kifumashi River, with levels ranging from 1 173 to 1 186 mamsl and having an average elevation of 1 180 mamsl. Mining activity, together with abstraction for dewatering and water supply purposes had since distorted the immediate surface water and groundwater dynamics, drawing water towards the pit, defining a cone of depression. Figure 4-10 depicts topography, hydrology and piezometric heads from the first (2010) available groundwater level data at Kinsevere. Groundwater strike intersected during historical drilling ranged between 6 mbgl within weathered rock units and 94 mbgl within fractures and contacts, giving rise to the aforementioned levels (SRK, 2016).

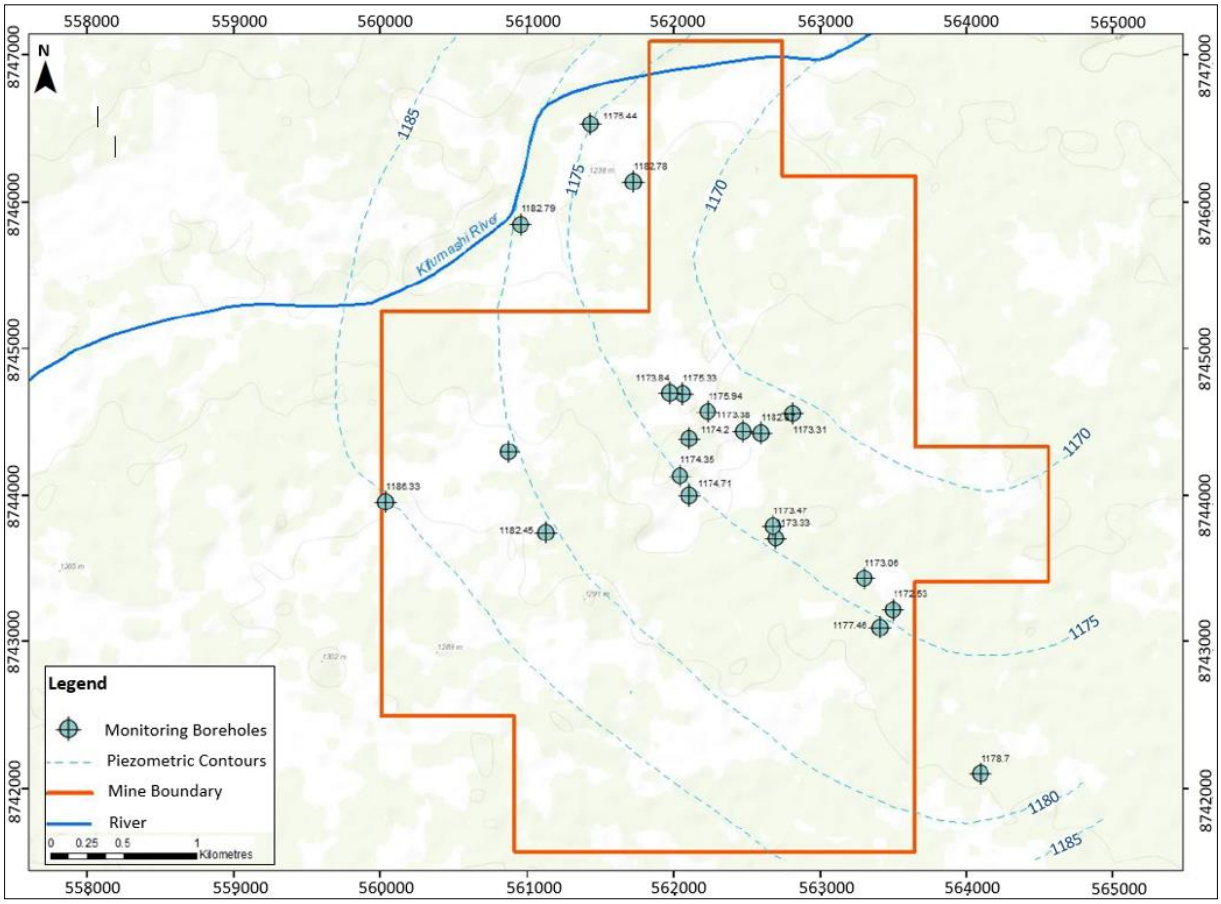


Figure 4-10: Map of Kinsevere topography, hydrology and piezometric heads in 2010 (base map source: SRK, 2018). Borehole water level and piezometric contour data collated by author.

4.4.3 Hydrostratigraphy

KP (2007) and SRK (2015) delineated aquifers at Kinsevere following hydraulic tests undertaken within the RSL, RBX, CMN, SD, Kundelungu formations and structures. The CMN was identified as the highest yielding rock unit due to extensive fracturing, weathering and dissolution at depth, making it more hydraulically connected and promoting high yields. Faulted zones and their associated weathering at depth act as preferential flow paths for groundwater and are higher yielding relative to the shallower weathered zones (<60 mbgl). KP (2007) and SRK (2015) defined the Kinsevere hydrostratigraphy as follows:

- The transition zone (saprock) between the saprolite and the fractured and fresh rock zones constituted a minor aquifer. The zone was considered permeable, with dominant lateral flow;
- A well developed, high yielding dolomitic aquifer comprising CMN and SD units. It was defined as a confined aquifer with well-interconnected cavities, faults and fractures acting as preferential groundwater flow paths and providing high storage capacity;
- A highly fractured RBX of moderate yield. The aquifer was weak with irregular to parallel bedding and occurred within the highly fractured fault zones; and
- A poorly developed, low yielding argillitic aquifer comprising the RSL unit, ungrouped sandstones and shales.

5 Observations and Findings

5.1 Hydrocensus

A hydrocensus was undertaken with the assistance of Kinsevere's mining, environmental and exploration departments. Over 35 boreholes visited were appropriately marked and in good condition, each fitted with a lockable cap for protection. Coordinate and collar elevation data was collected from each borehole. The departments provided data for boreholes not visited due to access issues and time constraints. Water levels were measured and adjusted to mamsl.

Surface water bodies and structures encompassing the Kifumashi River, discharge line, sediment ponds, process water dams, together with trenches and ponds around the WRDs, TSFs and OSs were visited, and their conditions assessed. Figure 5-1 presents boreholes and surface water bodies visited. See Appendix A for hydrocensus data.

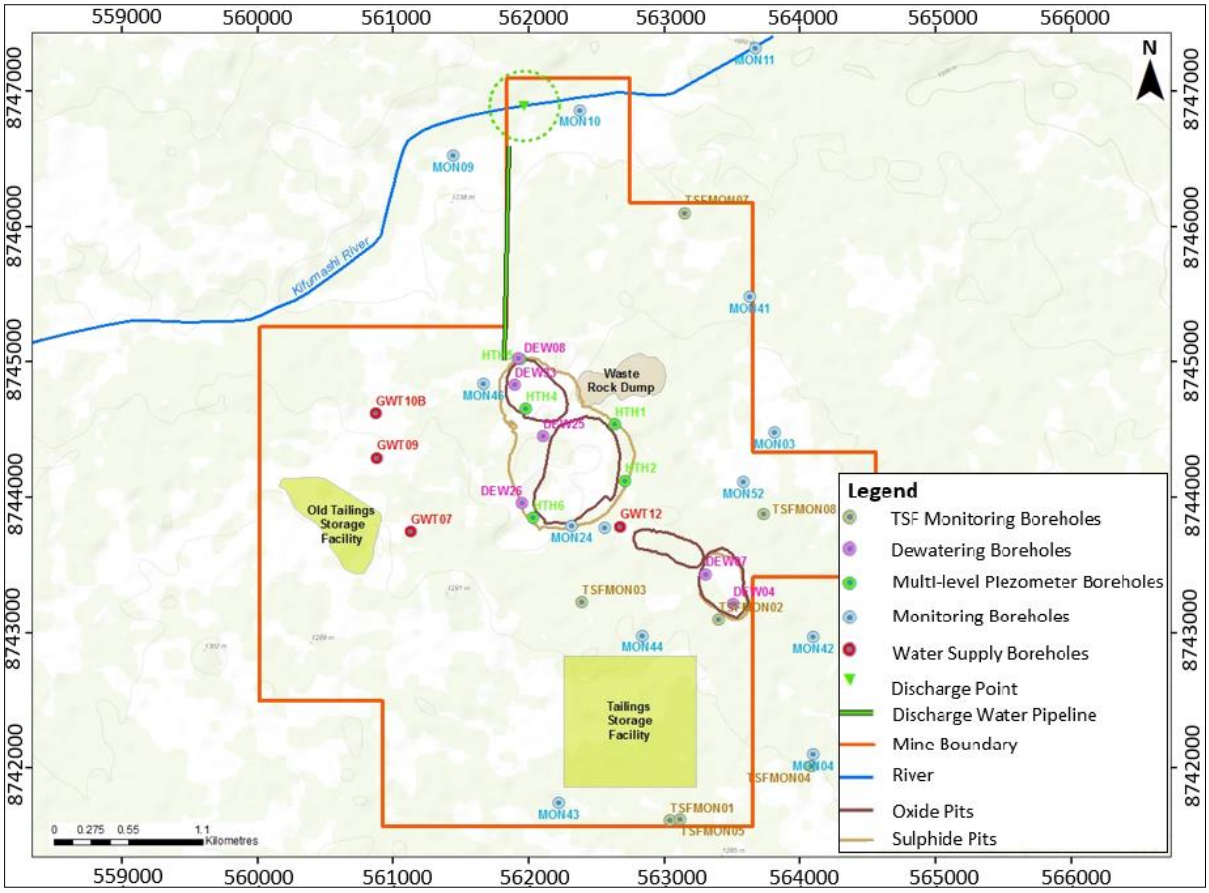


Figure 5-1 Boreholes identified during the hydrocensus (Base map source: SRK, 2018). Borehole data collated by author.

5.1.1 Groundwater Level Measurements and Abstraction

Groundwater levels fluctuate seasonally, falling during the dry season and rising during the rainy season due to rainwater infiltrating through the saprolite (weathered zone) into the underlying fractured siliceous and dolomitic units. Groundwater level measurements across Kinsevere ranged between 1 142 mamsl and 1 184 mamsl, with an average elevation of 1 174 mamsl (39 mbgl). Levels around the TSF, WRD and OS facilities were slightly elevated, ranging between 1 174 mamsl (MON44) and 1 179 mamsl (TSFMON01) and appearing as mounds relative to groundwater levels across the site (Figure 5-2). Water seeping through these facilities and into the underlying groundwater system stemmed from rainfall and dust suppression activities.

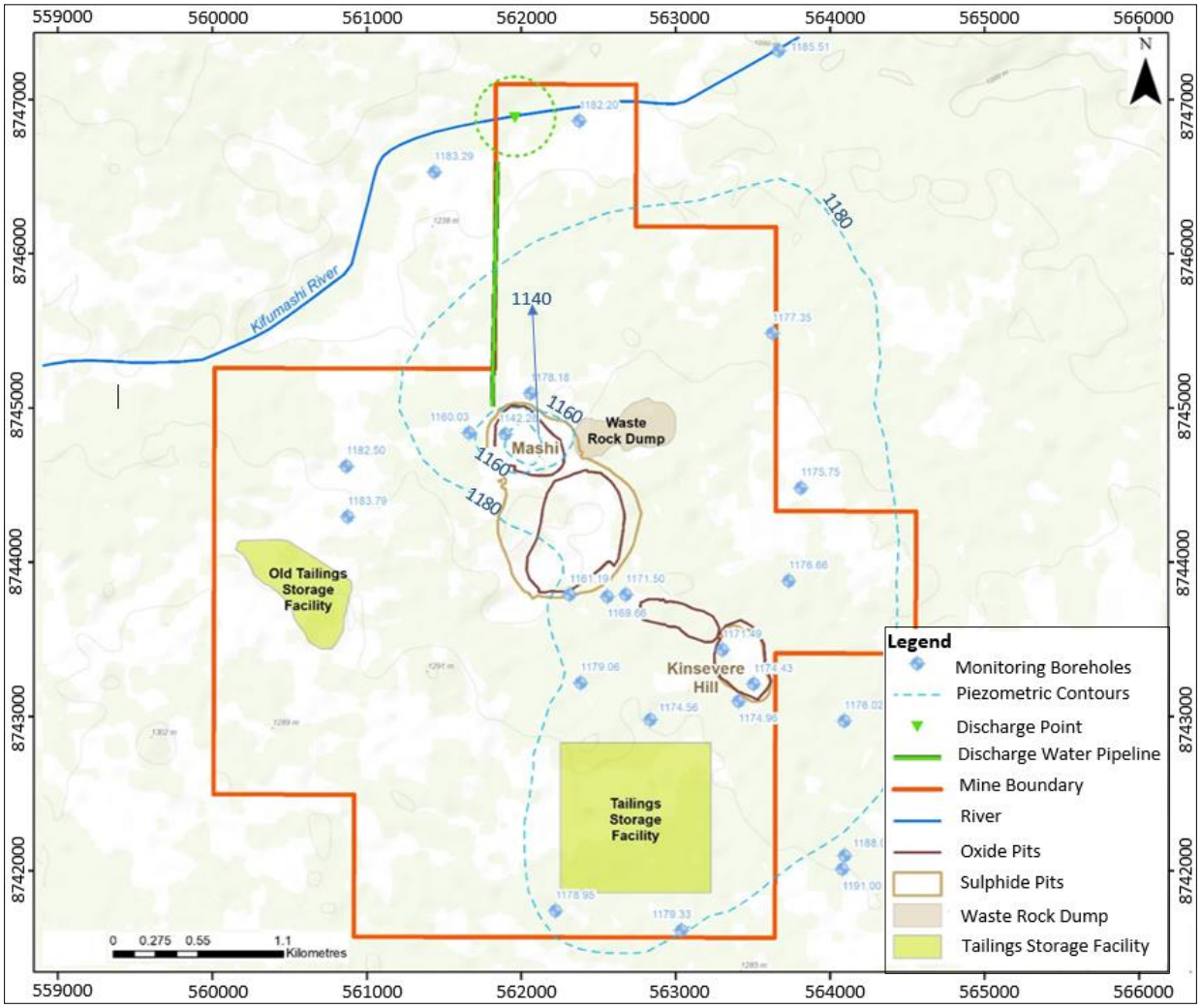


Figure 5-2: Piezometric map (Base map source: SRK, 2018). Borehole water level and piezometric contour data collated by author.

Groundwater levels had been falling gradually due to abstraction from water supply (GWT) and dewatering (DEW) boreholes. Abstraction from GWT boreholes occurred on a need basis or as per prescribed duty cycle for processing and domestic purposes. Groundwater levels in these boreholes were not severely affected due to sustainable pumping. Levels in these boreholes dropped by less than 1 m since 2010, with an average elevation of 1 180 mamsl.

Abstraction from dewatering boreholes was continuous, at an average rate of 280 L/s, aimed at keeping the groundwater levels below the pit floors (Figure 5-3). Dewatering activity was primarily concentrated on the western portion of the pits, predominantly comprising dolomitic rock units that introduced significant volumes of water into the pits. Groundwater levels across the pits dropped by a minimum of 31 m and a maximum of 64 m since 2010 (Figure 5-4). This variation in the groundwater levels was caused by stoppage of pumping in some of the dewatering boreholes because of maintenance and numerous pump failures, leading to levels rebounding.

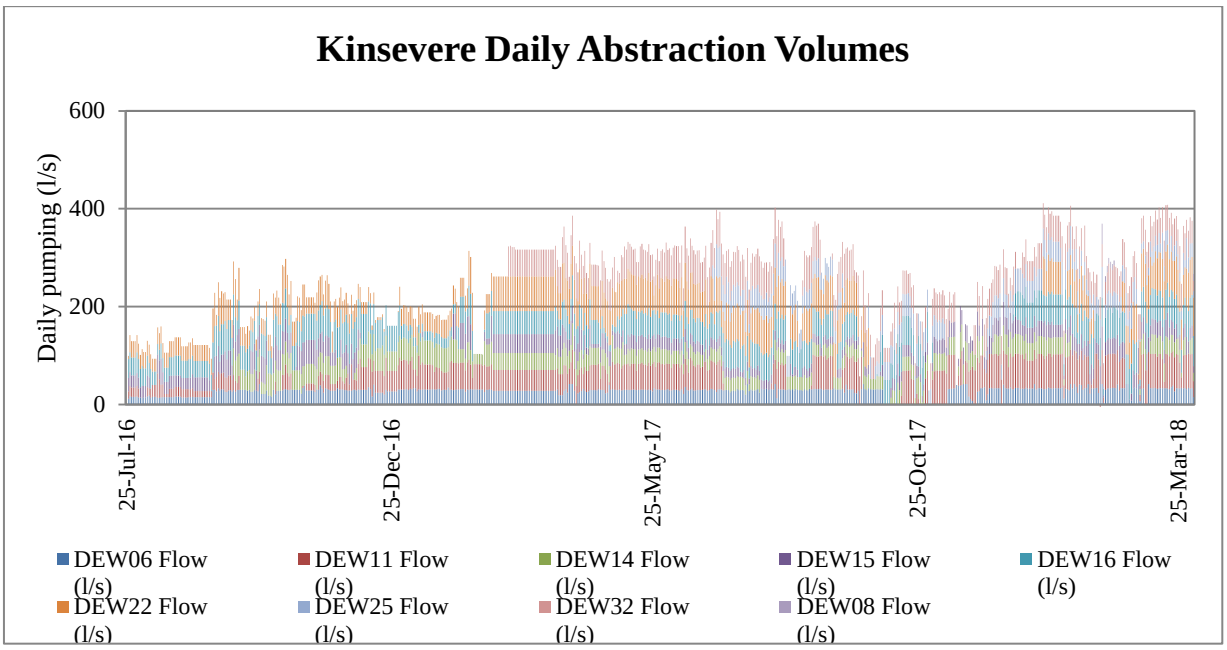


Figure 5-3: Daily abstraction volume for 2016 to 2018 (Source: Kinsevere Pumping Sheets, 2018).

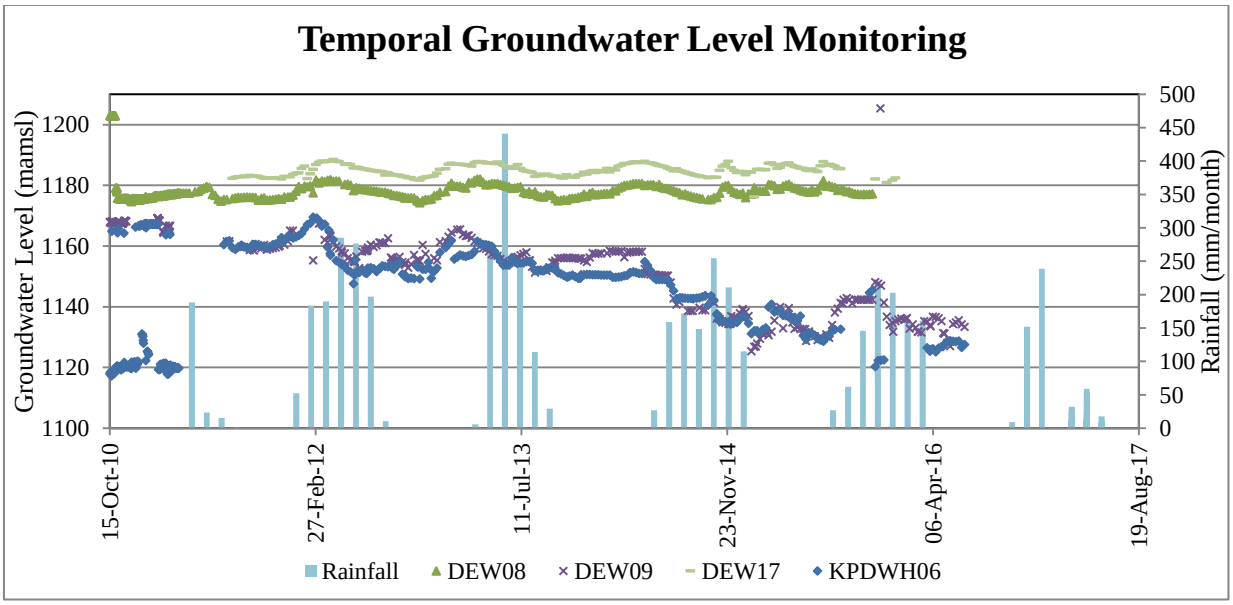


Figure 5-4: Temporal groundwater level monitoring plot between 2010 and 2016 (Data source: SRK, 2016).

As mining was ongoing in the Mashi Pit, dewatering of the rock units intersected by the pit was of primary focus. Levels in this pit dropped by 33 m since 2010, sitting between 1 142 mamsl (DEW33), 1 160 mamsl (MON45) and 1 178 mamsl (DEW08). Groundwater levels remain slightly above the pit floor on the northeastern (DEW08) and northwestern (MON45) portions, leading to groundwater ingress through the highwalls.

At the time of this research, the Central Pit was undergoing a cutback and dewatering was not prioritised. Pumps were either poorly maintained, shutoff, moved to dewatering boreholes in the Mashi Pit, failed due to over-pumping or electricity outages, leading to the groundwater levels rebounding to just below the DEW15 collar, sitting at 1 095 mamsl. A pit lake in the Central Pit was a consequence of this process.

Dewatering boreholes DEW06, DEW08, DEW11, DEW14, DEW15, DEW16, DEW22, DEW25 and DEW32, together with sump pumps, were used to remedy the rebound so mining could continue as planned in 2019. Groundwater levels in these boreholes could not be measured due to access, hence, the DEW15 collar was used for inference.

There was no mining activity in the Kinsevere Hill North Pit at the time of this research. From groundwater monitoring data, groundwater levels around the pit ranged between 1 169 mamsl (MON47) and 1 171 mamsl (DEW07). A small volume of water collected on the central portion of the pit, sourced from beneath the pit floor. Extensive weathering and the resultant clayey nature of the rock units on this portion limited rain water infiltration and promoted lateral flow, hence, the presence of stagnant water.

The abstraction for dewatering purposes distorted the groundwater patterns across the site, leading to a drop in the hydraulic gradient towards the pits, defining a cone of depression where abstraction was concentrated. Abstraction, structural occurrence (geological) and variation in lithological and hydraulic attributes of rock units found at Kinsevere led to miscorrelation between groundwater levels and topography.

Geological structures and significant differences in hydraulic attributes of rock units promoted compartmentalization, whereby groundwater levels in boreholes located within 100 m of each other show significant differences.

At Kinsevere, the compartmentalization was more pronounced with depth, as dewatering and resultant drop in levels progressed deeper. Dewatering boreholes DEW18-1 and DEW34 support this as they are located 90 m apart on the saddle between the Mashi and Central pits, divided by the SW – NE sinistral strike-slip fault. Groundwater levels on the saddle were initially (2010) at 1 173 – 1 175 mamsl but were found to have levels of 1 096 mamsl (DEW18-1) and 1 116 mamsl (DEW34) at the time of this research. Groundwater levels between the Mashi and Central Pits had an average difference of 42 m.

5.1.2 Observed Groundwater Inflows

Groundwater inflows were observed on the northeastern and northwestern highwalls of the Mashi Pit. Inflows on the northeastern portion occurred via dissolution fissures between the fractured RBX, SD, RSL and NE – SW trending faults, while inflows on the northwestern portion occurred through the RBX-CMN contact and NW – SE trending faults. Minor seepage delineated fault and fold structures on the northwestern highwall, stemming from rainfall. Inflows observed were driven by relatively higher water levels measured on the OS located to the immediate west of this portion. Ingress on the northeastern portion may have stemmed from a discharge trench and an unlined sediment to the north and northeast, respectively. There was no dewatering on this portion, hence the slightly elevated groundwater levels had sufficient driving head to induce groundwater ingress. Inflows from the pit floor were observed. Highwall and pit floor inflows were directed to sumps via trenches and pumped ex-pit, while some of the water flowed into cavities exposed during mining, thereby recharging the groundwater system. Inflows into the pit were determined to be less than 58 L/s (SRK, 2018).

In the Central Pit, no major groundwater ingress was observed on the highwalls. The 25 m column of rebound water within the pit masked highwall inflows. Minor inflows were observed in the Kinsevere Hill Pit stemming from the pit floor on account of a 1 m water level difference observed in DEW07 and the pit floor. This difference was not sufficient to drive significant inflows into the pit. The Central and Kinsevere Hill pits had inflows of 520 L/s and less than 58 L/s, respectively (SRK, 2018). See Figure 5-5 for photographs of groundwater conditions observed within the Kinsevere pits.



a) Pit floor inflows and direction of inflows in the Mashi Pit (facing NE).



b) Exposed cavities (red) receiving water (green) in Mashi Pit (facing NE).



c) Seepage on the northwestern highwall in Mashi Pit.



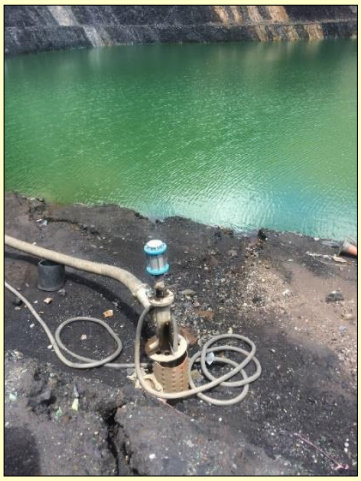
d) Seepage through a horizontral drain hole on the northeastern highwall of Mashi Pit.



e) Folds and faults delineated by seepage (facing NW).



f) Pit-lake conditions in Central Pit (facing SE).



g) DEW15 and the pit-lake in the Central Pit (facing SE).



h) Minor pit floor inflow in the Kinsevere Hill Pit (facing NE).

Figure 5-5: Photographs of groundwater conditions at Kinsevere.

5.2 Pore Pressure Assessment

Six HTH boreholes were installed in 2015, each fitted with three vibrating wire transducers (VWTs) to monitor pore pressures around the Mashi and Central pits within RBX, RSL and CMN units in isolation, with each VWT measuring the head above it and resultant hydrostatic pressure. See Table 5-1 for installation details and Figure 5-1 for their respective locations. From the data provided, spanning from 2015 to 2016, pressures fluctuated in response to the degree of saturation, induced by rainfall and its intensity (Figure 5-6 and Figure 5-7). The extent and rate of response was also dependent on the degree of weathering, fracturing together with hydraulic capacity and connection. Changes in dewatering activity also induced fluctuations.

RBX and RSL monitored on the eastern (HTH02- Figure 5-8) and western (HTH03- Figure5-9) portions of the Central Pit showed evidence of hydraulic connection between sections monitored and upward maximum pressures ranging between 0.6 MPa and 1.8 MPa in the RBX and RSL units, respectively. The top RBX monitoring VWT (T1) on the eastern portion (HTH02) showed a pronounced response to rainfall relative to the lower VWTs on account of extensive weathering and fracturing at the upper sections.

Faulting, fracturing and degree of weathering with depth promote hydraulic connection. Similar observations were made on the southwestern portion of the Mashi Pit (HTH04), where the CMN unit was connected to the RSL unit and induced maximum upward pressures of 1.8 MPa (Figure 5-10). The shallow CMN unit on the southwestern portion of the Central Pit (HTH06) was isolated from the underlying RSL and CMN units at depth. In addition, maximum upward pressures of 1.2 MPa were evident (Figure 5-11). Semi-confined to confined conditions prevailed across the pit, induced by the SD, CMN and RSL units. Variations in the groundwater levels across the pits, as observed in the HTH plots, suggested compartmentalisation.

Table 5-1: Details of HTH boreholes installed.

HTH I. D	Location	VWT No.	Depth Installed (mamsl)	Target Rock Unit and Lithology
HTH01	Immediate northeast of Central Pit	T1	1 139	RSL– moderately weathered and oxidized
		T2	1 072	RSL– fresh
		T3	1 008	RSL– fresh
HTH02	Immediate east of Central Pit	T1	1 126	RBX– moderately weathered and oxidized
		T2	1 069	RBX– moderately weathered and oxidized
		T3	994	RBX– fresh
HTH03	Immediate west of Central Pit	T1	1 107	RSL– moderately weathered and oxidized
		T2	1 049	RSL– fresh and slightly oxidized
		T3	967	RSL– moderately weathered and oxidized
HTH04	Immediate south of Mashi Pit	T1	1 106	RSL– fresh
		T2	1 044	RSL– fresh
		T3	965	CMN– fresh
HTH05	Immediate north of Mashi Pit	T1	1 123	RBX– fresh and slightly oxidized
		T2	1 103	RBX– fresh
		T3	1 063	RSL– fresh
HTH06	Immediate southwest of Central Pit	T1	1 107	CMN– fresh
		T2	1 047	CMN– fresh
		T3	967	RSL– highly weathered

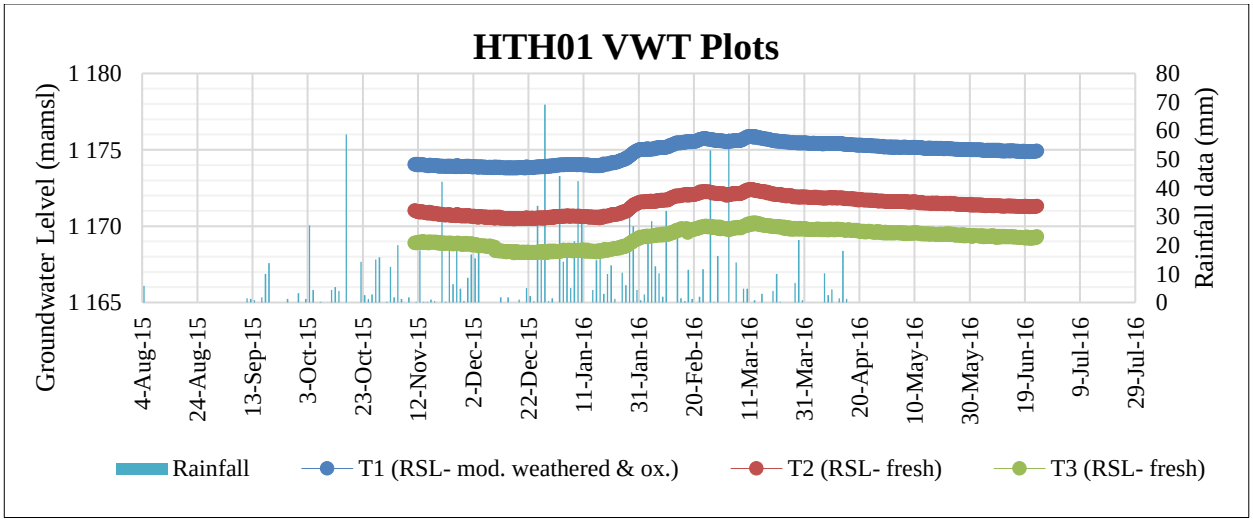


Figure 5-6: HTH01 Plot– evidence of rainfall influence on groundwater levels (Data source: SRK, 2016).

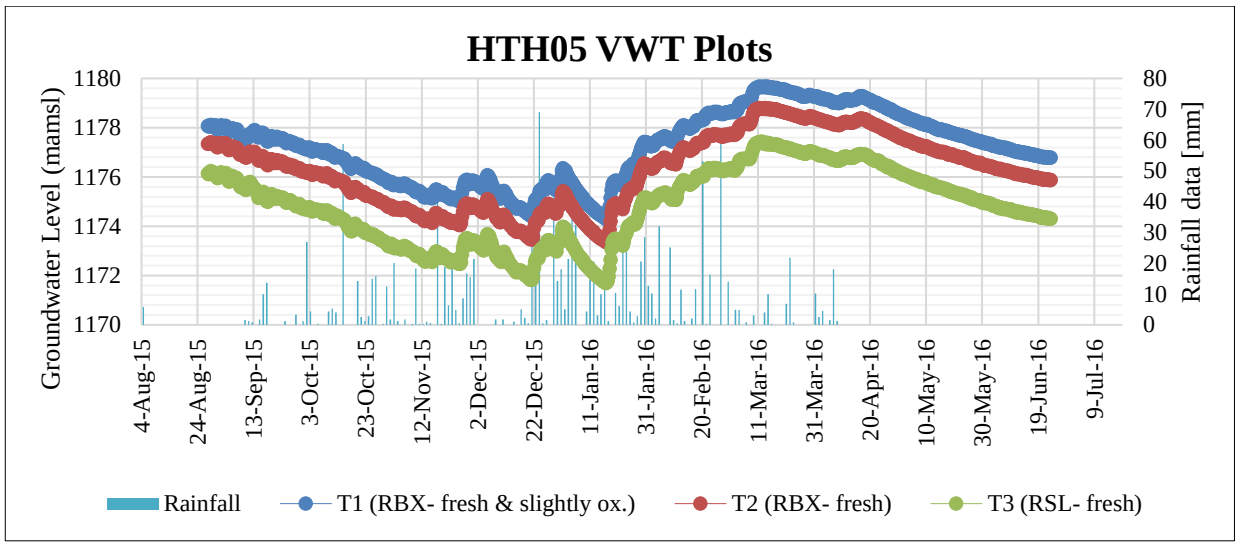


Figure 5-7: HTH05 Plot– evidence of rainfall influence on groundwater levels (Data source: SRK, 2016).

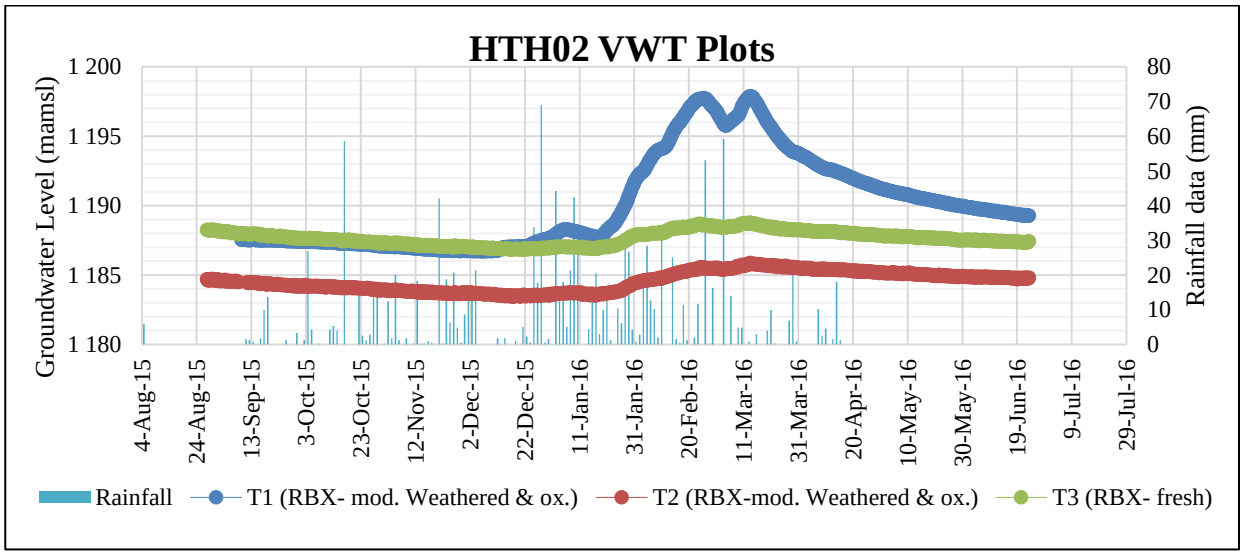


Figure 5-8: HTH02 Plot– evidence of hydraulic connectivity and upward hydrostatic pressures (Data source: SRK, 2016).

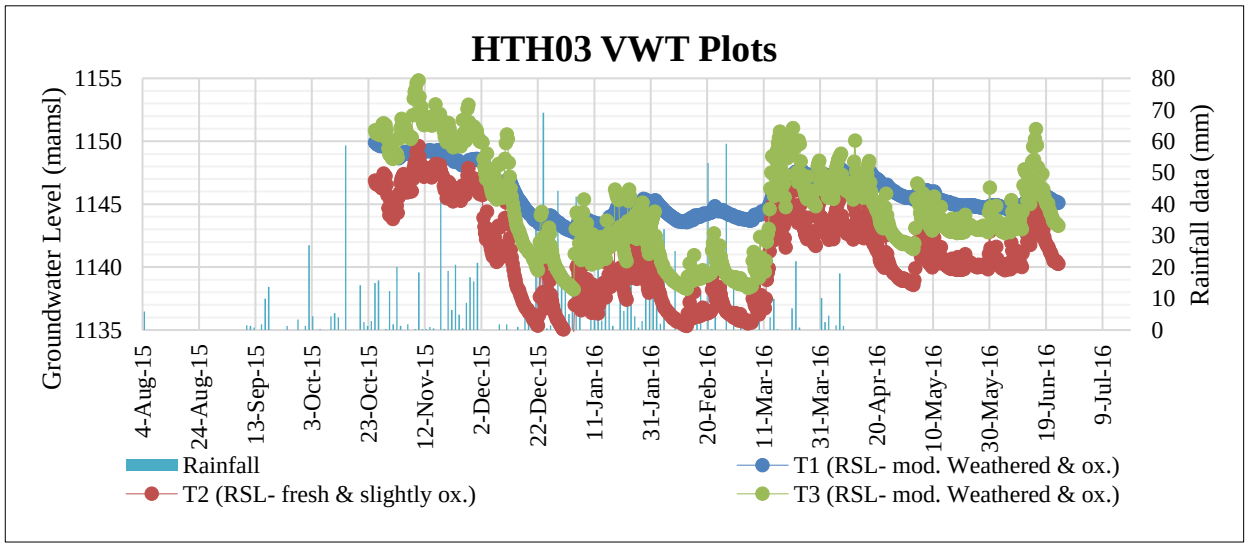


Figure 5-9: HTH03 Plot– evidence of hydraulic connectivity and upward hydrostatic pressures (Data source: SRK, 2016).

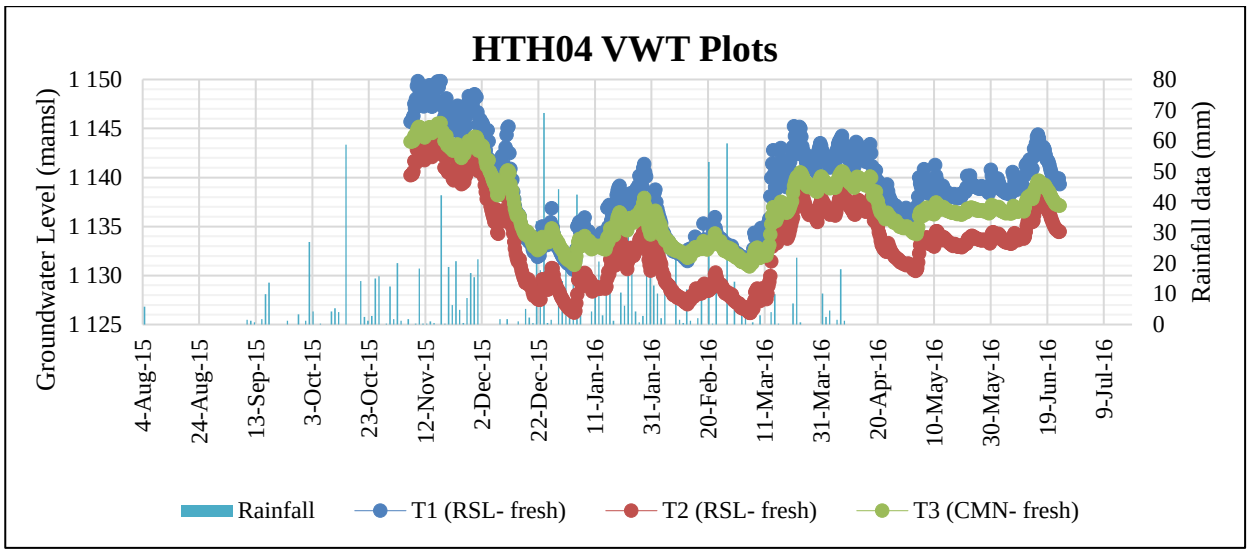


Figure 5-10: HTH04 Plot– evidence of hydraulic connectivity and upward hydrostatic pressures (Data source: SRK, 2016).

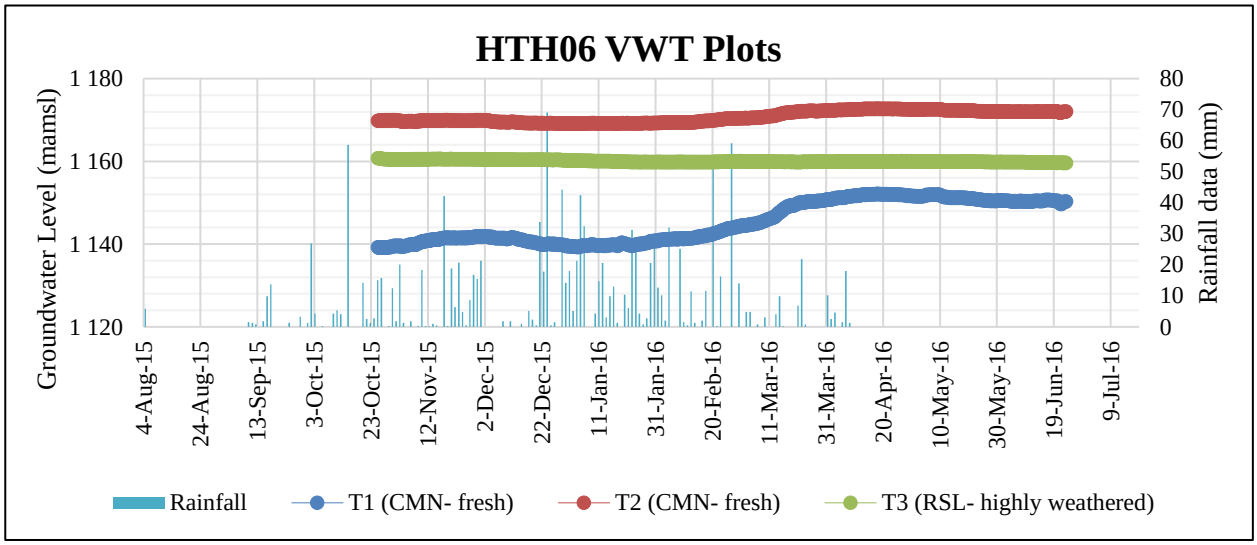


Figure 5-11: HTH06 Plot– evidence of disconnection between upper CMN and underlying RSL and CMN units (Data source: SRK, 2016).

5.3 Drilling

Boreholes drilled during the course of this research are presented in Figure 5-12. The Mining Department drilled four dewatering pilot boreholes, three of which were drilled using the DC technique, while the fourth borehole was drilled using the CSRC technique (Table 5-2). In addition, the department drilled and installed three dewatering boreholes (Table 5-3). The Exploration Department drilled eleven resource boreholes, three of which were drilled using the CSRC technique and were completed as monitoring boreholes, while eight boreholes were drilled using the CCRC technique (Table 5-4). Additional boreholes were drilled, but this research only focused on boreholes hydraulically tested during drilling.

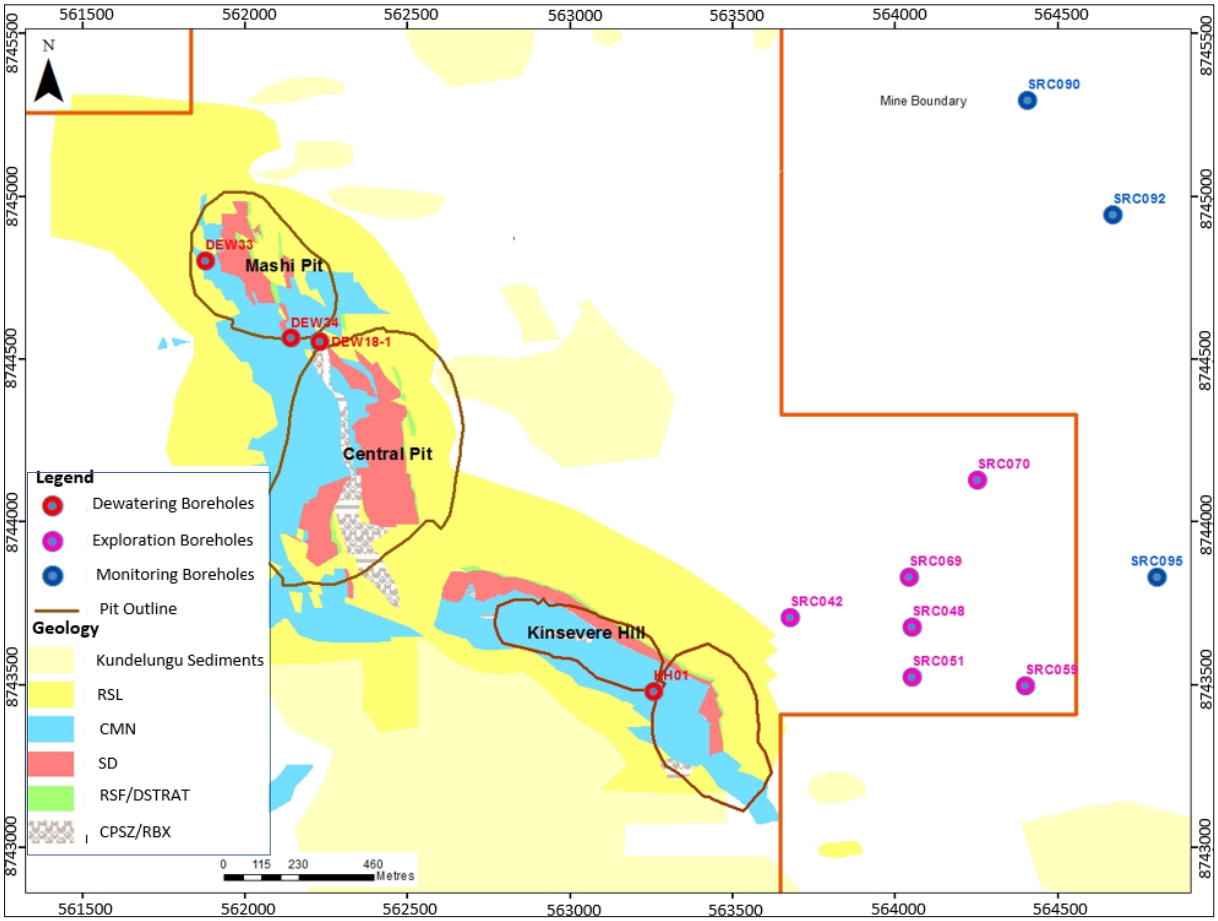


Figure 5-12: Map showing boreholes drilled during research (Base map source: SRK, 2018). Borehole data collated by author.

Table 5-2: Details of pilot boreholes drilled.

Borehole I. D	Location	Purpose	Drilling Technique	Diameter Drilled (cm)	Depth Drilled (mbgl)	Final Depth (mbgl)
DEW18-1	Mashi & Central pits saddle	Dewatering pilot borehole	DC	8.3 (PQ)	0 – 153	200
				6.4 (HQ)	153 – 200	
DEW33	Northern part of Mashi Pit	Dewatering pilot borehole	DC	8.3 (PQ)	0 – 124	124
DEW34	Mashi & Central pits saddle	Dewatering pilot borehole	CSRC	91.4	0 – 10	200
				35.6	10 – 200	
KH01	South of Kinsevere Hill	Dewatering pilot borehole	DC	8.3 (PQ)	0 – 35	110
				6.4 (HQ)	35 – 110	

Table 5-3: Details of dewatering boreholes.

Borehole I. D	Location	Purpose	Drilling Technique	Diameter drilled (cm)	Depth Drilled (mbgl)	Final Depth (mbgl)	Water Strikes (mbgl)	Airlift Yield (L/s)
DEW18-1	Mashi & Central pits saddle	Dewatering borehole	CSRC	-	-	200	88	0.36
DEW33	Northern part of Mashi Pit	Dewatering borehole	CSRC	71.1	0 – 6	140	30	24
				61.0	6 – 80			
				50.8	80 – 140			
DEW34	Mashi & Central pits saddle	Dewatering borehole	CSRC	91.4	0 – 10	200	63	5.5
				61.0	10 – 88			
				50.8	88 – 200			
KH01	Dewatering borehole to be drilled when mining of Kinsevere Hill Pit continues							

Table 5-4: Details of resource exploration boreholes.

Borehole I. D	Location	Purpose	Drilling Method	Water Strikes (mbgl)	Diameter Drilled (cm)	Depth Drilled (mbgl)	Airlift Yield (L/s)	RWL (mbgl)	Comment
SRC042	TSF3	Resource exploration borehole	CCRC	-	11.4	96	-	-	Collapsed to 42 mbgl
SRC048	TSF3		CCRC	-	11.4	120	-	-	Collapsed to 44 mbgl
SRC051	TSF3		CCRC	-	11.4	81	-	-	Collapsed to 37 mbgl
SRC059	TSF3		CCRC	-	11.4	111	-	-	Collapsed to 23 mbgl
SRC064	TSF3		CCRC	-	11.4	-	-	-	Collapsed to 48 mbgl
SRC066	TSF3		CCRC	-	11.4	-	-	-	Collapsed to 34 mbgl
SRC069	TSF3		CCRC	-	11.4	-	-	-	Collapsed to 21 mbgl
SRC070	TSF3		CCRC	-	11.4	91	-	-	Collapsed to 32 mbgl
SRC090	TSF3	Resource exploration & groundwater monitoring borehole	CSRC	72 & 83	20.3	0 – 6	6.8	20.4	Installed & capped
					16.5	6 – 102			
SRC092	TSF3		CSRC	73 & 91	20.3	0 – 6	5.7	20.7	Installed & capped
					16.5	6 – 120			
SRC095	TSF3		CSRC	84 & 103	20.3	0 – 6	3.4	29.3	Installed & capped
					16.5	6 – 120			

5.3.1 Rock Units Intersected

Pilot and Dewatering Boreholes

The pilot and dewatering boreholes drilled around the pits intersected saprolite, saprock, SD, CMN, RSL and RBX units. The saprolite units intersected were fine grained, highly weathered, clayey, oxidized and argillaceous, appearing as pink, purple or reddish brown, suggesting variability in Redox, petrographic and geochemical conditions. The saprock units were reddish brown in colour, fine to medium grained, moderate to highly weathered, with a combination of clayey, silty and sandy features, marking the transition section from a highly weathered derivative (saprolite) into the parent rock.

The SD rock unit appeared dark brown or dark grey to black, fine-grained, massive with minor laminations (rhythmic in places) and with magnesite, quartz and pyrite filled veins, slight to moderately weathered and fractured with depth, comprising vugs and cavities with depth, with carbonaceous shale interbedded with dolomitic siltstone at depth. Weathering was more extensive towards the contacts with the RAT and CMN units.

The CMN unit occurred as grey, fine to medium grained, massive or rhythmically laminated with magnesite-filled veins, dolomitised, weathered, faulted, fractured and having vugs (with quartz crystals) and cavities at depth. The RSL unit varied between being red, purple, brown and white in colour, with features such as being fine-grained, massive with a silty matrix, weathered and fractured in places, while the RBX unit appeared as either pink to light brown or grey depending on the dominant cementing agent. The pink to light brown RBX was fine to medium grained, dominantly siliceous with sub-angular clasts, slight to moderately fractured and brecciated, while the grey RBX had similar features with the exception of a dolomitised cement. The unit was therefore polymictic and occurred along the shear zone, where it was in contact with the RSL, SD and CMN units.

See Table 5-5 for descriptions of rock units intersected by pilot and dewatering boreholes and their respective lithological attributes. Water strikes were intersected at shallow depths of 9 mbgl within the upper weathered transition section (saprock) and as deep as 194 mbgl within faulted, fractured, brecciated and in places, karstified units. See Figure5-13 for photographs of rocks intersected during pilot and dewatering drilling.

Resource Exploration Boreholes

The resource exploration boreholes drilled in the TSF3 area intersected saprolite and saprock derivatives of shale, siltstone and SD units. The saprolite was reddish brown to brown, fine grained, highly weathered, oxidized, slightly gritty and soft, while the saprock unit had similar attributes as the saprolite unit, with the exception of hardness and extent of clay composition. The shale unit occurred as purple or light brown in places, fined grained, moderate to highly weathered, slightly oxidized and slightly fractured, while the siltstone unit was brown, purple or light grey in places, fine to medium grained, gritty, slightly weathered and fractured. The shale and siltstone units may be associated with the Kundelungu Group, as they were located further (*c.*1.7 km) east and northeast of the Kinsevere Hill Pit. The SD unit occurred as brown, reddish brown and grey with depth, fine grained, moderate to highly weathered, slightly oxidized, vuggy and interbedded with siltstone which appeared reddish brown to brown with depth, fine to medium grained, silicified and brecciated in places. Table 5-6 presents rock units intersected by resource exploration boreholes completed as monitoring boreholes in the TSF3 area. Minor seepage was observed within the saprolite and saprock (transition section) units at depths of 11 mbgl, while major water strikes were intersected as deep as 103 mbgl in fractured units. See Figure 5-13 for photographs of rocks intersected during resource exploration drilling.

Table 5-5: Details of rock units intersected by dewatering pilot boreholes and their respective lithological attributes.

Borehole I. D	Depth Drilled (mbgl)	General Rock Unit and Lithology
DEW18-1	0 – 1	Saprolite – reddish brown, fine grained, clayey, soft, oxidized and highly weathered.
	1 – 4	Saprock – reddish brown, fine to medium grained, locally sandy, clayey, and moderate to highly weathered.
	4 – 97	SD – dark brown to black, fine grained, slightly laminated, carbonaceous, slightly fractured, moderate to highly weathered with depth, interbedded with Dolomitic Siltstone – dark grey, fine grained, laminated, slightly fractured with quartz filled veins and evidence of faulting.
	97 – 99	Cavity.
	99 – 108	SD – black, fine grained, slightly laminated, carbonaceous slightly fractured and weathered, interbedded with Dolomitic Siltstone - grey, fine grained, laminated and slightly fractured.
	108 – 109	Cavity.
	109 – 118	SD – black, fine grained, slightly laminated, carbonaceous slightly fractured and weathered, interbedded with Dolomitic Siltstone– grey, fine grained, laminated and slightly fractured
	118 – 121	Cavity.
	121 – 147	SD – black, fine grained, slightly laminated, fractured and weathered, and comprised Magnesite-filled veins.
	147– 151	Cavity.
	151– 178	SD – black, fine grained, slightly laminated, fractured and weathered, and comprised Magnesite-filled veins.
	178 – 180	Cavity.
	180 – 185	SD – black, fine grained, slightly laminated, slightly fractured, slightly weathered, carbonaceous, interbedded with Dolomitic Siltstone – grey, fine grained and comprised Magnesite-filled veins.
	185 – 200	CMN – grey, fine to medium grained, laminated and comprised Magnesite-filled veins.
DEW33	0 – 16	SD – brown, fine grained, mottled, moderate to highly weathered, carbonaceous, fractured and slightly laminated.
	16 – 19	SD – dark brown to black, fine grained, carbonaceous, moderate to highly weathered, carbonaceous and fractured.
	19 – 22	SD – greyish-brown, fine grained, carbonaceous, variably weathered, fractured and laminated with cherty bands
	22 – 26	Cavity.
	26 – 30	CMN – grey, fine to medium grained, laminated, highly fractured and moderate to highly weathered.
	30 – 33	SD – grey to black, fine grained, carbonaceous, highly fractured, moderately weathered and slightly oxidized.
	33 – 69	CMN – grey to brown, fine to medium grained, laminated, moderate to highly fractured, silty and moderately weathered and comprised quartz filled veins.
	69 – 70	Cavity.
	70 – 85	CMN – grey to brown, fine to medium grained, laminated, moderate to highly fractured, silty and moderately weathered, with quartz filled veins and was slightly oxidized.
	85 – 96	SD – black, fine grained, carbonaceous, slightly laminated, moderate to highly fractured, interbedded with Dolomitic Siltstone – fine to medium grained, laminated and fractured.
	96 – 113	CMN – grey, fine to medium grained, laminated, fractured, brecciated in places, quartz filled veins and had evidence of faulting.
	113 – 115	SD – black, fine grained, carbonaceous, slightly laminated, moderate to highly fractured, interbedded with Dolomitic Siltstone – fine to medium grained, laminated and fractured.
	115 – 140	CMN – grey, fine to medium grained, laminated, fresh, fractured, quartz filled veins, with evidence of faulting.
DEW34	0 – 50	SD – dark brown, fine grained, laminated, soft, carbonaceous, moderate to highly weathered, interbedded with Siltstone – brown, fine to medium grained, silty and moderate to highly weathered.
	50 – 51	Cavity.
	51 – 70	SD – brown, fine grained, laminated, soft, moderate to highly weathered, interbedded with Siltstone – brown, fine to medium grained, silty and moderate to highly weathered.
	70 – 71	Cavity
	71 – 97	SD – brown, fine grained, laminated, soft, carbonaceous moderate to highly weathered, interbedded with RAT- brown, fine to medium grained, silty, moderate to highly weathered.
	97 – 200	CMN – grey, fine to medium grained, massive and slightly laminated, fractured and variably weathered.

Borehole I. D	Depth Drilled (mbgl)	General Rock Unit and Lithology
KH01	0 – 2	Saprolite – reddish brown, fine grained, clayey, moderate to highly weathered, soft and oxidized.
	2 – 8	Saprock – reddish brown, fine to medium grained, clayey, silty, harder relative to above and oxidized.
	8 – 16	SD – black, fine grained, slightly laminated, clayey, moderate to highly weathered and carbonaceous.
	16 –40	RBX – brown, fine to medium grained, silty, moderate to highly weathered with clasts in places, brecciated and interbedded with SD – black, fine grained, carbonaceous and moderate to highly weathered.
	40 – 59	RBX – grey, fine to medium grained with clasts, brecciated, fractured, silty and slight to moderately fractured.
	59 – 106	CMN – grey, fine to medium grained, laminated, moderate to highly fractured, vuggy with quartz-filled veins and brecciated in places.
	106 – 110	SD – grey to black, fine grained, slight brecciation in places, slightly laminated, slight to moderately fractured and vuggy.

Table 5-6: Summary of rock units intersected by resource exploration boreholes in the TSF3 area.

Borehole I. D	Depth Drilled (mbgl)	General Rock Unit and Lithology
SRC042	0 – 3	Saprolite – brown, fine grained, highly weathered, soft, clayey and oxidized.
	3 – 17	Saprock – reddish brown, fine to medium grained, moderate to highly weathered, soapy, clayey
	17 – 45	Shale – reddish brown, fine grained, moderate to highly weathered, siliceous and clayey.
	45 – 76	SD – brown to yellow, fine grained, carbonaceous, moderate to highly weathered, highly oxidized, and interbedded with Dolomitic Siltstone.
	76 – 96	SD – brown to greyish black in places, fine grained, dolomitic, carbonaceous, silicified in places and vuggy.
SRC048	0 – 4	Saprolite – reddish brown, fine grained, highly weathered, soft, oxidized and clayey.
	4 – 12	Saprock – reddish brown, fine to medium grained, silty and moderate to highly weathered.
	12 – 120	SD – reddish brown to grey with depth, fine grained, carbonaceous, silicified, dolomitic, brecciated in places, vuggy and moderately weathered.
SRC051	0 – 15	Saprolite – reddish brown, fine grained, highly weathered, soft, clayey and oxidized.
	15 – 35	Saprock – reddish brown, fine to medium grained, Siltstone interbedded with Shale with depth.
	35 – 50	Siltstone – brown, fine to medium grained, silicified, interbedded with Shale and brecciated in places.
	50 – 81	SD – brown, fine to grained, oxidized, silicified, interbedded with Dolomitic Siltstone and vuggy.
SRC090	0 – 12	Saprolite – reddish brown, fine grained, highly weathered, oxidized, mottled, soft, slightly gritty and clayey.
	12 – 36	Saprock – light brown, fine grained, moderate to highly weathered and slightly fractured.
	36 – 102	Shale – purple, fined grained, moderate to highly weathered, slightly oxidized and fractured.
SRC092	0 – 13	Saprolite – reddish brown in places, fine grained, highly weathered, oxidized, soft, slightly gritty and clayey.
	13 – 24	Saprock – reddish brown, fine to medium grained, moderate to highly weathered and slightly fractured.
	24 – 50	Shale – purple, fine grained, moderately weathered, slightly oxidized and slightly fractured.
	50 – 58	Siltstone – brown, fine to medium grained, moderate to highly weathered, silty and slightly fractured.
	58 – 91	Shale – purple, fine grained, moderately weathered, slightly oxidized and slightly fractured.
	91 – 120	Siltstone – light grey, fine to medium grained, moderate to highly weathered, silty, and slightly fractured.
SRC095	0 – 13	Saprolite – reddish brown and brown in places, fine grained, highly weathered, oxidized, slightly gritty and clayey.
	13 – 15	Saprock – light brown, fine grained, moderate to highly weathered and slightly fractured.
	15 – 73	Shale – purple to light brown in places, fined grained, moderate to highly weathered, slightly oxidized and slightly fractured.
	73 – 120	Siltstone – light brown to grey in places, fine to medium grained, slightly weathered and fractured.



a) Highly weatherd and oxidized saprolite and saprock (DEW18-1).



b) Faulted, fractured and laminated CMN and fractured SD (DEW33).



c) Fractured CMN with brecciation and weathered RAT Breccia (KH01).



d) Fractured CMN interbedded with fractured and friable SD (DEW33).



e) Fractured CMN with rythmic laminations and silicified nodules.



f) Vuggy CMN with quartz crystal and veins.



g) Vuggy SD with pyrite and magnesite veins.



h) RBX with clasts.

Figure 5-13: Photographs of rock units intersected during drilling.

5.4 Hydraulic Testing

5.4.1 Pumping Test

Dewatering borehole DEW08 was subjected to a pumping test. The borehole was drilled down to the depth of 140 m at the time of Anvil but was found to have silted or collapsed up to 125 mbgl at the time of the test and this research. The borehole intersected fractured RSL, SD and CMN units (from top to bottom). SD and CMN units promote confining conditions at depth. Dewatering borehole DEW17 and monitoring borehole SRK06 located 15 m south and 50 m north of DEW08, respectively, were used as observation boreholes during the pumping test to determine storativity and the radial influence of DEW08 when pumping. Groundwater levels in the three boreholes were at 13 mbgl. Prior to pumping, the pump was installed at 120 m depth. A 150 m long discharge line was laid out, leading to a sump at the bottom of the Mashi Pit. The water level was measured and zeroed to determine the extent of available drawdown (AD). The AD was determined to be 107 m. The borehole was then subjected to SDT and CDT tests, having RT tests undertaken after the aforementioned tests.

Step and Constant Discharge Rate Tests

Three SDT steps at rates of 5, 10 and 20 L/s at 60-minute intervals were undertaken. The pump choked towards the end of the third step, whereby the pumping rate exceeded inflows into the borehole. In addition, a no flow boundary was encountered at the end of the third step. The borehole had a drawdown of 100 m over the course of the steps. The residual drawdown was measured immediately after the third step, with the water level rebounding to its initial level within 100 minutes of termination of the SDT. Analysis of the step drawdown vs. time scatter plot overlain with the Non-linear FC Method line of best fit generated a bulk T of $1.4x10^{1}$ m^2/d, K of $1.3x10^{-1}$ m/d, and S of 0.1 (Figure 5-14). See Appendix B for pumping test data.

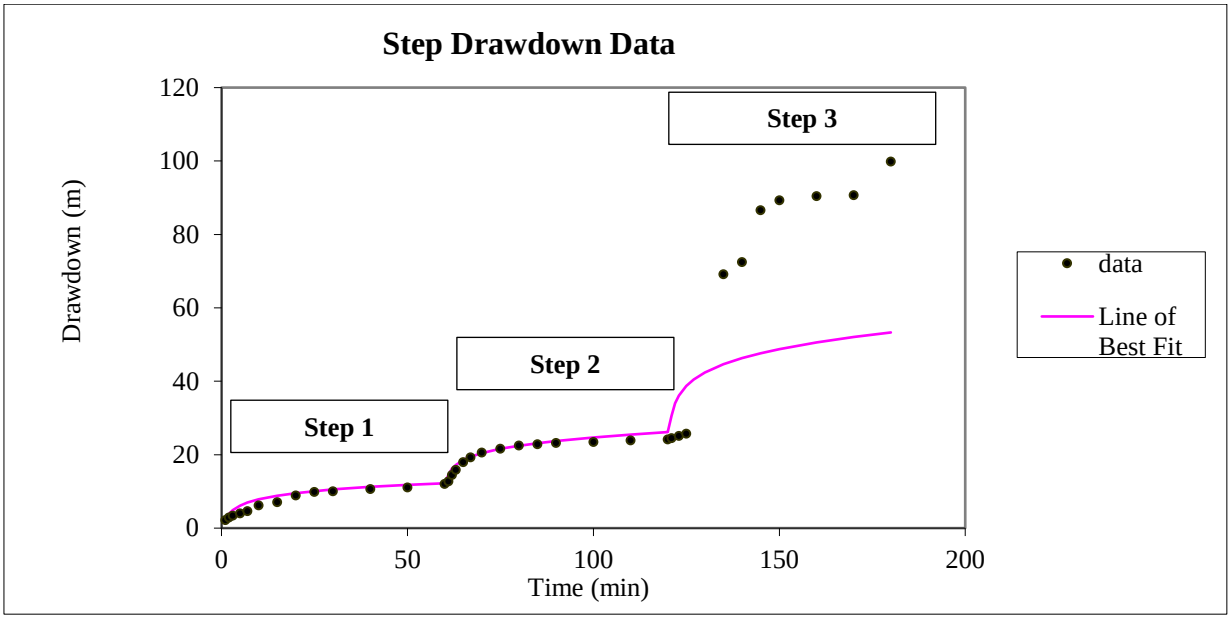


Figure 5-14: Step drawdown data vs. time graph of DEW08 overlain by the Non-Linear FC Method line of best fit (pink).

The CDT ran for 48 hours at a rate of 13 L/s. The groundwater level in DEW08 had a drawdown of 65 m, while the levels stabilized (dropping by cm) during the last four hours of the test, suggesting that the rate of groundwater ingress into the borehole matched the discharge rate during this phase of pumping. The pump was shut-off and the RT test initiated.

The DEW08 borehole groundwater level rebounded by 95% within the first hour of the test. During the CDRT test, the drawdown in the DEW17 borehole was 10 m and rebounded within 70-minutes of the RT, while levels in the SRK06 borehole had a drawdown of 4 m over 28 hours. The residual drawdown in SRK06 was also as miniscule, rising in centimetres at hourly intervals.

Analysis of the Drawdown vs. Time plot of all three boreholes suggested flow conditions to be under unsteady state. This was made evident by variable drawdown and recovery between the boreholes during the CDT. Diagnostic and derivative plots of Drawdown derivative vs. Time derivative were analysed to determine aquifer hydraulic boundaries, water-bearing zones and their respective depths, together with the flow models and their respective method of analysis.

Analysis of diagnostic and derivative plots from CDT drawdown data showed evidence of double porosity (linear, bi-linear and radial flow) and a Theis Model (Figure 5-15 and Figure 5-16). The early pumping phase drew well-bore storage (linear flow), while the intermediate phase drew water from the matrix, fractures and dissolution features (bi-linear and radial flow) immediate to the borehole that were dewatered, and the late (final) phase indicated minor fracture (linear flow) followed by a no-flow boundary. Two major water strikes at depths of 59 mbgl and 63 mbgl were confirmed from analysis of Derivative Plots (Figure 5-17). The water strikes sat below the 13 mbgl groundwater level, thereby, supporting the notion of SD and CMN units as confining units.

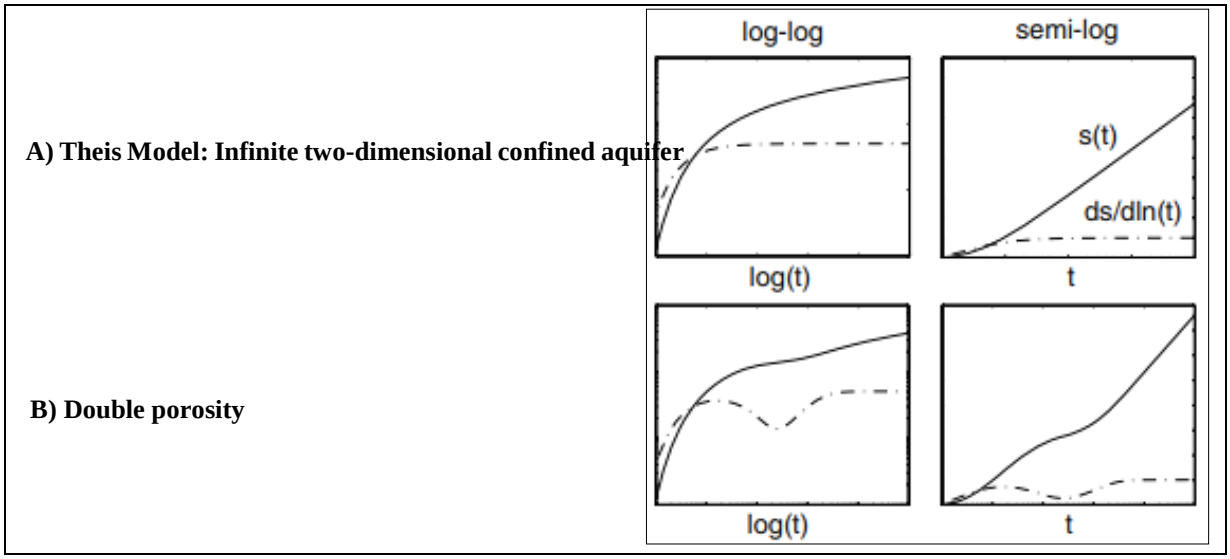


Figure 5-15: Diagnostic plots showing trends observed during pumping test (Source: Renard, 2005b).

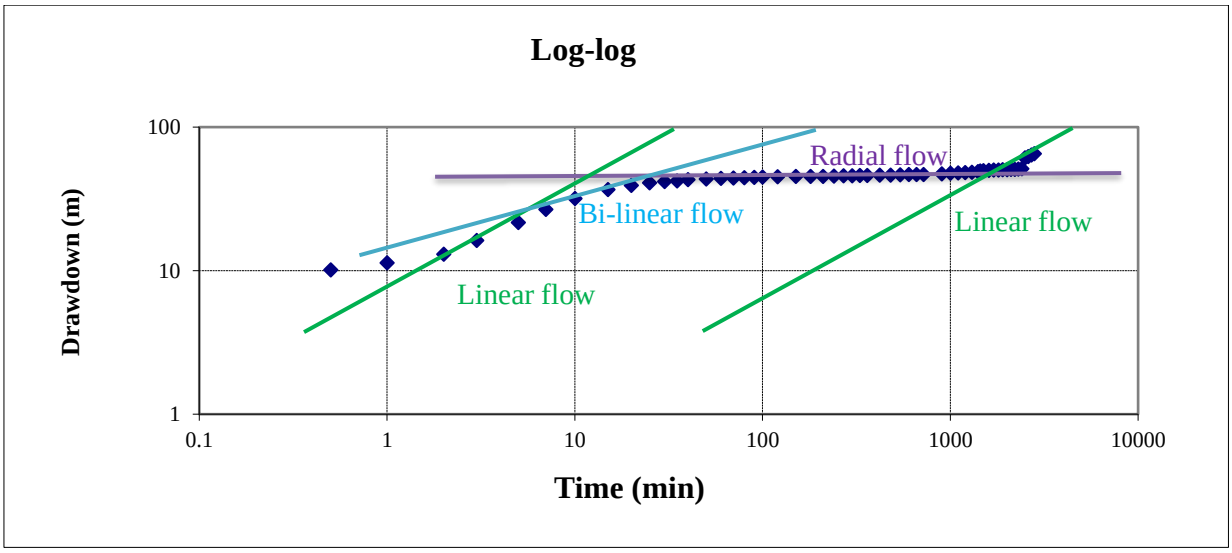


Figure 5-16: Log-log Diagnostic Plot of DEW08 constant drawdown data.

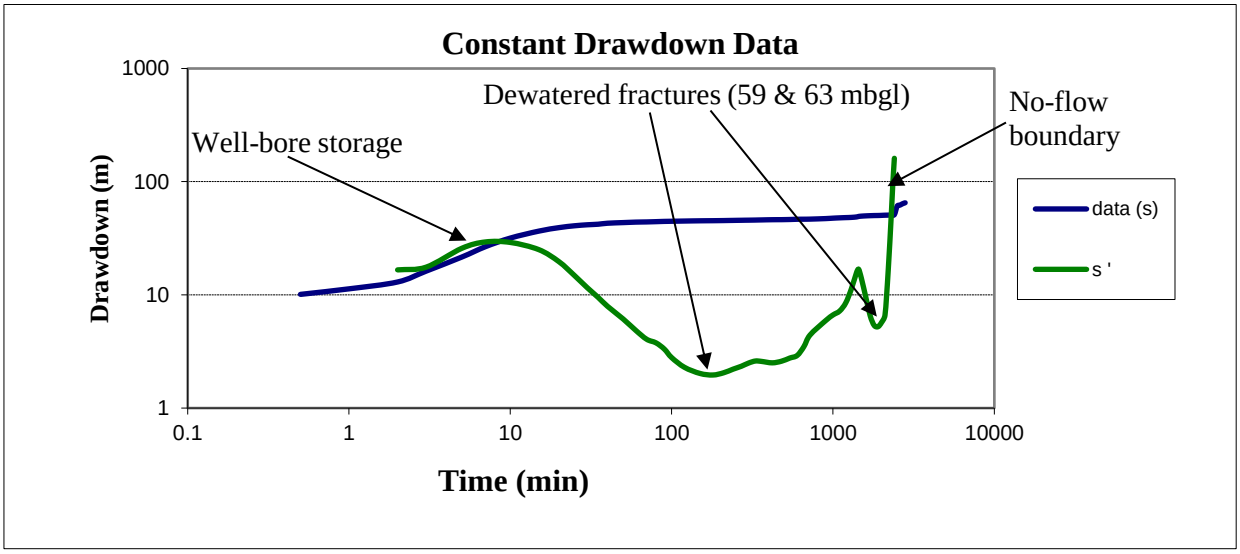


Figure 5-17: Derivative Plot of DEW08 constant drawdown data.

Recovery Test

The Theis (1935) Recovery Method was applied to determine T and K from residual drawdown data based on prevailing unsteady-state flow and confining conditions determined previously. Application of the method assumed the following:

- The aquifer was of infinite radial extent;
- The aquifer was homogeneous, isotropic and of uniform thickness;
- The borehole fully penetrated the aquifer;
- Lateral flow was dominant and unsteady;
- The aquifer was confined; and
- Water discharge from the borehole drew directly from storage.

Figure 5-18 shows residual drawdown plot produced and the line fitted per log cycle between the intermediate and late time to determine residual drawdown change. The method generated a bulk T of 3.4 $x10^{0}$ m^2/d and K of $3.2x10^{-2}$ m/d (saturated thickness of 107 m) as per equation 2.

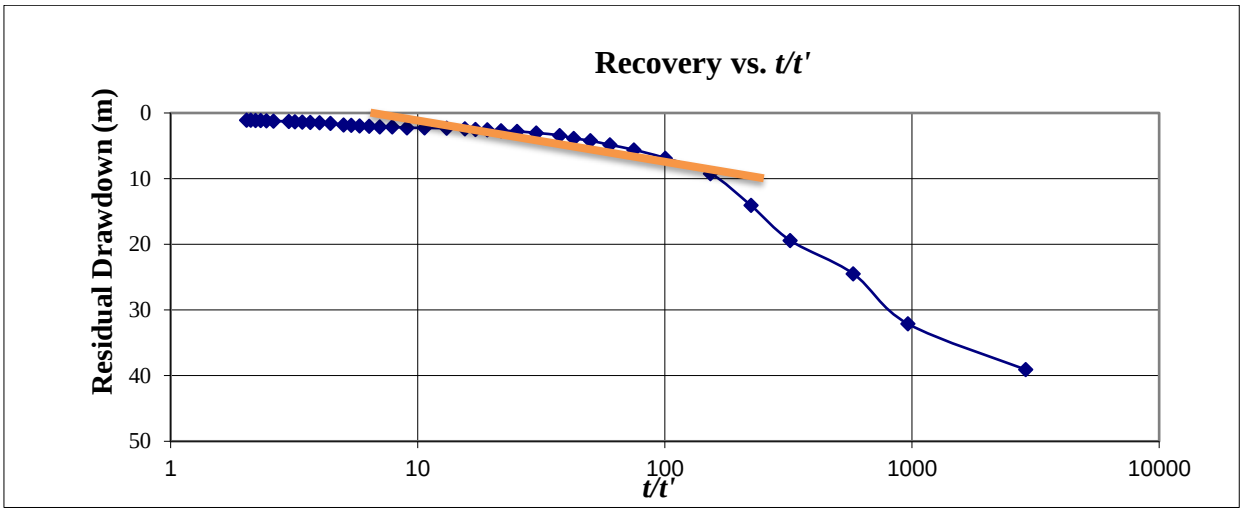


Figure 5-18: Residual drawdown data plot of DEW08.

5.4.2 Airlift Tests

Dewatering pilot boreholes DEW18-1, DEW33 and KH01 were subjected to airlift tests to determine T and K of the rock units (RBX, RSL, SD and CMN) they intersected. Core logs from these boreholes were reviewed during drilling to identify test sections that could potentially have significant water-bearing potential. The boreholes intersected the fractured, faulted and weathered RSL, RBX, SD and CMN units. Analysis of the airlift test data collected from the boreholes and the 22 additional resource exploration and dewatering pilot boreholes tested previously was undertaken using the Theis (1935) Recovery Method. The aforementioned rock units promoted confined and unsteady-state condition, warranting the use of the method. See Table 5-7 for ranges of T and K per rock unit tested for the 25 boreholes tested. See Appendix C for airlift test data analysis per borehole and sections tested. Figure 5-19 illustrates how each analysis was undertaken.

Table 5-7: K and T ranges determined from newly drilled pilot boreholes and an additional 22 boreholes.

Rock Unit	K (m/d)			T (m^2/d)		
	Minimum	Maximum	Average	Minimum	Maximum	Average
SD	$4.2x10^{-3}$	$1.5x10^{0}$	$4.9x10^{-1}$	$3.0x10^{-1}$	$8.4x10^{1}$	$2.9x10^{1}$
CMN	$1.3x10^{0}$	$1.6x10^{2}$	$4.1x10^{1}$	$4.7x10^{1}$	$1.2x10^{4}$	$1.8x10^{3}$
RSL	$3.3x10^{-3}$	$1.5x10^{-2}$	$7.4x10^{-3}$	$1.9x10^{-1}$	$9.5x10^{-1}$	$4.4x10^{-1}$
RBX	$1.7x10^{-2}$	$5.4x10^{1}$	$8.5x10^{0}$	$1.0x10^{0}$	$1.3x10^{3}$	$2.0x10^{2}$

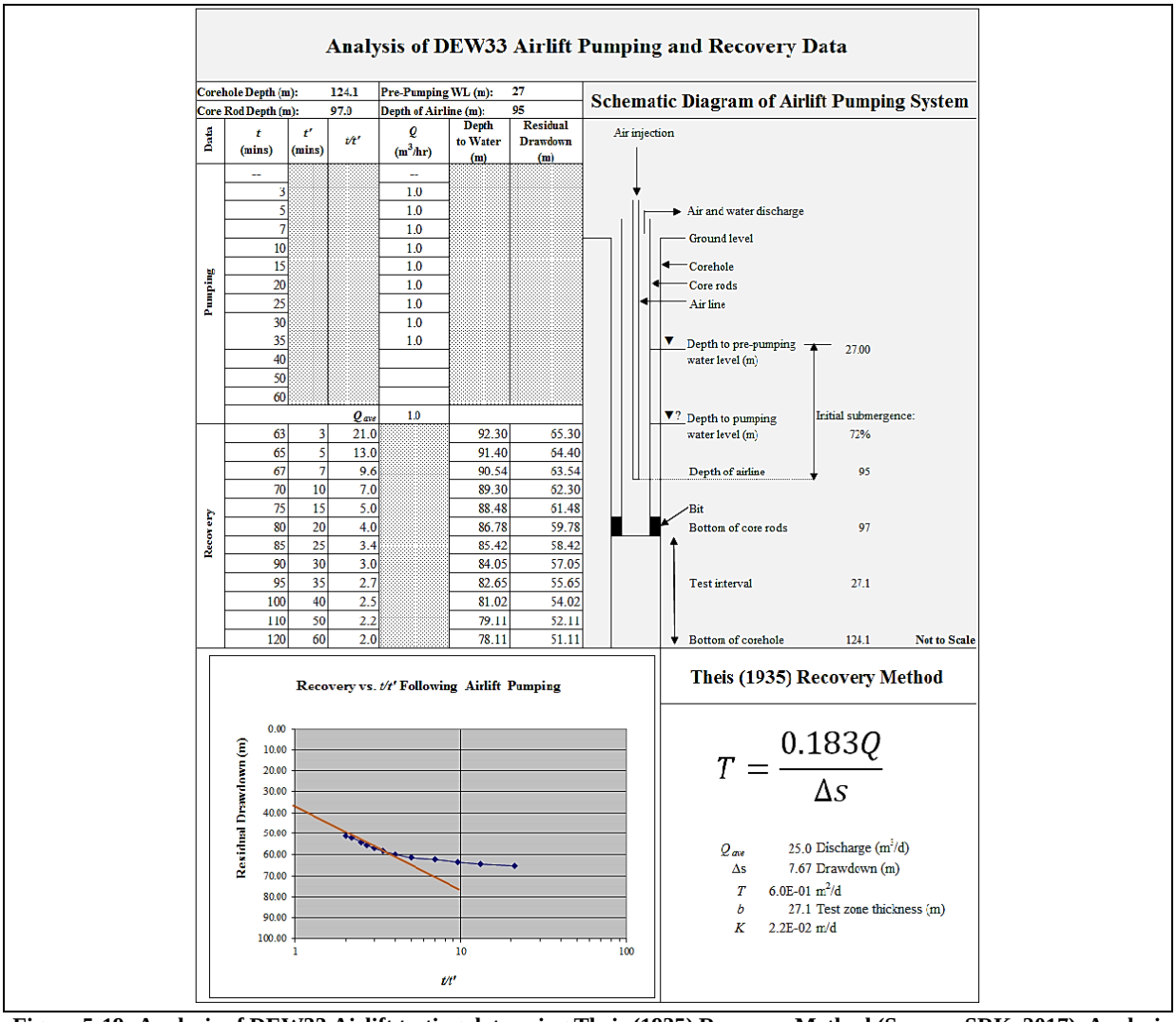


Figure 5-19: Analysis of DEW33 Airlift testing data using Theis (1935) Recovery Method (Source: SRK, 2017). Analysis spreadsheet updated by author.

5.4.3 Slug Tests

Slug tests were conducted in eleven open exploration boreholes located in the eastern part of the Kinsevere concession, targeting saprolite, saprock, shale, siltstone and SD units. The 16 L slug used in the three boreholes could not induce sufficient displacement, so only eight boreholes were analysed using the Bouwer-Rice (1976) Method (equation 3). Table 5-8 presents K and T ranges of rock units intersected and tested. See Appendix D for slug test analysis of boreholes tested and Figure5-20 for illustration of slug test analysis.

Table 5-8: K and T ranges determined from eight resource exploration boreholes.

Rock Unit	K (m/d)			T (m^2/d)		
	Minimum	**Maximum**	**Average**	**Minimum**	**Maximum**	**Average**
Saprolite and saprock – SD	$1.6x10^{-1}$	$7.0x10^{-1}$	$4.3x10^{-1}$	$7.1x10^{0}$	$2.9x10^{1}$	$1.5x10^{1}$
Saprolite and saprock – shale and siltstone	$8.0x10^{-3}$	$2.6x10^{-2}$	$1.5x10^{-2}$	$2.4\ x10^{-1}$	$8.7x10^{-1}$	$5.0x10^{-1}$

See Figure 5-21 for location of boreholes subjected to hydraulic tests. Tables 5-9 and 5-10 present details of boreholes tested.

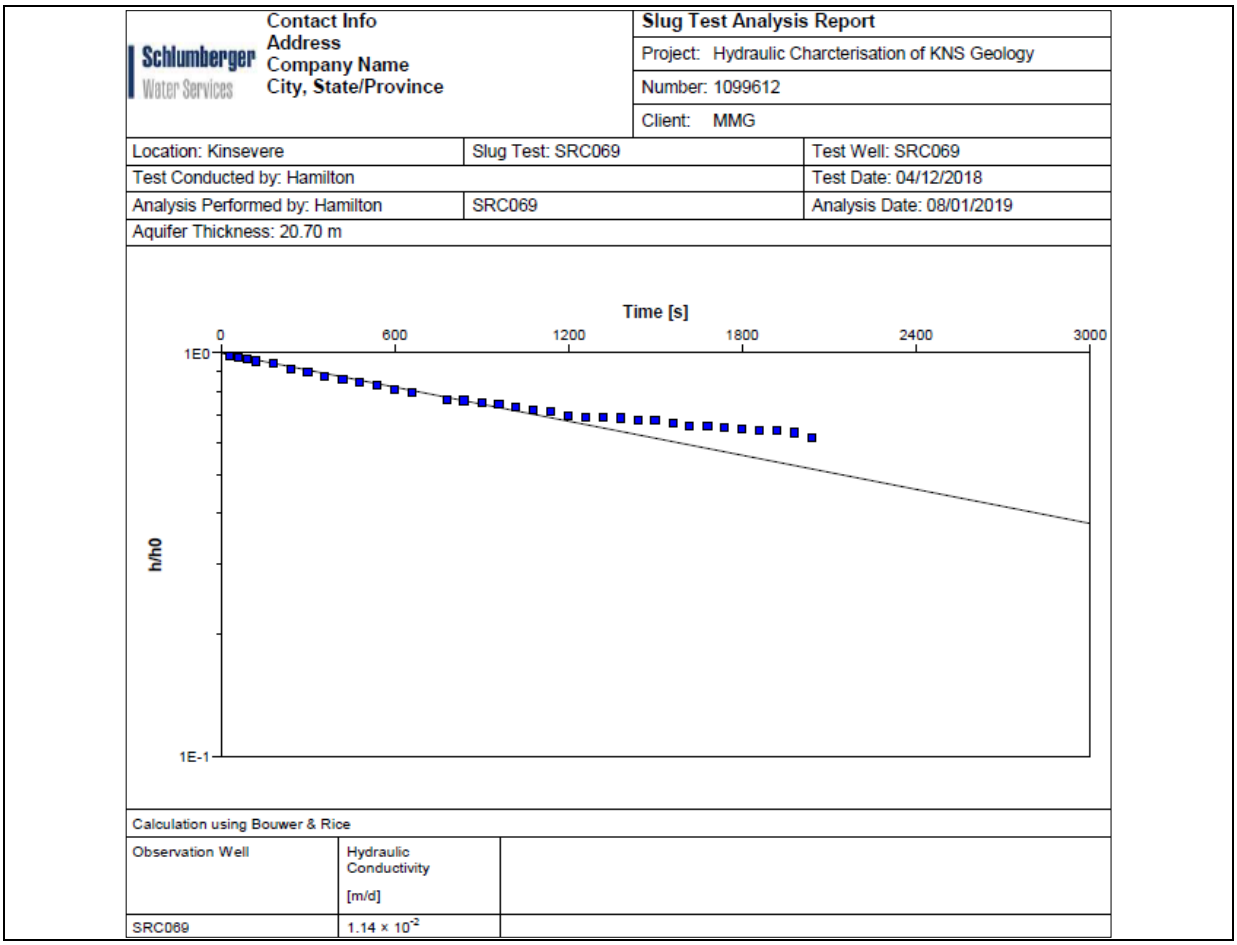


Figure 5-20: Slug test analysis for SRC069 using Bouwer-Rice (1976) in Aquifer Test Pro (2015.1).

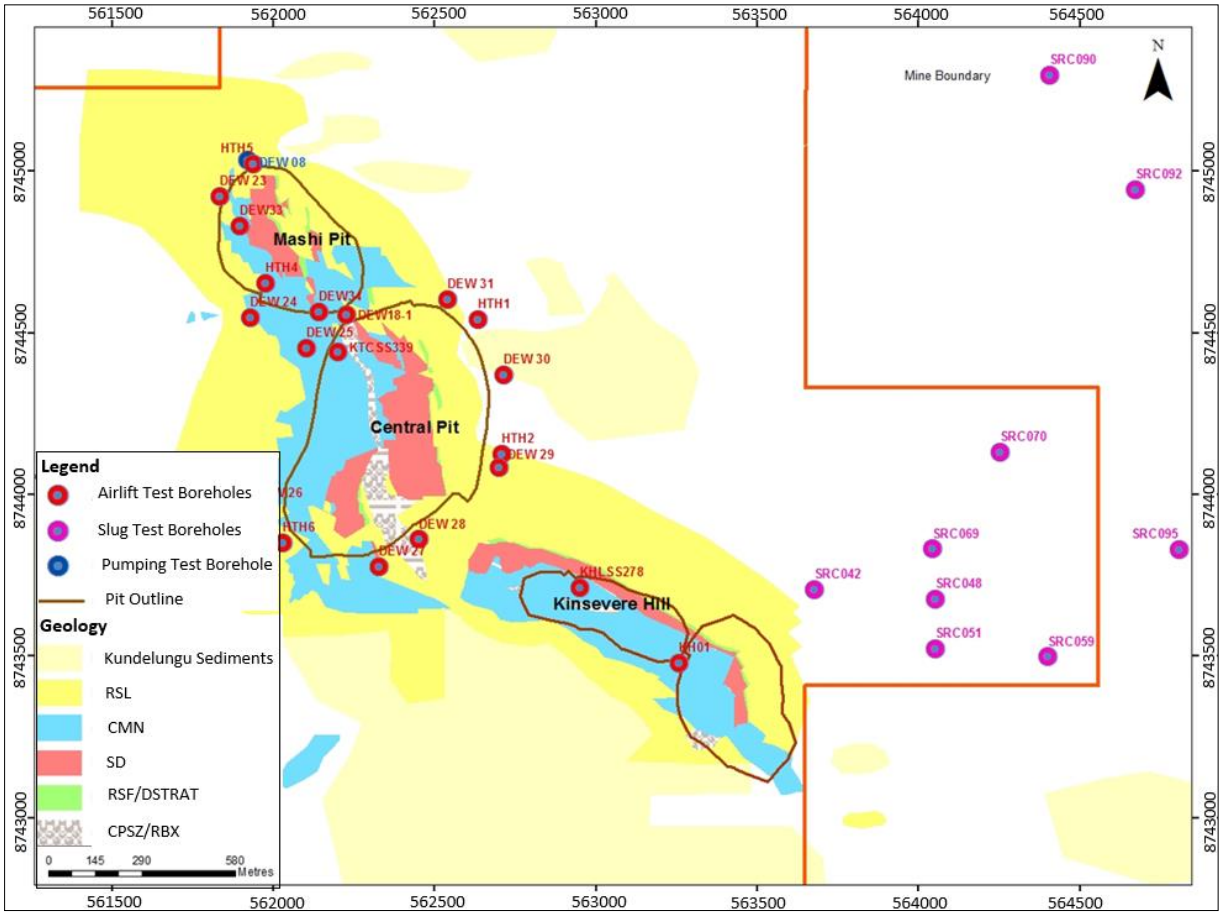


Figure 5-21: Location of boreholes subjected to hydraulic tests (Base map source: SRK, 2018). Borehole data collated by author.

Table 5-9: Summary of hydraulic conductivity (K) and transmissivity (T) data determined from airlift tests.

Borehole I. D	Test	Use	Section Tested			Lithology	Hydraulic Attributes	
			From (mbgl)	To (mbgl)	Saturated Thickness (m)		K (m/d)	T (m^2/d)
DEW18-1	1	DWPB	160	200	40	SD interbedded with fractured CMN	$1.5x10^{0}$	$6.0x10^{1}$
DEW23	1	DWPB	178	255	77	Vuggy massive CMN (178-194m) underlain by massive grey RSL (194-255m)	$7.5x10^{-3}$	$5.8x10^{-1}$
DEW24	1	DWPB	185	251	66	Massive and fractured Red RSL	$7.1x10^{-3}$	$4.7x10^{-1}$
DEW25	1	DWPB	185	250	65	Laminated CMN interbedded with grey RSL (next to fault zone)	$1.5x10^{-2}$	$9.5x10^{-1}$
DEW26	1	DWPB	185	252	67	Vuggy massive CMN	$7.4x10^{0}$	$4.9x10^{2}$
DEW27	1	DWPB	178	250	72	Fractured RBX	$3.1x10^{-2}$	$2.2x10^{0}$
DEW28	1	DWPB	180	250	70	Weathered SD (180-219m) underlain by fractured RBX (219-250m)	$4.2x10^{-3}$	$3.0x10^{-1}$
DEW29	1	DWPB	190	250	60	Fractured RBX	$1.7x10^{-2}$	$1.0x10^{0}$
DEW30	1	DWPB	178	250	72	Fractured, karstified and massive CMN	$1.6x10^{2}$	$1.2x10^{4}$
DEW31	1	DWPB	180	250	70	Massive CMN (180-201m) underlain by SD interbedded with grey RSL (201-250m)	$4.4x10^{-3}$	$3.1x10^{-1}$
DEW33	1	DWPB	97	124	27	Fractured CMN interbedded with SD	$2.2x10^{-2}$	$5.9x10^{-1}$
KH01	1	DWPB	80	110	30	Vuggy, brecciated and fractured CMN	$5.3x10^{1}$	$1.6x10^{3}$
	2		50	80	30	Fractured RBX (50-59m) underlain by vuggy CMN (59-80m)	$6.3x10^{0}$	$1.9x10^{2}$
HTH01	1	HTB	133	157	24	Weathered and fractured RBX	$5.4x10^{1}$	$1.3x10^{3}$
	2		167	187	20	Weathered and fractured RBX	$3.7x10^{1}$	$7.3x10^{2}$
HTH02	1	HTB	126	168	42	Fractured RBX	$3.5x10^{-1}$	$1.5x10^{1}$
	2		174	210	36	Fractured RBX	$4.0x10^{-1}$	$1.4x10^{1}$
	3		264	290	26	Fractured RBX	$2.7x10^{-1}$	$7.0x10^{0}$
HTH03	1	HTB	91	98	7	Weathered grey RSL	$3.1x10^{1}$	$2.1x10^{2}$
	2		110	134	24	Highly Weathered CMN	$1.2x10^{2}$	$2.9x10^{3}$
	3		146	213	67	RSL	$6.3x10^{-3}$	$4.2x10^{-1}$
	4		214	250	36	RSL	$5.2x10^{-3}$	$1.9x10^{-1}$
HTH04	1	HTB	106	133	27	Fractured and karstified CMN	$5.1x10^{1}$	$1.4x10^{3}$
	2		165	189	24	Fractured RBX	$2.0x10^{1}$	$4.8x10^{2}$
	3		220	250	30	Fractured and Fresh CMN and grey RSL	$8.2x10^{-3}$	$2.5x10^{-1}$

Borehole I. D	Test	Use	Section Tested			Lithology	Hydraulic Attributes	
			From (mbgl)	To (mbgl)	Saturated Thickness (m)		K (m/d)	T (m^2/d)
HTH05	1	HTB	64	111	47	Fractured RBX	$1.5x10^{-1}$	$7.0x10^{0}$
	2		108	150	42	Fractured RBX	$9.7x10^{-2}$	$4.1x10^{0}$
HTH06	1	HTB	98	105	7	Fractured RBX	$1.8x10^{0}$	$1.2x10^{1}$
	2		143	203	60	Fractured CMN and grey RSL	$6.2x10^{-1}$	$3.7x10^{1}$
	3		208	250	42	RBX	$3.0x10^{-2}$	$1.3x10^{0}$
KSV-SS-05	1	ERB	221	245	24	Fractured and karstified CMN	$2.6x10^{0}$	$6.2x10^{1}$
	2		245	281	36	Fractured and karstified CMN	$1.3x10^{0}$	$4.7x10^{1}$
	3		280	301	21	Fractured and karstified CMN	$4.5x10^{0}$	$9.5x10^{1}$
KSV-17003	1	ERB	120	145	25	Vuggy, brecciated, fractured and massive CMN	$6.2x10^{1}$	$1.5x10^{3}$
	2		120	181	61	Fractured and karstified CMN	$1.5x10^{1}$	$9.2x10^{2}$
KTC-SS-320	1	ERB	206	331	125	RBX	$3.6x10^{0}$	$4.5x10^{2}$
	2		220	274	54	Weathered and fractured RBX	$3.7x10^{0}$	$2.0x10^{2}$
KSV-17005	1	ERB	194	265	71	Fractured and laminated CMN	$2.4x10^{0}$	$1.7x10^{2}$
	2		265	307	42	Fractured RSL	$2.1x10^{-1}$	$8.6x10^{0}$
KSV-17004	2	ERB	104	197	93	RBX (104-128m) underlain by fractured, vuggy CMN (128-197m)	$9.0x10^{-1}$	$8.3x10^{1}$
KSV-SS-051	1		72	140	68	Fractured RSL	$3.3x10^{-3}$	$2.2x10^{-1}$
KSV-SS-69	1		104	197	93	Fractured SD	$9.0x10^{-1}$	$8.4x10^{1}$

* DWPB- Dewatering Pilot Borehole
* HTB- Hydrogeological Test Borehole
* ERB-Exploration/Resource Borehole

Table 5-10: Summary of hydraulic conductivity (K) and transmissivity (T) data determined from slug tests.

Borehole I. D	Use	Section Tested			Displacement Source	Volume (L)	Lithology	Hydraulic Attributes	
		From (mbgl)	To (mbgl)	Thickness (m)				K (m/d)	T (m^2/d)
SRC042	REB	0	42	42	Water	729	Saprolite and Saprock – SD	$7.0x10^{-1}$	$2.9x10^{1}$
SRC048	REB	0	44	44	Water	2 700	Saprolite and Saprock – SD	$1.6x10^{-1}$	$7.1x10^{0}$
SRC051	REB	0	37	37	Water	370	Saprolite and Saprock – SD	$3.4x10^{-1}$	$1.3x10^{1}$
SRC059	REB	0	23	23	Water	-	Saprolite and Saprock – SD	$5.1x10^{-1}$	$1.2x10^{1}$
SRC064	REB	0	48	48	Water	-	Saprolite and Saprock – Shale and Siltstone	$1.3x10^{-2}$	$6.3x10^{-1}$
SRC066	REB	0	34	34	Water	-	Saprolite and Saprock – Shale and Siltstone	$2.6x10^{-2}$	$8.7x10^{-1}$
SRC069	REB	0	21	21	Water	-	Saprolite and Saprock – Shale and Siltstone	$1.1x10^{-2}$	$2.4x10^{-1}$
SRC070	REB	0	32	32	Water	-	Saprolite and Saprock – Shale and Siltstone	$8.0x10^{-3}$	$2.6x10^{-1}$
SRC090	MB	0	102	102	Slug	16	Saprolite, Saprock, Shale and Siltstone	Insufficient water displacement	
SRC092	MB	0	120	120	Slug	16	Saprolite, Saprock, Shale and Siltstone	Insufficient water displacement	
SRC095	MB	0	120	120	Slug	16	Saprolite, Saprock, Shale and Siltstone	Insufficient water displacement	

* REB- Resource Exploration Borehole
* MB- Monitoring Borehole

5.5 Groundwater Recharge

The chloride concentrations together with the MAP were used as input parameters (Table 5-11) into the CMB method equation (4) to determine groundwater recharge across the Kinsevere concession.

Table 5-11: Input parameters used for recharge calculation.

Recharge *(R)* Input Parameters	**Unit**	**Value**
Mean annual precipitation depth (P)	mm/yr	1 084
Chloride concentration in precipitation (Cl_p^-)	mg/L	0.6
Chloride concentration in groundwater within the pit area (Cl_{GW}^-)	mg/L	2.2
Chloride concentration in groundwater within the Kinsevere surrounds (Cl_{GW}^-)	mg/L	12.1

Recharge within the pits was determined to be 28% of MAP (298 mm/yr), attributed to the exposed fractured and karstified RBX, CMN and SD units. Kinsevere surrounds had a recharge of 5% of MAP (54 mm/yr) due to the highly weathered RSL and saprolite units of relatively low permeability. The estimates determined were in line with those determined by the KP (2010) and SRK (2016). Recharge values determined are typical of the Kinsevere area.

5.6 Groundwater Inflow Calculations

The Dupuit-Forchheimer Analytical Method (equations 5, 6, 7 and 8) was used to determine groundwater inflows into the pits. Groundwater inflows into the Mashi Pit were determined to be 83 L/s, with 42 L/s predominantly stemming from the pit highwall on the northeastern and northwestern portions attributed to dissolution fissures between the fractured RBX, SD, RSL, RBX-CMN contacts together with NE – SW and NW – SE trending faults. The difference (41 L/s) stemmed from the pit floor, through exposed cavities, fractures and RSL, RBX, CMN and SD units which had an upward flow due to hydrostatic pressure. The estimates fell in line with those determined by SRK (2018). Assuming no additional dewatering boreholes are installed, highwall inflows could increase to 130 L/s once terminal depths are reached. Total inflows could be 171 L/s. Inflows in the Central Pit were determined to be 545 L/s, with most inflows having stemmed from the highwall (335 L/s). Pit floor inflows accounted for the difference. The 25 m water column in this pit masked these inflows. Estimated inflows aligned with those estimated by SRK (2018). Inflows from the pit highwall are expected to increase as mining progresses with depth, with projected total inflows of 1 103 L/s at terminal depth, assuming no additional dewatering is undertaken.

No estimations were undertaken for the current Kinsevere Hill Pit as the pit had negligible ingress. Projected inflows into the Kinsevere Hill North and South pits were 27 L/s and 135 L/s, respectively. Pit floor (17 L/s) inflows exceeded the highwall (10 L/s) contribution in the Kinsevere North Pit. Pit highwall (79 L/s) contribution could be higher than the pit floor (56 L/s) contribution in the Kinsevere Hill South Pit once terminal depths are reached. Table 5-12 summarises pit inflows determined. Refer to Appendix E for equations, groundwater inflow input parameters and calculations.

Table 5-12: Summary of pit inflows determined.

Pit	**Pit Depth (mbgl)**	**Highwall Inflows (L/s)**	**Pit floor Inflows (L/s)**
Mashi	60	42	41
	135	130	41
Central	140	334	210
	305	893	210
Kinsevere Hill North	30	Minor inflows observed	
	40	10	17
Kinsevere Hill South	85	79	135

6 Discussion

6.1 Hydraulic Characterisation

6.1.1 Saprolite and Saprock Units

Saprolite and saprock units represent the in-situ chemically weathered derivative of parent rocks, both varying in the preservation extent of the parent rock fabric and volume. The saprolite occurred as variably coloured (reddish brown, grey and black), fine grained, clayey, soft and moderate to highly weathered material, while the saprock unit had similar attributes, with the exception of the degree of weathering, clay composition and competency, marking the transition zone between the highly weathered upper saprolite unit and the parent rock.

The saprolite and saprock stemming from weathering of shale and siltstone rock units had a low K of $8.0x10^{-3}$ – $2.6x10^{-2}$ m/d and a T of $2.4x10^{-1}$ – $8.7x10^{-1}$ m^2/d. The low K range was slightly higher than that typically assigned for siltstone and shale units. This contrast was attributed to the structural fabric of the shale and siltstone units induced by D1 – D3 phase deformation preserved within the saprock unit, enhancing hydraulic connection together with lateral and vertical flow. The relatively higher K of the shale unit was typical of the copperbelt, as noted at Ruashi Mine, having a K of $1.0x10^{-1}$ m/d.

The saprolite unit promoted water retention, lateral flow, confining and perched conditions due to its highly weathered fabric. Saprolites and saprock units of the SD parent rock had intermediate hydraulic attributes, with a K of $1.6x10^{-1}$ – $7.0x10^{-1}$ m/d and a T of $7.1x10^{0}$ – $2.9x10^{1}$ m^2/d, due to the structural and dissolution features retained within the saprock, promoting double porosity, moderate hydraulic connection, high storage capacity and both lateral and vertical flow.

6.1.2 RSL Unit

The RSL unit occurred as red or brown, fine to medium grained, massive to irregularly bedded, with a clayey to silty matrix, of moderate to high weathering and slight to moderate fracturing with depth. The unit had low hydraulic attributes, with a K of $3.3x10^{-3}$ – $1.5x10^{-2}$ m/d and T of $1.9x10^{-1}$ – $9.5x10^{-1}$ m^2/d. The extent of weathering together with the siliceous and argillaceous nature of this unit limit groundwater within the matrix, promoting water retention, lateral flow, confining and perched conditions. Fractured sections of this unit induced hydraulic connection with underlying and adjacent units, promoting double porosity and a vertical flow component. These attributes could expedite slope failure when the rock unit is extensively saturated and pore pressures increased. The low K values determined correlate to those determined at the Ruashi Mine and DIMA Area.

6.1.3 RBX Unit

The RBX unit predominantly occurred along a shear zone bisecting the pits, appearing as grey, fine to medium grained, with a siliceous and dolomitic matrix, moderately and highly weathered, moderate to highly fractured, with clasts of variable sizes, and brecciated. The unit had low to high K of $1.7x10^{-2}$ – $5.4x10^{1}$ m/d and a T of $1.0x10^{0}$ – $1.3x10^{3}$ m^2/d, attributed to its polymictic nature. Faulting, fracturing, brecciation and minor dissolution features observed promote high hydraulic attributes and double porosity, while its siliceous and argillaceous nature in places, limit hydraulic connection and retard flow. K ranges determined aligned with those of at Ruashi Mine.

6.1.4 SD Unit

The SD unit is the thickest dolomitic shale package at Kinsevere, occurring as dark brown, grey to black, fine-grained, laminated or rhythmically bedded, dolomitic with a shale constituent, carbonaceous, with pyrite and magnesitic veins, dissolution features in places, slight to moderately fractured, weathered and interbedded with dolomitic siltstone. It had a moderate to high K of $4.2x10^{-3}$ – $1.5x10^{0}$ m/d and T of $3.0x10^{-1}$ – $8.4x10^{1}$ m^2/d. The lower end of the K range was due to the argillaceous shale bedding, limiting hydraulic connection by promoting lateral flow and primary porosity, while the higher end was attributed to the faulting, fracturing and dissolution of the dolomitic component, promoting groundwater storage and transfer, together with secondary porosity. A similar case was observed at Ruashi, where the K was $3.0\ x10^{0}$ m/d, attributing to yields of up to 111 L/s.

6.1.5 CMN Unit

The CMN was the most water-bearing unit at Kinsevere, occurring as grey or pink, fine grained, laminated, dolomitic, and magnesitic, with siltstone of variable organic matter, extensive vein density, nodular in places, weathered and fractured in places and having extensive dissolution features (vugs and cavities). It had a high K of $1.3x10^{0}$ – $1.6x10^{2}$ m/d and T of $4.7x10^{1}$ – $1.2x10^{4}$ m^2/d. The high K was attributed to extensive faulting and fracturing stemming from D1 – D3 phase deformation, karstic and vuggy features, promoting high storage, hydraulic connection and double porosity

6.1.6 Bulk Units

A combination of RSL, SD and CMN units had a bulk K of $3.2x10^{-2}$ m/d, T of $3.4\ x10^{0}$ m^2/d and S of 0.1. In the DIMA Area, the CMN and SD units had a bulk K of $7x10^{-1}$ – $2.1x10^{1}$ m/d, T of $3.7x10^{3}$ – $4.0x10^{4}$ m^2/d and S of 0.0006 – 0.12. The K values fell within an order of magnitude of each other, while the T values showed significant differences because of variable thickness of the zones tested.

6.2 Pore Pressures

Increased pore pressures on account of oversaturation stemming from rainfall and groundwater inflows lead to failure in rocks of low permeability and weakened self-retainability. Pore pressure measurement undertaken within HTH boreholes in the Kinsevere concession suggested increased upward hydrostatic pressures of up to 1.8 MPa on the western portions of the Mashi and Central pits within the RBX, RSL and CMN units. Extensive saturation loading along this portion could potentially lead to slope failure as pore pressures increase within the rock units, more so, in the RSL unit and along its contact with other rock units and along faults zones. Increased upward hydrostatic pressures tend to result in heaving of the pit floor as mining progresses deeper. This will not be the case in Kinsevere as the rock units within the pit are predominantly competent and inclined, however, introduction of significant volumes of water through the pit floor could occur on account of these pressures. Slope failures experienced at Ruashi Mine occurred due to saturation loading of the highwalls by introduction of significant volumes of water.

6.3 Groundwater Inflows

Groundwater ingress into the pits predominantly occurred through the highwalls, with the Mashi and Central pits experiencing lateral inflows of 42 L/s and 335 L/s, respectively. Inflows in the Mashi Pit predominantly occurred in the northeastern and northwestern potions of the highwall, while those of the Central Pit were masked by the pit-lake. Inflows from the Mashi and Central pit floor were 41 L/s and 21 L/s, respectively. Mine progression could result in increased inflows as the siliceous and dolomitic rock units and structures are exposed.

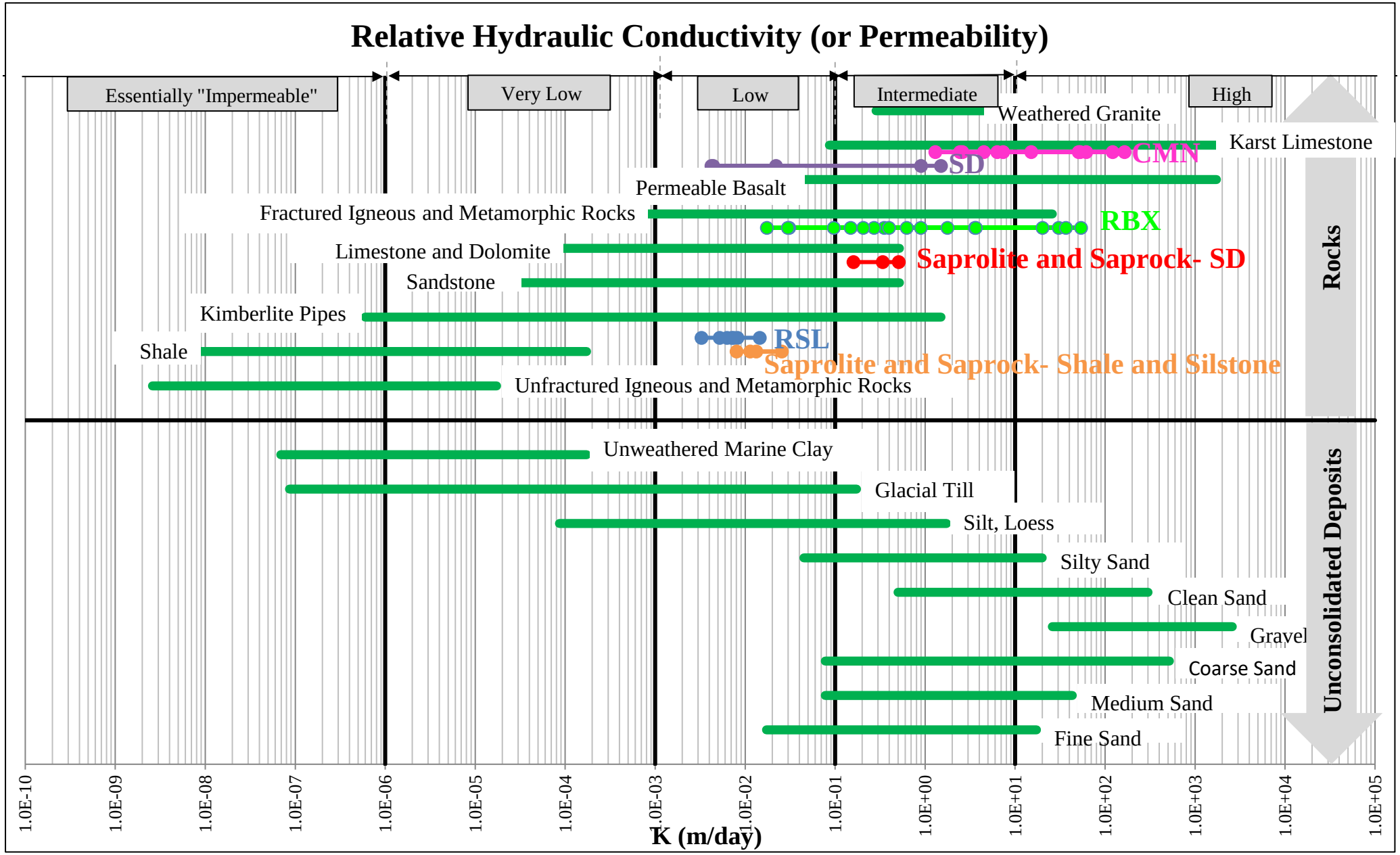


Figure 6-1: Hydraulic conductivity values determined from hydraulic tests plotted over generic results presented in USGS (2003).

7 Hydrogeological Conceptual Model

The Kinsevere operation comprised the Mashi, Central and Kinsevere Hill pits, sitting at depths of 1 150 mamsl, 1 070 mamsl and 1 170 mamsl, respectively. Surface elevations across the operation ranged from 1 180 mamsl in the north to 1 291 mamsl in the south. The concession experienced a MAP of 1 084 mm and a MAE of 1 071 mamsl, exceeding precipitation during dry months. Precipitation, as rainfall, either run off towards the river; collected atop TSFs, WRDs and OSs; evaporated; fell into pits or infiltrated through the saprolites, saprock and parent rock units and into the groundwater system as recharge. Groundwater recharge in the pit area was 28% of MAP (298 mm/yr) while the concession surrounds received 5% (54 mm/yr). Higher recharge in the pit area was attributed to the exposed fractured and karstified RBX, CMN and SD units, while the lower recharge in the concession was due to the highly weathered RSL and saprolite units of relatively low permeability. Groundwater levels in the pit area responded sooner to precipitation than the concession surrounds due to limited overburden on account of mining.

Groundwater levels across the concession ranged between 1 173 mamsl and 1 186 mamsl, with an average depth of 39 mbgl. Groundwater strikes were intersected at depths of 9 mbgl within the upper weathered and transition sections and as deep as 194 mbgl within the underlying fractured and karstified rock units. Levels in the Mashi Pit sat slightly above the pit floor, at elevations of 1 178 mamsl in the northeastern portion and 1 160 mamsl in the northwestern portion, leading to inflows of 42 L/s through the highwalls and 41 L/s through the pit floor. The Central Pit was under pit lake conditions, having a 25 m column of water, with levels at 1 095 mamsl, masking inflows of 545 L/s from the pit highwalls and floor. The Kinsevere Hill pit had levels of 1 m above the pit floor. Negligible inflows were observed due to hydraulic heads having negligible drive. Overall pit inflows exceeded the discharge rate.

Groundwater level mounds prevailed beneath the TSF, WRD and OS facilities. The saprolite, saprock, RSL, RBX, SD and CMN units together with their respective lithologic and hydraulic attributes, enhanced by extensive folding, faulting, fracturing, brecciation and/or dissolution, influence groundwater compartmentalisation and define their capacity to receive, store and transmit water as aquifers should. The hydrostratigraphy at Kinsevere was delineated as follows based on common lithologic and hydraulic attributes (Figure 7-1):

- **Siliceous Aquifer** – poorly developed, low yielding and comprised saprolite, saprock, shale, siltstone and RSL units of low permeability, predominantly limiting water to within the matrix and promoting lateral flow (unless fractured). Acted at confining layers in places and induced perched conditions. Had low structural integrity and capacity to retain significant volumes of water that may lead to slope failure along weak zones and as the upward hydrostatic pressures increase with saturation. The highest K in this unit was $7.0x10^{-1}$ m/d, with a T of $2.9x10^{1}$ m^2/d;
- **Polymictic Aquifer** – comprised the RBX unit and occurred along fault zones. It was of moderate yield on account of having both siliceous and dolomitic cementing agents. The unit was weak with irregular to parallel bedding. Groundwater transfer predominantly occurred along the fractured and brecciated zones. The polymictic nature promoted both lateral and vertical flow, together with double porosity. The K of this aquifer could get as high as $1.5x10^{0}$ m/d, with a T of $8.4x10^{1}$ m^2/d ; and
- **Dolomitic Aquifer** – comprised SD and CMN units that were well developed, confined and high yielding, with well-interconnected cavities, vugs, faults and fractures promoting significant groundwater storage and transfer. The aquifer had a K of up to $1.6x10^{2}$ m/d and T of $1.2x10^{4}$ m^2/d. The bulk S (including RSL) was 0.1.

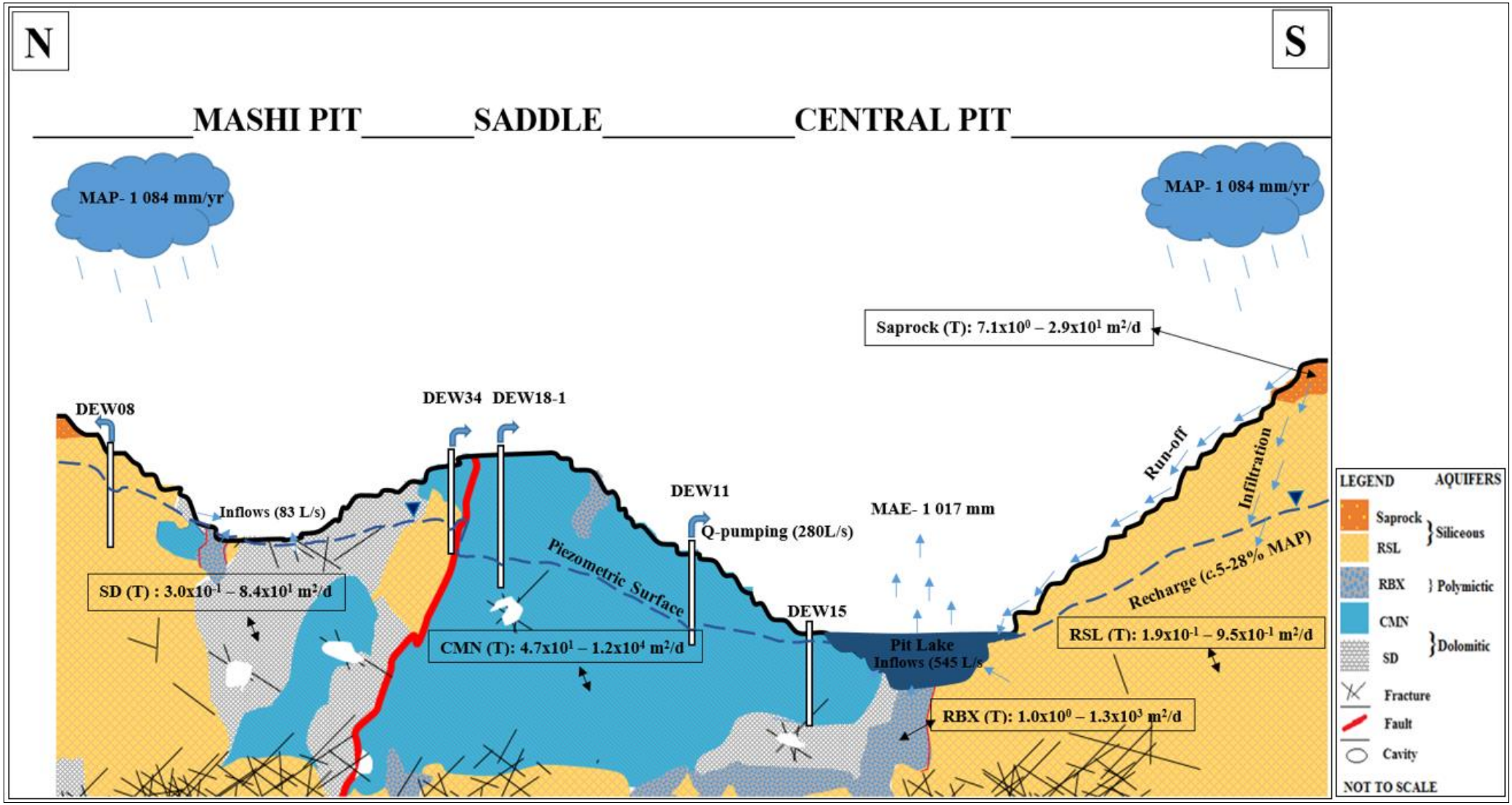


Figure 7-1: Hydrogeological conceptual model (Source: SRK, 2016). Updated and modified by author.

8 Conclusions and Recommendations

Rock units and structures underlying the Kinsevere concession define hydrogeological conditions. Their respective lithologic and hydraulic attributes influence the capacity of the rock units to receive, store and transmit groundwater. The Siliceous Aquifer had relatively low permeability, having capacity to retain water or promote lateral flow and confined conditions. Oversaturation of this unit in the pit area may often lead to slope failure as the unit was of poor structural integrity and had an upward hydrostatic pressure component. The highest K in this unit was $7.0x10^{-1}$ m/d, with a T of $2.9x10^{1}$ m^2/d, attributed to the saprolite and saprock unit derivatives of the SD unit that was fractured and vuggy.

The Polymictic Aquifer was extensively faulted, fractured, weathered, karstified, dolomitised and silicified, with a double porosity characteristic and enhancing hydraulic connection with adjacent units. Contact zones of the RBX unit with RSL, SD and CMN units were highly transmissive due to faulting and resultant weathering. Upward hydrostatic pressures were noted within this aquifer. This unit spanned through the centre of the pits, which may likely lead to groundwater ingress through the pit floor via this unit. The K of this aquifer was $1.5x10^{0}$ m/d, with a T of $8.4x10^{1}$ m^2/d. The Dolomitic Aquifer had the highest hydraulic capacity, introducing significant volumes of water into the pits. The K of this unit was $1.6x10^{2}$ m/d, with a T of $1.2x10^{4}$ m^2/d, attributed to extensive faulting, fracturing and dissolution cavities, promoting groundwater storage and transmission within the matrix and apertures. An upward hydrostatic component prevailed.

Mine progression has a potential to remove storage, increasing the groundwater sink towards the pit, leading to introduction of water into the pits via exposed structures and cavities on the highwall and pit floor. Although structural features such as faults, fractures and shear zones tend to promote groundwater storage and transfer between rock units, the SW – NE sinistral fault transecting the Mashi and Central pits behaved conversely, acting as a barrier to flow. In addition, the fault and its offshoots compartmentalized the area as highlighted by the 42 m difference in groundwater levels between the two pits. Groundwater ingress into the Central Pit was 535 L/s while that of the Mashi Pit was 83 L/s. The groundwater ingress exceeded the dewatering discharge of 280 L/s. Merging of the Mashi and Central pits into one large split pit could expose the sinistral fault and units at depth. Exposure of this fault could not contribute groundwater to the pits, however, groundwater ingress into the pits could increase as and when the CMN, SD and RBX units, of moderate to high hydraulic capacity and connection, get exposed.

All units need to be dewatered and the pore pressures monitored. Additional perimeter dewatering boreholes should be drilled to manage inflows. Horizontal drain boreholes should be installed to depressurize the highwalls. Rain water, horizontal borehole discharge and residual inflows should be directed to sumps using trenches and pumped ex-pit. Groundwater levels should be kept at least 10 m below the pit floors to ensure safe mining conditions.

The findings of this research are believed to add to the existing hydraulic knowledge of the shale, siltstone, RSL, RBX, SD and CMN rock units belonging to the Roan and Kundelungu groups of the Katanga Supergroup, together with their weathered derivatives (saprock and saprolite). The use of the airlift test method proved to be useful in isolating specific rock units and geological structures for hydraulic testing.

References

1. Anand, R. R. and Paine, M. (2002). Regolith geology of the Yilgarn Craton, Western Australia: implications for exploration. *Australian Journal of Earth Sciences*, vol. 49, pp. 3-162.
2. Batumike, M. J., Kampunzu, A. B. and Cailteux, J. L. H. (2003). Petrology and geochemistry of the Neoproterozoic Nguba and Kundelungu Groups, Katangan Supergroup, southeast Congo: Implication for provenance, paleoweathering and geotectonic setting. *Journal of African Earth Sciences*, vol. 44, pp. 97-115.
3. Beekman, H. E. (2000). Groundwater Recharge: Assessment and estimation Techniques in Southern Africa, Lecture notes WREM Hydrogeology Course UZ-Civil Eng. Dept. Zimbabwe, 17-18, pp. 25.
4. Beekman, H. E., Selaolo, E. T., Van Elswijk, R. C., Lenderink, N. and Obakeng, O. T. O. (1997). Groundwater recharge and resources assessment in the Botswana Kalahari-Chloride and isotope profiling studies in the Letlhaken-Botlhapatlou and Central Kalahari areas, GRES II Technical Report, pp. 112.
5. Batumike, M. J., Cailteux, J. L. H. and Kampunzu, A. B. (2007). Lithostratigraphy, basin development, base metal deposits and regional correlations of the Neoproterozoic Nguba and Kundelungu rock succession Central African Copper Belt. *Gondwana Research*, vol.11, pp. 432-447.
6. Bohlweki Environmental (Pty) Ltd. (2007). Air quality impact assessment for the Kinsevere mining and smelter operations, north of Lubumbashi, Democratic Republic of Congo.
7. Bourdet, D., Whittle, T. M., Douglas, A. A. and Whittle, T. M. (1983). A new set of type curve simplifies well test analysis. *World oil*, Gulf Publishing company, pp. 1-7.
8. Bourdet, D., Ayoub, J. A. and Pirard, Y. M. (1989). Use of pressure derivative in well-test interpretation. *SPEFE*, pp. 293-302.
9. Bouwer, H. and Rice, R. C. (1976). A slug test for determining hydraulic conductivity of unconfined aquifers with completely or partially penetrating wells. *Water Resources Research*, vol. 12 (3), pp. 423-428.
10. Bredenkamp, D. B., Botha, L. J., van Tonder, G. J. and van Rensburg, H. J. (1995). Manual on quantitative estimation of groundwater recharge and aquifer storativity. *Water Research Commission*, pp. 407.
11. Buffard, R. (1988). Un rift intracontinental du Precambrian superieur: Le Shaba meridionial (Zaire). PhD thesis. University of Maine, France.
12. Bull, S., Selly, D., Hitzman, M. (2010). A sequence- and chemo- stratigraphic interpretation of the Central African Copperbelt, CODES/AMIRA P872: Sediment-hosted copper deposits of Congolese, Zambian and Australian basin systems.
13. Bumby, A. J and Giraud, R. (2005). The geodynamic setting of the Phanerozoic basin of Africa. *Journal of African Earth Sciences*, vol. 43, pp. 1-12.
14. Cahen, L, Delhal, J. and Deutsch S. (1967). Rubidium-strontium geochronology of some granitic rocks from the Kibaran belt (Central Katanga, Rep. of the Congo). *Annales des Sciences Géologiques, Musée Royal de l'Afrique Centrale*, Tervuren, Série in 8, pp. 65.
15. Cahen, L., Snelling, N. J., Delhal, J., Vail, J. R., Bonhomme, M. and Ledent, D. (1984). The geochronology and evolution of Africa. *Clarendon Press Oxford*, pp. 512.

16. Cailteux, J. (1994). Lithostratigraphy of the Neoproterozoic Shaba-type (Zaire) Roan Group and metallogenesis of associated stratiform mineralisation. *Journal of African Earth Sciences*, vol. 19, pp. 279-301.

17. Cailteux, J. and Kampunzu A. B. (1995). The Katangan tectonic breccias in the Shaba Province (Zaire) and their genetic significance; In Wendorff, M. and Tack, L. (eds.) Late Proterozoic Belt in central and Southern Africa. *Annales des Sciences Géologiques, Musée Royal de l'Afrique Central*, vol. 101, pp. 49-62.

18. Cailteux, J., Kampunzu, A. B., Lerouge, C., Kaputo, A. K. and Milesi, J. P. (2005). Genesis of sediment-hosted stratiform copper-cobalt deposits, Central African Copperbelt. *Journal of African Earth Sciences*, vol. 42, pp. 134-158.

19. Campbell, M. D., Starret, M. S., Fowler, J. D. and Klein, J. J. (1990) Slug tests and hydraulic conductivity. I*n Proceedings of Petroleum hydrocarbons and organic chemicals in groundwater*, October 31- November, pp. 85-99.

20. Chironga, L. (2013). Designing a dewatering plan for the Ruashi Mine in the Democratic Republic of Congo, MSc thesis, University of the Free State.

21. Cooper, H. H. and Jacob, C. E. (1946). A generalised graphical method for evaluating formation constants and summarizing well field history, *Am. Geophys. Union Trans*., vol. 27, pp. 526-534.

22. Dresher, W. H. (2001). How hydrometallurgy and the SX/EW Process Made Copper the Green Metal. Copper Development Inc, pp. 4.

23. Eggleton, R. A. (2001). 'The regolith glossary. (Cooperative Centre for Landscape Evolution and Mineral Exploration, National Capital Printing: Canberra, ACT).

24. Erriksson, E. and Khunakasem, V. (1969). Chloride concentration in groundwater, recharge rate and rate of deposition of chloride in the Israel coastal plain. *Journal of Hydrology*, vol. 7, pp. 178-197.

25. Evans, D. G., Nunn, J. A. and Hanor, J. S. (1991). Mechanisms driving groundwater flow near salt domes. *Geophysical Research Letters*, vol. 18, issue 5, pp. 927-930

26. Francois, A., (1973). L'extrémité occidentale de l'arc cuprifère shabien. Etude géologique, Gécamines, Likasi (Shaba-Zaïre), pp. 65

27. François, A., (1974). Stratigraphie, tectonique et minéralisation dans l'arc cuprifère du Shaba (Rep. Du Zaïre) In; P. Bartholomé (éd) Gisements stratiformes et provinces cuprifères. Centenaire de la société géologique de Belgique. Liège, pp. 79-101.

28. Gigler, G. M. (2016). The Transition from hypogene to supergene mineralisation at the Mashitu South Cu-Co deposit, Katanga, Democratic Republic of Congo. MSc thesis (Unpublished), University of the Witwatersrand.

29. Groundwater Consulting Services (Pty) Ltd. (2006). Ruashi Copper and Cobalt Mine-Lubumbashi. Bankable Feasibility Study Hydrogeological Investigation, pp. 20-33.

30. Jackson, M. P. A., Warin, O. N., Woad, G. M and Hudec, M. R. (2003). Neoproterozoic allochthonous salt tectonics during the Lufilian Orogeny in the Katangan Copperbelt, central Africa, *Bull. Geo. Soc. Amer*, 115(3), pp. 314-330.

31. Johnson, R. D. (2014). Orebody characterisation and structural features that govern copper and cobalt mineralisation in the eastern limb of the Lufilian Arc, Democratic Republic of Congo, MSc Thesis (unpublished), University of the Witwatersrand.

32. Kazadi, B. S-B. (2012). Structural geology of the Kinsevere Copper Deposit, DRC. MSc thesis, University of Pretoria.

33. Knight Piésold Consulting (Pty) Ltd. (2007). Kinsevere copper mine draft hydrogeological modelling report.

34. Knight Piésold Consulting (Pty) Ltd. (2010). Anvil Mining Kinsevere copper mine numerical hydrogeological modelling saturated zone model update and optimization kinsevere pit dewatering report.

35. Knight Piésold Consulting (Pty) Ltd. (2012). Kinsevere copper mine update of the environmental impact study.

36. Kampunzu, A. B., Kapenda, D. and Manteka, B. (1991). Basic magmatism and geotectonic evolution of the Pan African belt in Central Africa: evidence from the Katangan and West Congolian segments. *Tectonophys*., vol. 190, pp. 363-371.

37. Kampunzu, A. B. and Cailteux, J. (1999). Tectonic evolution of the Lufilian Arc (central Africa copper belt) during Neoproterozoic pan African orogenesis. *Gondwana Research*, vol. 2, pp. 401-421.

38. Kampunzu, A. B., Cailteux, J. L. H., Kamona, A. F., Intiomale, M. and Melcher, F. (2009). Sediment-hosted Zn-Pb-Cu deposits in the Central African Copperbelt. *Ore Geology Review*, 35, pp. 263-297.

39. Kruseman, G. P. and d Ridder, N. A. (1994). Analysis and evaluation of pumping test data (2nd Ed). *International institute for land reclamation and improvement*, Netherlands, Publication 47, pp. 193-197.

40. Marjoribanks, R. (2010) Drilling: A general discussion the importance of drilling. In.: *Geological Methods in Mineral Exploration and Mining*. Springer, pp. 75-84.

41. Marinelli, F. and Niccoli, L. (2000). Simple analytical equation for estimating groundwater inflow to a mine pit. Department of Civil Engineering, Colorado State University, Fort Collins, *Groundwater*, vol. 38, pp. 311-314.

42. Master, S., Rainhaud, C., Armstrong, R. A., Phillips, D., and Robb, L. J. (2003). Provenance ages of the Neoproterozoic Katanga Supergroup (Central African Copperbelt), Based on Shrimp U-Pb and Laser 40Ar/39Ar Dating of Detrital Zircon and Muscovites, with implications for Basin Evolution. *Economic Geology Research Institute*, Information Circular no. 376, pp. 1-37.

43. McMaster, K., Dawborn, T., Ilongo, H., Olberg, D., Saleem, A., Sloan, M., Northcott, M., Reed, A., Tomkins, M., Williams, P., Bull, S., Davies, B., Murphy, B. and Blake, C. (2016). Geology of the Kinsevere Cu Deposit, Democratic Republic of Congo – Presentation.

44. McWhorter, D. B. and Sunada, D. K. (1977). Ground water hydrology and hydraulics, Highlands Rach, Colorado, *Water Resources Publications.*

45. Moine, B., Guilloux, L., and Audeoud, D. (1986). Major element geochemistry of the host rocks in some sediment-hosted copper deposit, in Friedrich, H. H., (ed). Geology and metallogeny of copper deposits, Berlin, *Springer-Verlag*, pp. 443-460.

46. Mulenga, S. C. (1991). Groundwater flow through Konkola (Bancroft) Copper Mine-Zambia, PhD Thesis.

47. Nahon, D. B. (1991) Introduction to the petrology of soils and chemical weathering.

48. Nepid Consultants. (2006). AMCK S.P.R.L. Joint venture Kinsevere copper-cobalt project environmental impact assessment: Aquatic ecology.

49. Okitaudji, R. L. (1989) Geologie sedimentaire et concentration syndiagenetique et du cobalt dans la serie des mines du Shaba, Zaire. Unpublished PhD thesis. Institut national Polytechnique de Lorraine.

50. Porada, H. and Berhorst, V. (2000). Towards a new understanding of the Neoproterozoic-Early Palaeozoic Lufilian and Northern Zambezi belts in Zambia and Congo/Zaire: *Journal of African Earth*.

51. Porada, H. (1989) Pan-African rifting and orogenesis in southern to equatorial Africa and eastern Brazil. *Precambrian Research*, vol. 44, pp. 103-136.

52. Renard, P. (2005). Hydraulics of well and well testing. In: Anderson MG (ed) Encyclopaedia of hydrological sciences

53. Renard, H., Glenz, G. and Mejias, M. (2008). Understanding diagnostic plots for well-test interpretation, *Hydrogeology Journal.*

54. Roger H. Airlift Testing in Exploration Coreholes, SRK Consulting, pp. 1-6.

55. SRK Consulting (South Africa) (Pty) Ltd. (2016). Kinsevere Primary Copper Project: Phase 1 – scoping study.

56. SRK Consulting (South Africa) (Pty) Ltd. (2016). Kinsevere Mine pre-feasibility study, groundwater management system design.

57. SRK Consulting (South Africa) (Pty) Ltd. (2016). Kinsevere Mine groundwater management system design model report.

58. SRK Consulting (South Africa) (Pty) Ltd. (2017). Kinsevere Copper Mine feasibility study, Hydrogeology – airlift testing.

59. SRK Consulting (South Africa) (Pty) Ltd. (2017). Summary of dewatering boreholes at kinsevere mine.

60. SRK Consulting (South Africa) (Pty) Ltd. (2017). Kinsevere Mine groundwater management: installation of dewatering boreholes, 2016.

61. SRK Consulting (South Africa) (Pty) Ltd. (2018). Kinsevere Mine groundwater management: installation of dewatering boreholes, 2017/18.

62. Straskraba, V., Placet, J. and Holubec, M. (1985). Hydrogeology and drainage of copper-cobalt mines in the Kolwezi area of Shaba, Republic of Zaire. *International Mine Water Association*, pp. 125-139.

63. Straskraba, V., Sharma, D. and Naish, E. J. H. (2012). Konkola Mine dewatering study. *International Mine Water Association*, pp. 163-174.

64. Summa, G. (2010). A new approach to step-drawdown test. *Water SA*, vol. 36 no.3 pp. 279-285.

65. Summers, W. K. (1983). The hydraulic properties of the pierres hale, A comparison of methods.

66. Theis, C. V. (1935). The relation between the lowering of the piezometric surface and the rate and duration of discharge of a well using groundwater storage, *Am. Geophys. Union Trans.*, vol. 16, pp. 519-524.

67. Theron, S. J. (2013). The origin of the Central African Copperbelt: in a Nutshell. *The Southern African Institute of Mining and Metallurgy*. Base Metals Conference 2013, pp. 1-15.

68. United States Geological Survey. (2003). Relative hydraulic conductivities of geological formations.

69. Unrug, R. (1983) The Lufilian Arc: a microplate in the Pan-African collision zone of the Congo and the Kalahari cratons. *Precambrian Research*, vol. 21, pp. 181-196.

70. Unrug, R. (1988). Mineralisation controls and source of metals in the Lufilian Fold Belt, Shaba (Zaire), Zambia and Angola. *Economic Geology*, vol. 83, pp. 1247-1258.

71. Unrug, R. (1997). Rodinia to Gondwana: the geodynamic map of Gondwana supercontinent assembly. *GSA Today*, vol. 7, pp. 1-6.

72. van Tonder, G. J., Botha, J. F. and van Bosch, J. (2001). A generalised solution for step-drawdown tests including flow dimension and elasticity, Institute for Groundwater Studies. *Water SA*, vol. 27 No.3, pp. 345-353

73. van Tonder, G., Bardenhage, I., Rieman, K., van Bosch, J., Dzanga, P. and Xu, Y. (2002). Manual on pumping test analysis in fractured rock aquifers, Institute for Groundwater Studies, University of the Free State.

74. van Tonder, G., de Lange, F. and Gomo, M. (2014) FE program for aquifer test analysis, Institute for Groundwater Studies, University of the Free State.

75. Wendorff, M. (2005). Evolution of Neoproterozoic-Lower Palaeozoic Lufilian Arc, Central Africa: a new model based on syntectonic conglomerates. *Journal of the Geological Society*, vol. 162, pp. 5-8.

76. Xiao, L. (2014). Evaluation of groundwater flow theories and aquifer parameter estimation, PhD Thesis, University of the Western Cape.

77. Zeintek, M. L., Bliss, J. D., Broughton, D. W., Denning, P. D., Hitzman, M. W., Horton, J. D, Parks, H. L., Wilson, A. B., Wintzer, B. W. and Woodhead, J. (2010). Sediment-hosted stratabound copper assessment of the Neoproterozoic Roan Group, Central African Copperbelt, Katanga Basin, Democratic Republic of Congo and Zambia. Global Mineral Resource Assessment. *United States Geological Survey*, pp. 1-178.

Appendices

Appendix A: Hydrocensus Water Level Data

Appendix B: Pumping Test Data

Appendix C: Airlift Testing Data

Appendix D: Slug Test Data

Appendix E: Groundwater Inflow Calculations